This is to certify that the

dissertation entitled

Diffusion Barriers for Silicon Carbide Particle Reinforcements by Ion-Beam Assisted Deposition: Effects On Interphase Stability in SiC_p/beta-NiAl and Sic_p/gamma-Ni_3Al Composites

presented by

Zhiwei Cai

has been accepted towards fulfillment
of the requirements for

Ph.D. degree in Materials Science and Engineering

Major professor

Date 10/7/2000

DIFFUSION BARRIERS FOR SILICON CARBIDE PARTICLE REINFORCEMENTS BY ION-BEAM ASSISTED DEPOSITION: EFFECTS ON INTERPHASE STABILITY IN SiC_P/β-NiAl AND SiC_P/γ-Ni_3Al COMPOSITES

By

Zhiwei Cai

A DISSERTATION

Submitted to
Michigan State University
in partial fulfillment of the requirements
for the degree of

DOCTOR OF PHILOSOPHY

Department of Materials Science and Mechanics

2000

ABSTRACT

DIFFUSION BARRIERS FOR SILICON CARBIDE PARTICLE REINFORCEMENTS BY ION BEAM ASSISTED DEPOSITION: EFFECTS ON INTERPHASE STABILITY IN SiC_P/β-NiAl AND SiC_P/γ-Ni_3Al COMPOSITES

By

Zhiwei Cai

In this study, aluminum nitride and aluminum oxide films were used as diffusion barriers for SiC particles that were consolidated with β-NiAl and γ- Ni_3Al matrices at temperatures of 1673 K and 1373 K, respectively. The focus of this study was to understand factors influencing the effectiveness of the diffusion barriers during the consolidation processes of the two composite systems.

The barrier films were deposited on SiC particles by ion-beam assisted vacuum evaporation during which the SiC particles were radiantly heated and acoustically levitated. The nitride film formed reactively on SiC particles, and consisted of 95% aluminum nitride (balanced with aluminum nitrate and oxide). The oxygen content in the nitride film was a result of the impingement of residual oxygen and water molecules in the deposition environment.

A voided globular structure of fine-grained clusters was found in a nitride film deposited on SiC particles at 593 K, which was attributed to the levitation of the particles and the deposition temperature. Nitride films deposited at a higher temperature of 793 K consisted of a fine-grained dense structure with few voids. The oxide film deposited at room temperature had a fine-grained dense structure with some globular features.

This study found that film material affected film's ability of retaining integrity during compositing process, which was important for the success of the barrier films. Annealed at 1673 K, grains in a nitride film (deposited at 793 K) coalesced to an average size of 0.5 μm that was comparable to the film thickness. Grain boundaries in the film were widened by the pore agglomeration, resulting in micro-cracks. The oxide film exhibited a similar phenomenon of uninhibited grain growth and micro-crack formation at a lower temperature of 1273 K. Both films failed to be an effective barrier in SiC/β-NiAl composite during the compositing process at 1673 K.

This study showed the influence of film structure on grain growth in films at high temperatures. With a voided globular structure, the nitride film deposited at 593 K experienced a grain growth that was primarily restricted within each individual grain clusters at elevated temperatures. Solid-state sintering at 1673 K densified the nitride film because of the film's originally voided structure. After annealing at 1673 K for 4 hours, an average 0.5 μm thick nitride film deposited at 593 K retained film integrity on SiC particles, and succeeded as a diffusion barrier in the SiC/β-NiAl composite.

This study indicated that the chemical reaction potential in a composite system was a critical factor in determining the effectiveness of diffusion barriers. SiC/γ-Ni_3Al composite had a higher chemical reaction potential at 1373 K, comparing to SiC/β-NiAl system at 1673 K. Although being effective as a diffusion barrier in the SiC/β-NiAl composite at 1673 K, the same 0.5 μm thick nitride film (deposited at 593 K) did not protect the SiC particles in the SiC/γ-Ni_3Al composite at 1373 K.

A cursory study performed in this research indicated that Ni has low diffusivities in aluminum nitride lattice. From a γ-Ni_3Al source, the upper-bound lattice diffusivity was estimated to be 2.2×10^{-14} cm^2/sec at 1473 K. From a β-NiAl source, the upper-bound lattice diffusivity at 1673 K was estimated to be 5.8×10^{-14} cm^2/sec.

I dedicate this dissertation to my wife, Fang Li.

And to the memories of my late grandmother.

ACKNOWLEDGEMENTS

I wish to express my sincere appreciation to Dr. D. S. Grummon, my advisor, for his generous support, patient guidance, creative ideas and scientific expertise. I would also like to thank my committee members, Dr. M. A. Crimp, Dr. T. R. Bieler, and Dr. K. L. Klomparens for their helpful discussions and valuable criticisms of the dissertation. Also, the generosity of the Composite Materials and Structures Center for letting me use their equipment is appreciated.

I would like to give a heartfelt thanks to my dear wife, Fang Li, for her love. It would be impossible for me to finish this dissertation without her enormous patience and encouragement throughout the entire unbelievable length of time to complete this dissertation.

I am deeply indebted to our parents for their caring, support, and wisdom. I am particularly grateful for our parents' sacrifices in their senior years helping my wife and I to raise our young family in an environment so alien to them.

I would also like to thank my two little angels, Phillip and Louis, for all the joy they bring into my life.

TABLE OF CONTENTS

LIST OF TABLES

LIST OF FIGURES

CHAPTER 1. INTRODUCTION

Ceramic-reinforced intermetallic matrix composites are of interest for elevated-temperature applications because of their better theoretical high-temperature properties as compared with the materials currently in service [Brindley, 1987; Metcalfe, 1974; Schoutens, 1982]. However, many of these composite systems suffer from inter-diffusion and/or interfacial reactions during composite consolidation and application at high temperatures, which in turn degrades the performance of these composites.

Silicon carbide (SiC) reinforced nickel aluminide-based matrix composites (SiC/β-NiAl and SiC/γ-Ni_3Al systems) are examples of high-temperature composites that have both potentials and problems. Although attractive from the standpoint of oxidation resistance and good theoretical mechanical properties at temperatures above 1273 K, these composites suffer from strong and debilitating interfacial chemical reactions of the carbide reinforcement with the nickel-bearing matrices. Because of the potential benefits of these composites as the next generation of high-temperature structural materials, studies have been done to understand the problems involved and their possible solutions [Chou, 1991a; Nieh, 1989; Pope, 1987; Yang, 1989 a&b].

SiC reacts strongly with nickel-bearing intermetallics at temperatures below the expected composite processing and service temperatures, producing graphite and ternary compounds. The reaction of SiC with β-NiAl has a modest rate and occurs at temperatures above 1573 K [Chou, 1991a], while γ-Ni_3Al reacts with SiC more strongly even at a lower temperature of 1073 K [Nieh, 1989; Yang, 1989b]. The interface zones formed have inherently poor mechanical properties. A continuous supply of free Ni atoms into the SiC region is the controlling factor in these reactions [Chou, 1991 a&b].

For this reason, concept of diffusion barrier against Ni diffusing into SiC was suggested for improving the viability of these composites.

Aluminum oxide (Al_2O_3) thin film has been studied as a diffusion barrier candidate in SiC/γ-Ni_3Al composite system. The results were not consistent, though. Nieh [1989] reported that an Al_2O_3 film formed on the surface of a Ni_3Al-based alloy plate demonstrated the ability to function as a diffusion barrier between a *planar* SiC and the Ni_3Al plate[1]. However, Al_2O_3 films deposited on SiC particles by reactive sputtering consistently failed to protect the SiC particles from the reactions at the consolidation temperature of 1373 K for γ-Ni_3Al matrix composites [Cai, 1992].

Because of the inconsistent results of Al_2O_3 as a diffusion barrier in SiC/γ-Ni_3Al composite system, this study evaluated several factors that influenced the effectiveness of diffusion barriers. These factors included barrier film materials, barrier film deposition conditions and resultant film structures, barrier film thermomechanical behavior at elevated temperatures, and chemical potentials in different composite systems.

In this study, SiC particle reinforced β-NiAl and γ-Ni_3Al matrix composites were selected for different levels of chemical potential in the composite systems. Aluminum nitride (AlN) was selected as a diffusion barrier material for SiC at elevated temperatures because AlN has more attractive thermomechanical properties (chiefly a more favorable thermal expansion coefficient) than Al_2O_3 [Poluboyarinov, 1980; Shaffer, 1964; Sheppard, 1990]. Aluminum oxide barriers were studied as a basis for comparison.

Both aluminum nitride and oxide films were deposited on SiC particles using an ion-beam assisted deposition (IBAD) technique. A novel particle levitation and heating

---

[1] In Nieh's experiment, a Ni_3Al plate was pre-oxidized to form a 0.13 μm thick Al_2O_3 layer on its surface. This oxide layer successfully prevented the inter-diffusion and reactions between the aluminide plate and a SiC plate at 1373 K.

system was designed to deposit films uniformly on the SiC particulate substrates. The nitride films were deposited reactively by using a nitrogen ion beam to react with evaporated aluminum atoms at the substrate surfaces. The composition of the nitride film was studied for evaluating the ability of such a reactive deposition process.

Two factors, the as-deposited film structure and films' thermomechanical behavior during compositing processes, were particularly interested in this study. The two factors were not only interrelated, but also underlay the viability of the films as an effective diffusion barrier. The effectiveness of the diffusion barriers was evaluated in model composites under high-temperature consolidation conditions after combining all the influencing factors analyzed in this study.

Because of the limited information on Ni diffusing in aluminum nitride, a cursory investigation was conducted to ensure that Ni has low lattice diffusivity in aluminum nitride at the temperatures applied in this research. Only the extent of Ni diffusing in aluminum nitride was of interest in this investigation.

Chapter 2 presents a review of the related fields of diffusion, the interaction between SiC and nickel aluminides, the concept of diffusion barriers, a property comparison between Al_2O_3 and AlN, vacuum evaporation and the IBAD processes, the resultant film structures, and grain growth in ceramics. The remaining chapters discuss the experimental procedures, results, and conclusions drawn from the study.

CHAPTER 2. BACKGROUND REVIEW

This chapter reviews fields related to this research, including diffusion, diffusion barriers and barrier materials, methods of thin film deposition, and thermomechanical behaviors in thin films during high-temperature treatment. Much of the discussion is focused on the aspects that directly apply to this study.

1. Diffusion in Thin Films

General Aspects

Diffusion is a time-dependent, thermally activated process that is driven by gradients in chemical potential, and rate-limited by atomic mobility in a material system. The rate factor for a diffusant in a material system, the diffusivity (D), can be expressed in terms of a frequency factor (D_o), temperature (T) and an activation energy (Q):

$$D = D_o \exp\left(-\frac{Q}{RT}\right)$$

Here, R is the molar gas constant. Both Q and D_O depend on the matrix as well as the diffusant. The distance of diffusion is proportional to $2\sqrt{Dt}$, where t is the appropriate diffusion duration [Gupta, 1988; Shewmon, 1963].

Diffusion in solids involves atomic exchange with lattice imperfections. The concentration of defects has a profound impact on diffusivity. In ionic compounds with negligible deviation from their stoichiometries, such as in Al_2O_3, the diffusivities are often small because of low point defect concentrations [Gupta, 1988; Kingery, 1976]. Compared with lattice-bound atoms, less tightly bound atoms at non-lattice sites, such as

grain boundaries, dislocation cores, surfaces, and interfaces, are more mobile. Diffusion through these sites requires less activation energy than through lattice sites, resulting in higher diffusivities at low temperatures (so-call *fast-diffusion*) [Ohring, 1991]. At high temperatures, lattice diffusion generally dominates mass transport in materials.

Figure 2.1 illustrates the corresponding dominant temperature regimes for lattice diffusion and grain-boundary diffusion. In most materials, grain-boundary diffusion dominates at temperatures below 0.3 T_m, where T_m is the melting point of the material [Ohring, 1991]. The available number of fast-diffusion site influences the temperature division between the dominant diffusion mechanisms. Higher defect concentration pushes the division to a higher temperature.

Compared with bulk materials, thin films from physical vapor deposition have higher density of defects such as vacancies, voids, grain boundaries and dislocations, which make the fast-diffusion important even at relatively high temperatures. Over a wide range of temperatures, diffusion in a thin film is a combined result of the lattice diffusion and fast-diffusion mechanisms. Among the latter, grain-boundary diffusion is the most important because of the small grain sizes of these materials. Figure 2.2 illustrates the regimes of dominant diffusion mechanisms in FCC metal films at various temperatures [after Balluffi, 1975]. For typical metal films with a grain size of 1 μm or less, grain-boundary diffusion dominates at all practical temperatures.

Grain Boundary Diffusion

Grain-boundary diffusion can seldom be fully de-coupled from lattice diffusion since the diffusing species may leak from grain boundaries into the adjoining lattice. Three types of kinetic behavior, A-, B-, and C-kinetics, are used to describe this lateral

leakage [Gupta, 1978]. Mathematical models have been established to solve the diffusant concentration for each kinetic regime.

A-kinetics describes the situation where the diffusant has high diffusivity in the matrix lattice. Extensive lattice diffusion causes the fields of diffusing species from adjoining grains to overlap. In C-kinetics, on the other extreme, lattice diffusion is considered negligible and significant atomic transport occurs only within the grain boundaries. C-kinetics requires very low lattice diffusivity in the diffusion system, and relatively short diffusion duration [Gupta, 1978][1].

B-kinetics deals with an intermediate situation, where one boundary is assumed to be isolated from the other and where the lateral flux of the diffusant approaches zero at large distances from the grain boundary. The diffusant concentration in the lattice is the sum of the contribution from lattice diffusion and material leakage from the grain boundaries. Whipple [1954] has given a solution for B-kinetic diffusion in a bulk material under a constant diffusant source.

The concentration profile for B-kinetics diffusion has two distinguishable regions. A high concentration region is dominated by the lattice diffusion, with a large gradient and a shallow penetration depth near the source interface. The followed second region is of a low level and less gradient of diffusant concentration, which arises from grain-boundary diffusion [Gilmer, 1976a]. The diffusant concentration from a grain boundary diffusion is proportional to $y^{6/5}$, where y is the diffusion distance [LeClaire, 1961]. The dotted lines in Figure 2.3 indicate the two regions in the concentration profile of B-kinetics based on diffusion in a bulk material.

---

[1] For C-kinetic diffusion, only the material residing in the grain boundaries themselves contributes to the total amount of diffusing species. In the case of diffusion barriers with low lattice diffusivities, grain-boundary diffusion may be treated as the only diffusion mechanism if the grain boundary itself has a thickness greater than 10 times of the extent of lattice diffusion of $2\sqrt{D_l t}$ [Gupta, 1978].

In thin films, the solutions for diffusant concentration are more complex because of the additional boundary condition imposed by the film surface[1] [Gilmer, 1976 a&b]. The diffusant concentration raises significantly near the free surface. Compared with the diffusion in a bulk material, the diffusant profile in a thin film has higher concentrations and lower gradient at the grain-boundary diffusion dominated region near the film free surface. Near the source/ film interface, the diffusant concentration profile is similar to that for diffusion in the bulk model because of the dominant of the lattice diffusion. In Figure 2.3, the solid line indicates the difference between the diffusion in a thin film and that in a bulk material. The y-axis of the profile uses a normalized distance (y/Y_0) away from the diffusion source (Y_0 is the film thickness). On the source/film interface, $y/Y_o=0$, whereas on the free film surface, $y/Y_o=1$.

In films with small grain sizes, the ratio between the grain size and the distance of diffusion influences the diffusant concentration profile [Gupta, 1978]. When the ratio is relatively large, smaller grain size allows the diffusant fields in the lateral direction to overlap inside the grains more easily, making it closer to A-kinetics grain-boundary diffusion [Gupta, 1978]. The A-type diffusion may be found in thin film materials with a small grain size even if the lattice diffusivity (D_l) is small. For instance, in a material with a grain size of 0.1 μm, a D_l of 5×10^{-15} cm^2/s and a diffusion duration of one hour correspond to a ratio of 1.2, which is at the junction of the A- and B-kinetics.

2. Interaction between SiC and Nickel Aluminides

A sharp gradient in chemical potential at the interface between the reinforcement and matrix in composites is the driving force for diffusion during processing or

[1] To find a mathematical solution for diffusant concentration profile in thin films, an imaginary source was used in order to maintain the free-surface boundary condition for thin films [Gilmer, 1976 a&b].

application of the composites at high temperatures [Chou, 1985; Reedy, 1989]. Inter-diffusion and/or diffusion-controlled interfacial reactions often degrade the reinforcement. The reaction products in the interfacial region are often brittle, and thus detrimental to composite strength [Broutman, 1974; Schoutens, 1982]. SiC-reinforced nickel aluminide matrix composites are typical examples of high temperature composites [Pope, 1987; Yang, 1989a].

SiC reacts with γ-Ni_3Al -based alloys at temperatures above 1073 K [Nieh, 1989; Yang, 1989b]. Graphite and a ternary compound, $Ni_{5.4}Al_1Si_2$, are formed in the reaction zone. A layer of NiAl is also formed near the matrix side [Chou, 1991b]. The reaction is controlled by the diffusion of Ni. Figure 2.4 schematically presents the reaction zone between a SiC and a γ-Ni_3Al plate after a 23-hour diffusion bonding treatment at 1273 K (0.76 T_m of γ-Ni_3Al). The width of the reaction zone is found to be approximately 100 to 150 μm under these conditions [Chou, 1991b].

SiC also reacts with β-NiAl-based intermetallic alloys, but at higher temperatures. Above 1573 K, a Ni-Al-Si ternary compound, $Ni_{14}Al_9Si_2$, and graphite are formed [Chou, 1991a]. In Figure 2.5, the interface region from this reaction is schematically illustrated. An annealing treatment at 1573 K (0.82 T_m of β-NiAl) for 20 hours produces a 10 μm thick reaction zone [Chou, 1991a]. This reaction is controlled by the decomposition rate of SiC in the presence of free Ni. Compared with the SiC/γ-Ni_3Al system, the thermal stability of the SiC/β-NiAl system is about one order of magnitude better.

The interface zones formed in the aforementioned reactions have inherently poor mechanical properties [Nieh, 1989; Yang, 1989b]. Hence, there is a need for a diffusion barrier between SiC reinforcement and the nickel aluminide matrices for the successful development of these composites.

3. Diffusion Barriers

Principles of Diffusion Barrier

Diffusion barriers are thin-film layers used to prevent two materials from coming into direct contact, thus preventing inter-diffusion and interactions between the two materials [Ohring, 1991]. The selection of the barrier material is largely determined by the characteristics of inertness and low diffusivities. Ideally, the barrier materials should be chemically inert, and have negligible mutual solubility and diffusivity at the highest temperature of application with respect to other materials in the system.

Other factors are important in choosing the barrier material as well. These factors include ease of fabrication, similar coefficients of thermal expansion between the barrier and its substrate, stress-state in the barrier after fabrication, and compatibility with other processing steps. Practically, some of the requirements for an ideal barrier are difficult to satisfy or even mutually exclusive. As a result, less ideal systems have to be adopted instead [Kattelus, 1988]. Based on to the operational mechanisms, diffusion barriers are divided into three categories: stuffed, passive, and sacrificial barriers [Nicolet, 1978].

The imposition of a diffusion barrier upon a thermodynamically unstable system slows down the equilibration process. Nevertheless, the instability in the system is never actually removed. Enhanced reliability is achieved with a diffusion barrier at the cost of increasing structural complexity and added processing expense [Ohring, 1991].

Candidates for Diffusion Barriers

Many high-temperature alloy coatings (Ni-, Fe-, Co- based alloys with Cr, Ti, Al, V additives) are used as barriers for prevention of diffusion bonding. The protection

mechanism is based on adherent impervious surface films of Al_2O_3, SiO_2, CrO_2, or a spinel-type, which grow on high temperature exposure to air [Grayson, 1983].

Low lattice diffusivity is crucial for high-temperature diffusion barriers because lattice diffusion becomes dominant at high temperatures. Candidates for high-temperature diffusion barriers are often stable compounds with limited deviations from their stoichiometries. They include the transition metal carbides (HfC, TaC, TiC), nitrides (AlN, HfN, TiN), borides (TiB_2), and oxides (Al_2O_3, Y_2O_3) [Walters, 1988].

Al_2O_3 as a Diffusion Barrier in SiC/γ-Ni_3Al System

Al_2O_3 is a diffusion barrier candidate for many high-temperature systems. The advantages of Al_2O_3 as a diffusion barrier includes a high melting point (2345 K), moderate thermal shock resistance, and good chemical stability at high temperatures in a wide variety of atmospheres. Al_2O_3 has a reasonably good and nearly constant strength that can be maintained at temperatures up to 1373 K.

Al_2O_3 has a moderately high coefficient of thermal expansion (CTE) of 8×10^{-6}/K, as compared with other ceramics like SiC (4.7×10^{-6}/K). The CTE of Al_2O_3 fits in between SiC and Ni_3Al (12×10^{-6}/K), which may limit the internal stress due to the thermal cycling when an Al_2O_3 film is coated on SiC reinforcements in SiC-reinforced Ni_3Al -based matrix composites [Grayson, 1983; Nourbakhsh, 1989].

Furthermore, the diffusion coefficients of Ni in oxides are low. For instance, Ni has a diffusivity ranging from 10^{-13} to 10^{-12} m^2/s in amorphous SiO_2 over a temperature range of 1273 to 1473 K [Goshtagore, 1969]. Nieh [1988] has shown the ability of Al_2O_3 film to function as a diffusion barrier between planar SiC and a Ni_3Al-based alloy.

In Nieh's experiment, the nickel aluminide was IC-50 (Ni - 23 at% Al - 0.5 at% Hf - 0.2 at% B) which was pre-oxidized to form an Al_2O_3 surface film. The pre-oxidation was performed at 1273 K in air for 60 hours, after which a 0.13 μm thick Al_2O_3 scale was formed on the surface of the Ni_3Al plate. Subsequent diffusion bonding tests were conducted using the pre-oxidized aluminide plate and a SiC disc. No bonding was found even at 1373 K.

4. Comparison of Aluminum Oxide and Aluminum Nitride

Aluminum oxide is an effective barrier to Ni diffusion, and has demonstrated its potential as a diffusion barrier between SiC and a Ni_3Al-based alloy [Nieh, 1989]. The mismatch of the coefficients of thermal expansion (CTE) between Al_2O_3 and SiC, however, may induce large thermal stress[1] in an Al_2O_3 film deposited on a SiC substrate when subjected to a large temperature excursion. Al_2O_3 has a CTE with an average value of 8×10^{-6}/K in a temperature range from 298 to 2123 K. The CTE is 4.7×10^{-6}/K for SiC from 293 to 1173 K [Shaffer, 1964]. Thus, the calculated result of the thermally induced stresses in the Al_2O_3 film could exceed 1 GPa when the temperature of an Al_2O_3 coated SiC changes between room temperature and 1273 K, assuming that the film is still intact and behaves elastically.

---

[1] The thermal stress is induced by the difference between the deposition temperature and the application temperature because of the difference in thermal expansion coefficients of a film and its substrate. The thermal stress in a film is estimated in one-dimensional approximation (neglecting the Poisson effect) by

$$\sigma_{film} = E_{film}(\alpha_{film} - \alpha_{sub})(T_{deposition} - T_{application})$$

where E_{film} is Young's modulus of the film, α_{film} and α_{sub} are the average coefficients of thermal expansion for the film and substrate respectively. $T_{deposition}$ is the substrate temperature during deposition and $T_{application}$ is the temperature at application. A positive value of σ_{film} corresponds to a tensile stress.

Aluminum nitride, on the other hand, possesses an average CTE of 4.8×10^{-6}/K from 293 to 2073 K [Poluboyarinov, 1980; Shaffer, 1964]. The closeness of the CTEs of aluminum nitride and SiC makes aluminum nitride an attractive candidate as a diffusion barrier material on SiC particles. The thermally induced compressive stresses in an aluminum nitride film on a SiC substrate are calculated to be 31 MPa when temperature reaches 1273 K from room temperature, and 38 MPa when reaching 1673 K, given an elastic behavior of the film. Figure 2.6 compares the CTEs among aluminum nitride, Al_2O_3, and SiC, from room temperature to 873 K.

Aluminum nitride has attracted interest in recent years. This material has many useful properties, such as high thermal conductivity, low thermal expansion, low density, and high specific modulus [Sheppard, 1990]. Aluminum nitride is chemically stable at temperatures up to 1873 K with both β- and γ- nickel aluminides and SiC [Lowell, 1990; Zangvil, 1985]. Aluminum nitride has a relatively low strength and modulus at high temperatures, which makes aluminum nitride an unattractive reinforcement candidate by itself for high-temperature nickel aluminide matrix composites.

Aluminum nitride has a high resistance to thermal shock [Kingery, 1976], which is a desirable feature for ceramics undergoing a large temperature excursion. The resistance to thermal shock may be measured by the *maximum-quench-temperature difference* that the material is able to withstand [Kingery, 1976]. Compared with 150 K for Al_2O_3 [Kingery, 1976], the resistance to thermal shock of aluminum nitride is approximate 550 K [Poluboyarinov, 1980]. The better thermal shock resistance of aluminum nitride is attributed to a lower elastic modulus, a lower CTE, and a higher thermal conductivity for aluminum nitride comparing with aluminum oxide. Figure 2.7 compares the thermal conductivities among aluminum nitride, SiC, and Al_2O_3, in a temperature range from 297 to 573 K.

Aluminum nitride films have been deposited by a variety of methods, from physical vapor deposition (PVD) to chemical vapor deposition (CVD) [Ohring, 1991]. Among these techniques, ion-beam assisted PVD methods offer attractive features, especially for compound film deposition, as will be discussed in the following section.

5. Vacuum Evaporation and Ion-Beam Assisted Deposition

PVD Techniques for Thin Films

During physical vapor deposition (PVD), physical mechanisms (evaporation or collision impact) are used to bring materials into a gas phase from solid or molten sources [Ohring, 1991]. PVD is capable of depositing virtually any type of inorganic, as well as some organic materials, over a wide range of deposition rates and temperatures. PVD is a more controllable process than other thin film deposition processes, such as chemical vapor deposition (CVD) [Bunshah, 1984].

One PVD technique is sputter deposition. Sputtering is a vacuum process in which atoms of a target material are ejected by the bombardment of ions and energetic particles generated by an electrical discharge, and then condensed onto a substrate [Holland, 1974]. Sputter deposition offers many advantages, including reproducibility, continuous nature, and simplicity in operation. Sputtering itself is a complex process, and has been extensively studied [Behrisch, 1981, 1983 and 1991].

Sputter deposition offers depositing atoms with kinetic energies in the range of 5 to 30 eV. Such energetic atoms improves the adhesion of deposited thin film to its substrate [Westwood, 1988]. The deposition process usually occurs in a relatively high pressure range of 10^{-2} to 10^{1} Pa, which causes a relatively high degree of impurity

incorporation [Mattox, 1989; Ohring, 1991]. For an alloy or compound target, the film concentration can easily match the composition of the target with a little variation.

Vacuum Evaporation

Another widely used PVD technique is vacuum evaporation. In the evaporation process, the coating material is evaporated in a vacuum environment by heating. The evaporation process can offer a high deposition rate for virtually all kinds of materials [Glang, 1970; Ohring, 1991]. Among various heating sources for evaporation, the electron-beam source provides the possibility to deposit high purity films [Bunshah, 1984; Ohring, 1991].

Vacuum evaporation is a relatively "clean" deposition process because it is performed in a vacuum environment below 10^{-4} or 10^{-3} Pa. Nevertheless, gas molecules in the vacuum environment will impinge and be adsorbed on the growing film surface. Using the arrival rate of depositing atoms (J_a) on substrate surface and the gas impingement rate (J_g), the concentration of the impurity molecules (C_g in at%) is approximated as [Chambers, 1989; Ohring, 1991]:

$$C_g = \frac{J_g}{J_a + J_g} \approx 4.38 \times 10^{-4} \frac{M_a P}{\dot{s}\rho\sqrt{M_g T}}$$

Here, $\dot{s}$ is the deposition rate in cm/sec, ρ is the film density in g/cm^3, P is the partial pressure in Pa, M_a is the molar weight of the film material in g/mole, M_g is the molar weight of the gas molecule in g/mole, and T is the background temperature in Kelvin.

Because the sticking probability of a gas molecule to a film surface is usually less than unity [Ohring, 1991], the above equation overestimates the amount of impurity molecules residing in the film by assuming the sticking probability to be unity. Using a

density value for a bulk material, on the other hand, the impurity concentration may be underestimated by the above equation [Ohring, 1991]. For metallic materials, the film densities can be about 95% of their bulk value. Compound films usually have lower ratios, such as 70% for fluorides [Pulker, 1984].

Conformal coverage (the coverage of the steps on substrate surface) is another issue in vacuum evaporation. Evaporated atoms travel in essentially collisionless paths prior to condensation on the substrate [Bunshah, 1984]. Because the evaporated particles usually come from a point source, shadowing effect may cause unequal deposition between the top and sides of the step on substrates. Inadequate step coverage, or sometimes no step coverage at all, can lead to minute cracks in the film [Ohring, 1991]. Such problems may be solved by either physically exposing the shadowed area to the coating material flux during deposition, or improving the depositing atoms' mobilities on the substrate surface. The latter approach can be implemented by elevating the substrate temperature [Thornton, 1977].

Evaporating compounds or alloy sources may form films with compositions that differ from that of the source. The constituents of alloy sources evaporate almost independently of each other. Decomposition or dissociation occurs in compound evaporation [Bunshah, 1984; Ohring, 1991]. Additional material sources may be needed to form a compound or alloy film with the same composition as the primary evaporating source. For example, introducing oxygen flow into the evaporation environment is a common practice necessary to overcome oxygen deficiency in films deposited by evaporating a stoichiometric Al_2O_3 source.

Some compound films can also be deposited by evaporating pure metal evaporants in a relatively high partial pressure (0.1 - 5 Pa) of reactive gases, such as O_2, N_2, CH_4, C_2H_2, etc. [Ohring, 1991]. A plasma discharge may also be used within the

reactive zone between the metal source and substrate, helping to overcome the energy barrier of reaction by ionizing both the metal vapor and the reactive gases. The plasma discharge increases the reactivities of the coating particles on the surface of the growing films, and promotes stoichiometric compound formation [Bunshah, 1987; Ohring, 1991]. Compounds can be synthesized by this method include oxides (Al_2O_3, V_2O_3, TiO_2), carbides (TiC, ZrC, HfC, VC), and nitrides (TiN, MoN, HfN, BN).

Vacuum evaporation is a capable film deposition process by itself. Nevertheless, low kinetic energy associated with the evaporant atoms (about a fraction of an eV) results in a weak adhesion of the condensed films to their substrates. Also, decomposition or dissociation that occurs during compound and alloy evaporation may make it difficult to form stoichiometric compounds or alloy films. Ion-beam techniques are utilized to improve the evaporated film quality, as well as to form compound films.

Reactive IBAD for AlN Films

Introduction To improve the quality of a deposited film from evaporation and to form compound films, a hybrid technique has been developed which uses ion-beam technology with vacuum evaporation. It is called *ion-beam assisted deposition (evaporation)*, or IBAD.

The IBAD process provides independently controlled deposition parameters and the characteristics of ion bombardment on substrates [Harper, 1982 and 1983; Ohring, 1991]. During the process, ion bombardment on a growing film heightens diffusion and chemical reactivity of film atoms, and lowers the sticking probabilities of residual gas atoms. With proper ion-beam parameters, ion bombardment during deposition can alter coating stresses, and improve step coverage and packing density. In many cases, low

beam energies (about 100 eV or lower) and low ion-to-atom arrival ratios (a few percent or lower) are most effective [Harper, 1983]. Figure 2.8 shows an IBAD configuration that incorporates an ion source and an electron-beam evaporation source.

The IBAD technique has many advantages similar to those of the sputtering technique, because of the ballistic nature of the bombardment of energetic particles on substrates and growing films. In addition, the energetic bombarding particles can be either ionized or neutral, which makes the IBAD technique applicable to non-conducting substrates or films. The technique is medium-to-high vacuum compatible also results in less impurity incorporation into the growing film.

The Ion Source In the heart of many IBAD processes is the broad-beam (Kaufman) ion source [Harper, 1983; Kaufman, 1982; Ohring, 1991]. The Kaufman source operates in a background pressure of approximate 10^{-2} Pa that is compatible to both sputtering and evaporation. The resulting beams have a low-energy spread (typically 10 eV) and are well collimated (with divergence angle of a few degrees). Such ion sources have been widely employed in sputtering, etching, surface compound formation, and thin film deposition [Harper, 1982 and 1983].

The ion beam from a Kaufman-type source consists primarily of a mixture of single- and double-charged molecules. Triple-charged (or even higher) gas ions are rare under normal operational conditions of the source [Kaufman, 1987]. For nitrogen (N_2) gas, the single-charged species are N_2^+ and N^+, and the double-charged are N_2^{++} and N^{++}. Among these four species, one N_2^{++} molecule and a pair of N^+ ions are identical in terms of the number of atoms, momentum and energy.

Because the energy required to form a single-charged molecule is much lower [Harper, 1982; Kaufman, 1987], the probability of forming a single-charged molecule is much greater than the probability of a double-charged one. Consequently, the number of double- charged species such as N^{++} from a Kaufman source may be negligible. Taylor [1981] has found that approximately 96% of the nitrogen ions are N_2^+ and 4% of N^+. Netterfield [1988] has measured that the ratio of $N_2^+ : N^+$ emitted from a Kaufman ion source is 3.7: 1 under a normal operational conditions at a 5×10^{-3} Pa working pressure, which indicates 78.7% of N_2^+ and 21.3% of N^+.

Reactive IBAD Using a reactive gas, such as N_2 in the ion source, the Kaufman source produces a reactive ion beam which can be used to form compound films with an evaporating metal [Harper, 1982]. In such a process, the degree of incorporation of the reactive components in the growing film is the key parameter that controls stoichiometry, density, resistively, and many other properties of the film [Harper, 1983; Stelmack, 1989]. The atomic ratio between the arrival rate of the charged species in the ion beam and that of the metal atoms is the parameter that, in practice, affects the film properties the most. Hentzell [1985] has shown that a ratio of $N/Al \geq 1$ was necessary in order to form a stoichiometric aluminum nitride film without metallic aluminum grains, where the nitrogen atoms were assumed to be as N_2^+.

Aluminum Nitride Film Deposition with Reactive IBAD In the reactive IBAD process for aluminum nitride film deposition, aluminum atoms are supplied by a metallic aluminum source whereas the growing film is bombarded with a nitrogen ion beam [Harper, 1982; Hentzell, 1985; Netterfield, 1988]. The charged nitrogen ions are necessary for nitride formation because metallic aluminum atoms do not readily react to

neutral nitrogen molecules by chemisorption during depositions [Taylor, 1981]. The reaction starts, however, when the nitrogen molecules become charged [Hentzell, 1985; Netterfield, 1988; Taylor, 1981]. The sticking coefficient of nitrogen ions on aluminum is then close to unity [Harper, 1985].

The atomic arrival ratio of nitrogen to aluminum (the *N/Al ratio*) is critical to the properties of the deposited film [Harper, 1985; Hentzell, 1985]. There are well-defined grains of metallic aluminum and aluminum nitride existing even when the N/Al ratio is 0.96. Metallic aluminum grains will only disappear after the N/Al ratio reaches 1.0 (In their reports, it was assumed that the nitrogen ion beam consisted of 100% of N_2^+ ions).

The microstructure of deposited aluminum nitride films have a strong dependence on the energy of the nitrogen ion beam [Hentzell, 1985]. At low beam energy (100 eV), the films have well-defined fiber-type grains, whereas the grains are large and equiaxed under a 500 eV nitrogen ion beam. The grain size increases with the ion beam energy. The preferred grain orientation also depends on the beam energy. In low beam energy regime ($\leq$ 200 eV), the *c*-axis of aluminum nitride lattice is normal to the film plane. The c-axis becomes parallel to the film plane when the beam energy is above 400 eV.

The visual appearances of aluminum nitride films correlates with the film microstructures [Hentzell, 1985]. The film appears metallically shiny when the N/Al ratio is between zero and 0.54. When N/Al ratio is higher than 0.54, the film becomes dull gray until the ratio reaches 0.82. Between 0.82 and 1.0, the film is shiny gray. A pure aluminum nitride film (N/Al = 1.0) is transparent.

The electrical resistivity is dependent on film structure. The characteristic of the resistivity changes from a metallic aluminum film to a dielectric aluminum nitride film according to the N/Al ratio. In Hentzell's experiment [1985], the resistivity of the film became too high to be easily measured with their equipment when N/Al exceeded 0.75.

Thin Film Deposition on Particulate Substrates

In PVD techniques, line-of-sight transport is followed in dealing with the positioning of the substrate relative to the source. The location and orientation of a substrate relative to the source not only determines the film deposition rate, but also strongly influences the film structure and properties [Ohring, 1991].

Techniques have been developed for thin film deposition on particulate substrates [Cairns, 1972]. It has shown that small particles can be levitated by vibrating their container during deposition to achieve uniformly deposited thin films on the particulate substrates [Hillegas, 1990].

Al_2O_3 films have been deposited on SiC particles with the help of a particle levitation system [Cai, 1992]. Using an acoustic wave of 100 to 140 Hz in frequency, SiC particles were levitated in their container during deposition. The film deposited on the particulate substrates in the particle levitation system had a fairly uniform thickness and coverage.

6. Zone Structures of Thin Films from PVD

The film structure is greatly affected by the homologues substrate temperature (T_S) [Thornton, 1977]. The structures of a film deposited by sputtering or evaporation have been classified in terms of "zone structures". Three "zone structure" types have been used for describing electron-beam evaporated film morphologies [Movchan, 1969]. Each zone has distinguishable features, resulting from different film nucleation and growth mechanisms. Figure 2.9 shows schematically the zone-structure in evaporated thin films [after Movchan, 1969].

The structural differences among different zones are the result of differences in atomic mobilities on the substrate surface [Ohring, 1991]. At low substrate surface temperatures (below $0.3T_m$), the low atomic mobility both on the surface and inside film causes virtually all grain boundaries in the film to be immobile. Hence the film is formed at this temperature regime by continued re-nucleation of grains during deposition. The resultant film consists of small tapered crystals with voided boundaries. Such a film structure is termed as the Zone I structure.

The Zone II film structure is formed because the grain boundaries are mobile at the substrate temperature range of 0.3 to $0.5T_m$. Granular epitaxy and subsequent grain growth result in a film structure with columnar grains and dense grain boundaries. At higher temperatures, enhanced surface diffusion results in Zone III structure with large equiaxed grains.

A transition film structure, Zone T, is formed at the high-end of the Zone I temperatures because of the enhanced atomic mobility at this temperature regime. Films deposited in this temperature regime are produced by continued nucleation of grains during deposition and subsequent grain growth. Hence, the Zone T structure has a mixture of small and large grains. Large residual stresses could be formed in the Zone T region [Thornton, 1977 and 1989].

The grain sizes in evaporated films vary with the structure of the film. Hentzell [1985], *et. al.*, found that the grain sizes in 0.1 μm thick evaporated metal films ranged from 0.01 μm for Zone I structures to approximately 1 μm for the Zone III structures.

The temperatures dividing the structural regimes are affected by other factors as well [Ohring, 1991; Thornton, 1977]. Roughness on substrate surface and an oblique deposition angle promote the Zone I structure. An elevated inert gas pressure at low temperature regime causes grain boundaries to become more open in both sputtered and

evaporated coatings. Such an influence largely vanishes at elevated temperatures. Ion bombardment suppresses the Zone I structure, resulting in a structure similar to the Zone T type. In an IBAD process, the ion-beam energy affects the structure of the film. Hentzell [1985] reported that the aluminum nitride grains became larger at higher ion beam energy (500 eV). The grains tended to be equiaxed grains at high beam energy, whereas elongated grains resulted at lower beam energy (100 eV).

7. Grain Growth and Solid-state Sintering in Ceramics

The structure and properties of deposited thin films can evolve further under application conditions. Such an evolution in film structure and properties can have significant impact on the functionality of the films.

Three major changes usually occur on heating of fine-grained ceramic materials: there is an increase in grain size; there is a change in pore shape; there is change in pore size and number [Kingery, 1976]. At elevated temperatures, two transformation processes in the microstructures of fine-grained, porous ceramics usually take place, namely solid-state sintering and grain growth.

Solid-state sintering usually occurs in porous ceramic materials. In a porous ceramic material, both the pore size and shape change upon annealing. The pores become more spherical in shape and smaller in size as the annealing continues. Changing of free energy that gives rise to densification of the ceramic is associated with a decrease in surface area, and lowering of the surface free energy by elimination of solid-vapor interfaces. Lowering of the free energy usually takes place with the coincidental formation of new but lower-energy solid-solid interfaces [Kingery, 1976]. The rate of sintering is roughly proportional to the inverse of the grain size.

The grain growth process is more often associated with ceramics with an originally dense structure. In such materials, a reduction of free energy can be achieved by increasing the average grain size. As the average grain size increases, some grains shrink and disappear. The rate of growth increases exponentially with temperature, and the activation energy corresponds approximately to the activation energy for grain-boundary diffusion [Kingery, 1976; Smallman, 1985].

During grain growth in ceramics, pores on the grain boundaries may be left behind by the moving boundary or migrate with the boundary, gradually agglomerating at grain corners [Kingery, 1976]. In the early stages of annealing, a cluster of small pores in the corner of a grain is a commonly observed result. In the later stages of grain growth, when the grain size is larger and the driving force for boundary migration is low, it is more usual for pores to be dragged along by the boundary, slowing grain growth.

CHAPTER 3. EXPERIMENTAL PROCEDURES

In this study, aluminum nitride and aluminum oxide films were evaluated as diffusion barriers in composite systems of SiC particle reinforced β-NiAl and γ-Ni_3Al matrices. This study included the following tasks: to develop a heated particle levitation system; to deposit films on particulate substrates at various elevated temperatures; to characterize the deposited films; to study films' thermomechanical behaviors on SiC particles; and to examine the effectiveness of both films as diffusion barriers in the composite systems.

1. Materials

In this study, model composites were used to study the effectiveness of the diffusion barrier materials. Abrasive-grade SiC powders were chosen because of their relatively large size. SiC particles of a nominal size of 60 μm were purchased from Mager Scientific Inc. Figure 3.1 shows a SEM photo of an as-received SiC particle. The surface of the particle was characterized as flat cleavage surfaces joined by sharp edges.

Both β-NiAl and γ-Ni_3Al plates were used as composite matrices in this study. They were at their stoichiometries (±0.5 at%). The γ-Ni_3Al was doped in Oak Ridge National Lab (ORNL) with 0.25 at% of boron to enhance its room temperature ductility. The β-NiAl was donated by NASA.

Both aluminum nitride and aluminum oxide films were deposited using ion-beam assisted deposition (IBAD) process. Al_2O_3 rods of 6.3 mm in diameter (with 99.5% purity) were used as the feedstock in a 3-kW electron beam evaporator to form the oxide

films in an IBAD process. Argon gas of 99.99% purity was used to produce an assist ion-beam in a 3-cm Kaufman ion beam source (the Kaufman gun). 99.99% pure oxygen gas was leaked into the deposition environment as an oxygen content supplement for the oxide film depositions. For the nitride film depositions, commercially pure aluminum rods (99.0 wt% aluminum) of 6.3 mm in diameter were used. Nitrogen gas of 99.99% purity was used to produce a reactive ion assist-beam from the Kaufman gun.

Besides the SiC particulate substrates, planar substrates were also used for film characterization. Glass microscope slides and polished Si wafers of 50.8 mm in diameter (purchased from PureSil, Inc.) were used for film composition and morphology studies. Polished γ-Ni_3Al, β-NiAl and monolithic aluminum nitride plates were used for a cursory study of Ni diffusion in the nitride material. The aluminum nitride plates were donated by the Carborundum Company (Sanborn, NY) and had a nominal composition of 97.5% aluminum nitride, and 2.5% Y_2O_3 in balance.

2. Particle Levitation and Heating System

System Overview

To facilitate the IBAD process for particulate substrates, a deposition system was specially designed to achieve an uniformly deposited film on the particulate substrates. The system was designed based on the idea that particles can be levitated by vibrating their container at certain frequencies [Cairns, 1972; Hillegas, 1990]. In this study, a particle levitation system was designed to accommodate ion-beam assisted depositions at elevated temperatures. Radiant heaters were used to sustain the temperature on substrate surface during depositions.

There were three major components in the particle levitation system, as schematically shown in Figure 3.2. A particle holder assembly was located in the deposition chamber. A vibration generator system was outside of the vacuum chamber, which converted a sine wave signal from a signal generator into a mechanical vibration. The third component of the levitation system was a connector assembly communicating the holder and the vibrator. Proper cooling procedures and radiant shielding were designed to prevent the system and the vacuum chamber from overheating at elevated deposition temperatures.

In the next section, a detailed description of the three components of the levitation system will be given. Later, a heater assembly will be described, which was added to complete the system used in this study.

Levitation System

Particle Holder Assembly The holder assembly consisted of a quartz container and two stainless steel brackets. The container was a 76 mm long, 51 mm wide and 13 mm deep box with a maximum deposition area of 39 cm^2. The two brackets, which were made of 0.8 mm thick stainless steel, were locked onto four quartz stubs attached to the four corners at the bottom of the container. The brackets were also locked onto the quartz tube in the connector assembly (which will be described later in this section). The sturdy and yet flexible brackets provided a combination of friction fit, spring tension, and a good vibration transfer.

Vibration Generator System The central element of the generator system was a 6-inch, 8 Ω impedance audio loudspeaker (the acoustic transducer) which

generated a mechanical movement from an electronic signal. A quartz coupling was designed to connect the speaker to the quartz tube in the connector assembly. The coupling was attached to the speaker at speaker's axis, using a resin epoxy. A thin aluminum plate was used as a reinforcing rib between the coupling and the speaker to enhance the vibration efficiency and reduce warping of the transducer.

A frequency adjustable electronic signal generator was used to obtain a sine wave with an optimum frequency that could levitate particles with a limited bouncing effect. The sine wave was amplified to an appropriate input signal power level to the speaker. The optimum frequency was influenced by the characteristics of the levitation system and the particles involved. It was also a result of vacuum and deposition conditions. For the conditions used in this study, the optimum frequency for a sine wave signal was found in a range of 100 to 140 Hz. A 2 to 3 Watt power input was necessary for the particle levitation system to operate with a load of one gram of SiC particles.

Connector Assembly The connector assembly served as a communicator between the particle holder in a vacuum chamber and the vibration generator system outside. The assembly consisted of a quartz tube sealed at the inner end, an O-ring vacuum chamber sealing component, and a weight balancing mechanism. A coaxial air tube, 6.4 mm in diameter, was used for forced cooling of the interior of the quartz tube for elevated temperature applications.

The quartz tube of 38 mm in outer diameter was inserted through a 38.1 mm vacuum chamber port assembly with a Viton O-ring seal. As the fulcrum of the whole vibration system, a pin in the tube was locked on the cover of the port assembly. The fulcrum pin secured the orientation of the particle holder during depositions. The vertical movement of the tube at the O-ring position was negligibly small because of the short

distance (about 1 mm) from the O-ring to the fulcrum pin. There was practically no air-leakage found during the depositions in this study.

To achieve a balanced levitation system around the fulcrum pin, spring tensions were applied to the quartz tube near its outside end. Two springs were used. Because of the balance, there was little strain on the vibration generator.

Heating Zone

To maintain an elevated temperature on substrate surfaces during deposition, two heater compartments were placed symmetrically near the specimen holder. Figure 3.3 illustrates the construction of the heater compartments. Each compartment consisted of a heater enclosure and a water-cooled shield. The heater enclosure was made of 1.6 mm thick stainless steel, capable of containing up to three quartz-halogen radiant heaters (Sylvania BVE-type reflector heaters, rated 625 Watts at 110 Volts). An adjustable power transformer supplied the power to the heaters. Using three heaters in each of the heater compartments, the temperature in the particle holder could reach up to 973 K. The water-cooled shield was made of 1.6 mm thick copper sheet.

The heater enclosures were mounted to the water-cooled shield with adjustable set-screws, as shown in Figure 3.3. These screws maintained the height of the heaters relative to the substrates as well as the angle of the radiation. The heaters were placed as close to the substrates as possible to ensure heating efficiency.

Performance of the System

The levitation system functioned well at the frequencies normally used for levitation (100 - 140 Hz). For one gram of SiC particles (with an average size of 60 μm) in the particle container, a sine wave of 2 to 3 Watts to the vibration generator was sufficient for levitating the powders at an optimum frequency of 120 Hz in both ambient and vacuum conditions. During deposition, this optimum frequency varied in a range of 100 to 140 Hz. During levitation, particles were observed to gather at locations with minimum vibration magnitude inside the container.

The system was capable of sustaining at working temperatures up to 973 K in the deposition area of 76 mm×51 mm. A deposition temperature of 793 K was achieved using a total of 775 Watts input power. The temperature in the deposition area was relatively uniform. At an average temperature of 793 K, the temperature variation in the deposition area was measured at ±20 K.

The performance of this system was stable over a long working period of tens of hours. The system had been used more than 30 levitation hours at a deposition temperature of 793 K. The system was able to withstand thermal cycles between room temperature and the deposition temperature without apparent damage.

This system has been used for depositing aluminum nitride and oxide films at various temperatures and on various substrates. Both inert and reactive IBAD processes were compatible to the levitation system. On particulate substrates, the film thickness was found to be fairly uniform.

3. Film Deposition, System and Procedures

IBAD System

The configuration of an ion-beam assisted deposition system, the IBAD system, is schematically shown in Figure 3.2. An electron-beam evaporation source and a Kaufman broad-beam ion source were arranged in a vacuum chamber, together with a particle levitation system. During depositions, the down-firing, rod-fed electron-beam evaporation source supplied the coating material flux, while the 3-cm Kaufman ion source directed an assist ion-beam towards the substrate surfaces.

By using a cryo-pump, a base pressure less than 5×10^{-5} Pa was achieved in the deposition chamber at room temperature. Maintained by radiant heaters, the temperature of the substrate area during deposition was measured by a thermocouple placed near the substrates. Because the thermocouple was placed at the same area as the substrates, the heat fluxes for both the thermocouple and the substrates were the same during deposition.

The 3-cm ion source was equipped with a divergent accelerator grid that produced an ion beam with a divergence angle of 10 degrees. With a working distance of 10 cm from the substrates, the effective ion beam coverage area was calculated of 33.4 cm^2 at the substrate location. The current of the incident ion beam was measured with a Faraday probe during deposition.

In each deposition-run, one gram of SiC particles was used. During deposition, the particle charge was observed to cover roughly 40% of the area in the particle container of 39 cm^2. Hence, the average size of the particle covered area, which equals the total exposure surface area of the particulate substrates to the incoming depositing fluxes, was estimated to be roughly 16 cm^2.

Aluminum Nitride Film Depositions

A reactive IBAD process was applied for aluminum nitride depositions. During the deposition, metallic aluminum was evaporated from an electron-beam evaporation source. Nitrogen ions with 100 eV beam energy were supplied by a 3-cm Kaufman ion source. The nitrogen ion beam was also served as a ballistic assist-beam.

According to researches done by Kaufman [1987], Netterfield [1988] and Taylor [1981], N_2^+ ions constituted most of the ions generated in the ion source (from 78.7% to 96%). Other species in the ion beam were mostly N^+ ions. Only a negligible amount of the ion species was multi-charged ions. To calculate the atomic arrival rate, the nitrogen ion-beam was assumed consisting of only N_2^+ and N^+ molecules, with $x\%$ N_2^+ and $y\%$ N^+. The ion density (i) for an ion beam with a current density of I (in A/cm^2) was

$$i = \frac{I}{1.6 \times 10^{-19}} \text{ (ions/cm}^2\text{/sec)}$$

and the arrival rate of nitrogen atoms at the substrate surface (J_N) was consequently

$$J_N = (2 \times x\% + y\%)\frac{I}{1.6 \times 10^{-19}} = (2 \times x\% + y\%) \cdot i \quad \text{(atoms/cm}^2\text{/sec).}$$

To achieve an atomic ratio of *N:Al* of unity (i.e. $J_N = J_{Al}$), the ratio between the ion density (i) and the arrival rate of aluminum atoms (J_{Al}), the *i/a ratio*, was thus

$$i/a = i/J_{Al} = i/J_N = \frac{1}{(2x\% + y\%)}$$

Based on the reference data [Kaufman, 1987; Netterfield, 1988; Taylor, 1981], the required *i/a* ratio was between 0.51 and 0.56.

The film deposition rates on planar substrates were calculated by using step-test samples on planar substrates. The step-test samples were produced by depositing films on partially covered glass slides. Using a Dektak II profilometer, the film thickness was determined by measuring the step depth at the film edges on the step-test samples.

The deposition conditions for planar substrates are tabulated in Table 3.1. Conditions for the deposition of aluminum nitride films on both planar and particulate substrates were similar, except for the duration. For depositions at 593 K, an average *i/a* ratio of 0.56 was detected with an *i/a* range between 0.52 and 0.60. On planar substrates, the averaged film deposition rate at 593 K was measured of 0.18 nm/sec, and the average ion density of the ion beam was 4.9×10^{14} (ions·cm^{-2}·sec^{-1}). For depositions at 793 K, the ion density was averaged of 3.4×10^{14} (ions·cm^{-2}·sec^{-1}). An average film deposition rate of 0.14 nm/sec on planar substrates resulted in an average *i/a* ratio of 0.53. The range of the *i/a* ratio was between 0.42 to 0.64.

Table 3.1. Deposition Rates and *i/a* Ratios of AlN Films Deposited on Planar Substrates.

Sample	T (K)	l (μm)	t (min.)	$\dot{s}$	$\bar{\dot{s}}$	Ion Arrival Rate	i/a	$\overline{i/a}$
1-1	593	0.16	15	0.18	0.18	4.5×10^{14}	0.52	0.56
1-2		0.16	15	0.18		5.2×10^{14}	0.60	
2-1	793	0.10	10	0.17	0.14	3.4×10^{14}	0.42	0.53
2-2		0.20	30	0.11		3.4×10^{14}	0.64	

T: Deposition Temperature. l: Film thickness. t: Deposition Duration.

i/a : Ion-to-Atom Arrival Ratio. $\overline{i/a}$: Average Ion-to-Atom Arrival Ratio.

Ion Arrival Rate: in ($ion\cdot cm^{-2}\cdot sec^{-1}$). $\dot{s}$: Deposition Rate on Planar Substrate, in (nm/sec.).

$\bar{\dot{s}}$: Average Deposition Rate on Planar Substrate, in (nm/sec.).

Prior to deposition, the majority of the residual gas species in the chamber were nitrogen, oxygen, and water vapor. The partial pressures of oxygen and H_2O were both about 1.3×10^{-5} Pa. The working pressures were 3×10^{-3} Pa for depositions at 593 K, and 7×10^{-3} Pa for 793 K deposition.

Aluminum Oxide Film Depositions

Al_2O_3 films were deposited at room temperature using an IBAD process with an inert argon ion assist beam[1]. An Al_2O_3 rod was thermally evaporated. The argon ion beam of 100 eV was used as a ballistic assist-beam. The working pressure in the deposition chamber was 4×10^{-3} Pa. An oxygen flow was leaked into the deposition chamber to compensate for an oxygen deficit normally associated with evaporation of Al_2O_3 [Bunshah, 1984; Ohring, 1991]. The oxygen partial pressure before deposition was 3×10^{-4} Pa due to this oxygen supplemental flow. The deposition rate for planar substrates was measured to be 0.46 nm/sec. The *i/a* ratio was maintained at 0.02, with an ion density of 2.3×10^{13} (ions·cm^{-2}·sec^{-1}).

Deposition Conditions on Particulate Substrates

In this study, the targeted film thickness on SiC particles was 0.5 μm for all films. Because of the high surface-to-volume ratio of the particulate substrates, the effective film deposition rate on SiC particles was much lower than the rate on planar substrates [Cai, 1992]. To achieve the targeted film thickness, a total of 9.75 hours of deposition duration was required for aluminum nitride films deposited on SiC particles at 593 K.

---

[1] A reactive IBAD process for Al_2O_3 film deposition was not employed because the Kaufman ion source was not compatible with a high oxygen flow required for such a process.

The duration was 25 hours for depositions at 793 K. For Al_2O_3 film deposition, SiC particles were coated for 6 hours to achieve the targeted film thickness.

The deposition temperature was measured by a thermocouple placed at the deposition area. The thermocouple was located so that it was subjected to the same radiant heat and deposition fluxes as the substrates. Thus, the temperature reading reflected the temperature of the substrate surfaces that were exposed to both radiant heat and deposition fluxes. In this experiment, the reading of the thermocouple was assumed to be the deposition temperature of the substrate surface.

For depositions on particulate substrates, the deposition area was static. However, the substrates were levitated, moving in and out the deposition area dynamically. This levitation of the substrates caused the cycling of the depositing surface on each particulate substrate. This cycling not only interrupted the growth of the depositing film, but also cycled the temperature on the substrate surfaces.

With depositing fluxes and a direct radiant heat flux, the substrate surface experienced the full deposition temperature and deposition rate. The deposition rate on the surface was the same as the rate on planar substrates under the same deposition conditions. When the surface was orientated away from the fluxes, The film deposition stopped. The substrate surface gradually cooled down towards the surrounding temperature. In this case, the surrounding temperature was presumably the temperature of the quartz particle holder. The holder was measured to be approximately 423 K during depositions. Because of the limited size of the deposition area (about 16 cm^2) and the large surface area of the particle charge (estimated of over 300 cm^2), the particles spent most of their time (about 95% of the total deposition time) in the non-coating stage during the deposition period.

4. Film Characterization

The microstructure, thickness, and composition of the deposited thin films were studied in detail because of their importance in influencing the performance of the thin films as diffusion barriers.

Film Structure and Thickness

After deposition, the surface morphology of films on both planar and particulate substrates was examined in scanning electron microscopy (SEM, Hitachi S-2500C). The SEM samples were coated with a thin layer of gold to reduce surface charging associated with dielectric materials. Secondary electron images (with electron beam accelerate voltages between 10 to 20 kV) were used of film structure and thickness study. The internal scale provided by the SEM was used for size measurement.

To measure the film thickness on SiC particles, as-coated SiC particles were embedded in resin and polished with diamond compounds to reveal the cross-section of the films. The polished samples were then gold coated and studied in SEM. The magnification rates of the SEM were in a range between 25000 and 35000. Multiple thickness measurements (more than 20 in each case) were made, and the results were averaged to determine the film thickness on the particulate substrates.

The measured film thickness on particles from SEM images varies depending on how the film is fractured after sectioning. A perfectly sectioned film along the polishing direction (Case 1) produces the highest film thickness measurement on SEM images. On the other hand, the lowest film thickness reading on SEM images arises when the film is fractured perpendicular to film surface (Case 2). The following discussions focus on the average value of the film thickness from SEM images for both cases.

The general assumptions of the discussions are as follow. Particles are spherical and of a radius of r_0. The film thickness is uniform on the particles and of a value of d. $d<<r_0$. SEM images are taken from a direction perpendicular to the polishing direction. The last assumption is that there is no error in the measurement on SEM images.

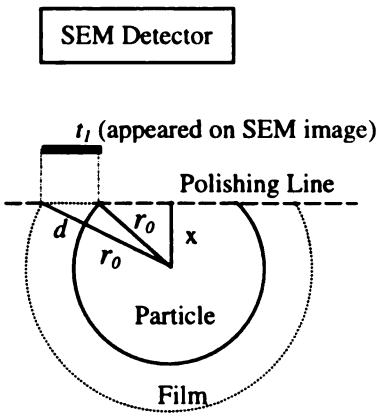

Case 1. Film Sectioned along the Polished Line.

In Case 1, the measured film thickness (t_1) is a function of the location of the polishing line (x):

$$t_1(x) = \sqrt{(r_0+d)^2 - x^2} - \sqrt{r_o^2 - x^2}$$

The average value of the thickness measurement is averaged over an x range from 0 to r_0:

$$\bar{t}_1 = \frac{\int_0^{r_0} t_1(x)dx}{\int_0^{r_0} dx} = \frac{(r_0+d)^2}{2r_0}\sin^{-1}\left(\frac{r_0}{r_0+d}\right) + \frac{r_0+d}{2}\cos\left(\sin^{-1}\left(\frac{r_0}{r_0+d}\right)\right) - \frac{r_0\pi}{4}$$

$$\because d << r_0$$

$$\therefore \bar{t}_1 \approx \frac{(r_0+d)^2}{4r_0}\pi - \frac{r_0}{4}\pi \approx \frac{\pi}{2}d = 1.57d.$$

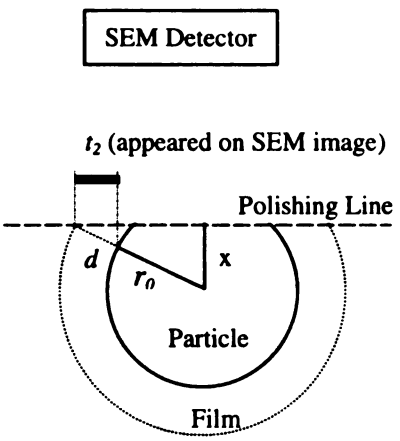

Case 2. Film Fractured Normal to Film Surface.

In Case 2, the measured film thickness (t_2) is a function of the location of the polishing line (x):

$$t_2(x) = \frac{d}{r_0+d}\cdot\sqrt{(r_0+d)^2 - x^2}$$

The average value of the thickness measurement is averaged over an x range from 0 to r_0:

$$\bar{t}_2 = \frac{\int_0^{r_0} t_2(x)dx}{\int_0^{r_0} dx} = \frac{d(r_0+d)}{2r_0}\sin^{-1}\left(\frac{r_0}{r_0+d}\right) + \frac{d}{2}\cos\left(\sin^{-1}\left(\frac{r_0}{r_0+d}\right)\right)$$

$$\because d << r_0$$

$$\therefore \bar{t}_2 \approx \frac{d(r_0+d)}{4r_0}\pi \approx \frac{\pi}{4}d = 0.79d.$$

Therefore, the ratio between the measured film thickness from SEM images (t) and the real film thickness (d) on particles is estimated to be between 0.79 and 1.57, depending on the way the film fractured after polishing.

Composition Study

The composition of the oxide film was studied with a Link AN1000 Energy Dispersive X-ray spectrometer (EDX) installed on a Hitachi S-2500C SEM. The EDX equipped with a windowless detector. By using a bulk Al_2O_3 material as a standard, the composition of a deposited oxide film was measured with quantitative corrections computed using the manufacturer's ZAF-4 code.

A Perkin-Elmer's PHI 5400 X-ray photoelectron spectroscope (XPS) was used for composition studies of the films used in this study. With X-rays exciting photoelectrons from the surface of a sample, the XPS was a surface analysis technique that provides both elemental and chemical bonding information [Moulder, 1992; Walls, 1898]. Appendix I of this paper states the principles of the XPS technique.

The XPS unit used in this study was equipped with an argon-ion sputter gun for surface contamination removal and film composition profiling. The sputter gun was

mounted off the axis of the photoelectron collector. The sputtering rate with this ion gun was measured of 0.3 nm per minute for the aluminum nitride film.

Because the shadowing effect among particles interfered with the removal of surface contamination (mostly CO, CO_2 due to the exposure of air after film deposition), XPS study of the nitride films was performed on planar substrates.

Because a range of ion-to-atom ratio (the *i/a* ratio, ranging from 0.42 to 0.64) had been detected during the depositions of the nitride films on the SiC particles, planar samples for the composition study were made under the similar conditions. The first sample deposited at 793 K had an *i/a* ratio of 0.42. The *i/a* ratio for the second sample, which deposited at 593 K, was measured at 0.60.

5. Thin Film Thermomechanical Behavior: Annealing Tests

Experiments were conducted to study the structural thermomechanical behavior of both aluminum nitride and oxide films deposited on SiC particles after heat treatments in both ambient and vacuum conditions. SEM was used to search for evidence of any cracks or voids formed in the films after annealing. The SEM samples were gold-coated for improving surface conductivity. Carbon-tape was used as the carrier for the particles in SEM sample preparation.

Annealing at 1273 K in Air

The annealing was performed in air to study the capability of the aluminum nitride and oxide films to withstand a moderate annealing temperature of 1273 K. SiC

particles with aluminum nitride and oxide coatings were heated in air from room temperature to the annealing temperature (1273 K), and subsequently air-cooled.

In addition, some SiC particles with aluminum nitride film (coated at 593 K) were quenched in liquid nitrogen (77 K) from the annealing temperature of 1273 K. This test provided a greater temperature difference comparing with the air-cooling test. The greater temperature difference induced a higher thermal stress in the film.

Annealing of Aluminum Nitride Films in Vacuum

For annealing temperatures higher than 1273 K, the annealing tests were performed under vacuum conditions. Aluminum nitride films, deposited on SiC particles at various temperatures, were tested under conditions similar to those expected for high-temperature applications. The results from this experiment provided information about the films' behaviors during composite consolidation processes.

The coated SiC particles were heated to the annealing temperatures (1573 K and 1673 K) in one hour in a Centorr Vacuum furnace at a pressure of 5×10^{-3} Pa, and then annealed for 4 hours. After cooling down to 673 K in 30 minutes, the samples were subsequently cooled in 8 hours to reach room temperature in vacuum. The annealed samples were examined with SEM.

SiC particles with a nitride film (coated at 793 K) were also annealed at 1373 K for one hour in vacuum. Samples were examined with SEM after the annealing.

6. Ni Diffusion in Aluminum Nitride, a Cursory Study

Because of limited information on Ni diffusing in an aluminum nitride matrix, experiments were designed to examine the extent of Ni diffusing in the nitride at elevated temperatures applied in this study. Conclusion drawn from these experiments was informative to determine the barrier film thickness used in this study.

Diffusion in Bulk Aluminum Nitride

Monolithic aluminum nitride and nickel aluminides (β-NiAl and γ- Ni_3Al) plates were hot-pressed (diffusion bonding) at a vacuum level was of 5×10^{-3} Pa. A bonding pressure of 10 MPa was applied, which ensured sufficient contact between the plates.

To provide a better contact between the nitride and aluminide plates, the contacting surfaces of aluminum nitride, β-NiAl and γ-Ni_3Al plates were polished with diamond compounds prior to the hot pressing. With a γ-Ni_3Al plate, the aluminum nitride plate was hot-pressed for 32 hours at 1473 K (0.88 T_m of γ-Ni_3Al). A diffusion couple of an aluminum nitride plate and a β-NiAl plate was hot-pressed at 1673 K (0.88 T_m of β-NiAl) for 12 hours in vacuum. After the bonding procedures, the diffusion couples were cut to reveal the interface between the plates.

Energy dispersive X-ray spectroscopy (EDX) was applied to examine the distance of Ni diffusing into aluminum nitride lattice in the diffusion-bonded samples. Line-scan profiles of the Ni element across the interface were used to mapping the extent of Ni diffusing in aluminum nitride from the aluminide matrices. Because a typical EDX probe had a spatial resolution about 1 μm [Loretto, 1984; Russ, 1984], this spatial resolution limited the lowest diffusivity that could be estimated under the proposed conditions.

For instance, with the conditions of the nitride/γ-Ni_3Al diffusion couple (32 hours at 1473 K), the spacial resolution of 1 μm determined a minimum diffusivity of

$$D_{\min} = \frac{x^2}{4t} = \frac{\left(1\times 10^{-4}\right)^2}{4\times 32\times 3600} = 2.2\times 10^{-14}\ \text{cm}^2/\text{sec}.$$

Here the diffusion distance (x) is assumed to be the EDX's spatial resolution of 1 μm. For the conditions of the nitride/β-NiAl diffusion couple (12 hours at 1673 K), the detectable limit of the diffusivity of Ni was 5.8×10^{-14} cm^2/sec. For diffisivities less than the minimum values, the EDX method was not capable of measuring the diffusion distance accurately. Thus, when the diffusion distance was less than 1 μm, only an upper bound of diffusivity could be determined from the EDX method.

Ni Penetrating Aluminum Nitride Films

The penetration depth of Ni diffusing in an aluminum nitride film was studied. The nitride film of 225 nm thick was deposited on a γ-Ni_3Al plate at the same conditions of nitride film deposited on planar substrates at 793 K, as described in Section 3. The coated γ-Ni_3Al plate was annealed at 1373 K for 30 minutes in a vacuum of 5×10^{-4} Pa. The Ni concentration in the nitride film was then studied with XPS profiling.

7. Effectiveness of Diffusion Barriers

The effectiveness of the diffusion barrier films was examined under the different chemical potential levels. Composites of SiC particle reinforced β-NiAl and γ-Ni_3Al matrices were selected for the low and high chemical potential conditions, respectively.

The survivability of the SiC particles in the composites during the compositing processes was used as the gauge for evaluating the effectiveness of the diffusion barrier films.

Coated and non-coated SiC particles were sandwiched and hot-pressed uniaxially between two aluminide plates in a vacuum of 5×10^{-3} Pa. A high-temperature mechanical testing system (MTS 810) with a Centorr vacuum furnace was used for the hot-pressing process. The configuration of the hot-pressing process is shown in Figure 3.4.

The hot-pressing conditions for the β-NiAl matrix composite were 4 hours at 1673 K under 10 MPa compressive stress. Conditions of one hour at 1373 K under 40 MPa compressive stress were used for the γ-Ni_3Al matrix composites. Before the hot pressing, specimens were ramped in an hour to the process temperatures from room temperature. Samples were cooled in vacuum after the hot pressing for eight hours to reach room temperature.

SEM/EDX was used to study the interface of SiC and the aluminide matrices. The β-NiAl matrix composite samples were fractured compressively at room temperature to reveal the SiC particles. A sample of SiC particles with nitride films coated at 593 K were also electropolished to study the barrier films' conditions after the consolidation process. The polishing agent was a solution of 10% perchloric acid and 90% acetic acid.

The γ-Ni_3Al matrix composite samples were polished and etched to reveal the interface region. The etchant solution consisted of 5 grams of $CuSO_4$, 20 ml of HCl, and 20 ml of H_2O. The etched samples were studied with an optical microscope. The sample with SiC particles with the nitride film coated at 793 K was an exemption, which was fractured in tension at room temperature. This fractured sample was studied using SEM.

The next chapter presents the results from all the experiments described above. Discussions will be given for the results. Conclusions drawn for this study will follow

CHAPTER 4. RESULTS AND DISCUSSION

1. Film Characterization

Three characteristics of thin films were studied, which were film thickness, structure, and composition. These characteristics strongly influenced the effectiveness of the films as diffusion barriers. Furthermore, these features characterized the film deposition processes used in this study.

Film Thickness and Deposition Rate on SiC Particles

By polishing the coated particles that were embedded in resin, cross-sections of the films were exposed. After gold-coated, the polished sample was studied in a SEM. Film thickness was estimated with an internal scale provided by the SEM imaging. Figure 4.1 shows a SEM image example that captured the cross-section of an aluminum nitride film on a polished SiC particle. Measured directly on Figure 4.1 (b), a SEM image with a 25000× magnification, the averaged film thickness was 0.51 μm.

The same procedure was used to estimate the average film thickness of the aluminum oxide, aluminum nitride films on their SiC particulate substrates after depositions. It was estimated that the oxide films had an average thickness of 0.47 μm after a 6-hour deposition, corresponding to an effective deposition rate of 0.022 nm/sec. The nitride films deposited for 9.75 hours at 593 K were of 0.52 μm thick. The nitride film coated at 793 K was 0.54 μm in thickness after a 25-hour deposition. The effective deposition rates for the nitride film deposited on SiC particles at 593 K were thus 0.015

nm/sec, and 0.006 nm/sec for the nitride film deposited at 793 K. Table 4.1 lists the results of the film thickness on SiC particles.

The actual film thickness on particles could be different from the value measured from SEM images. As discussed in Chapter 3, the magnitude of the difference was determined by the way the film was fractured after polishing. The ratio between the measured film thickness from SEM images and the actual film thickness on particles was estimated between 0.79 (when film fractured normal to the film surface) and 1.57 (when film fractured along the polishing line). The average value of these two ratios was 1.18.

In this study, films were observed to have a tendency of fracturing normal to the substrate surfaces. Hence, the ratio between the measured and the actual film thickness on particles was estimated between 0.79 and 1.18. By this estimation, the uncertainty was about ±19% when using the measured value as the actual film thickness. Therefore, after considering the errors and the uncertainty of the measurement technique, the average values of film thickness of all three films deposited on SiC particulate substrates

Table 4.1. Measured Thickness of As-Deposited Films on SiC Particles.

Material	T(K)	t(hour)	AvgThk	MaxThk	MinThk	$\bar{\dot{s}}$ (nm/sec)	$\dot{s}_e$ (nm/sec)
Al_2O_3	300	6	0.47 μm	0.6 μm	0.3 μm	0.022	0.024
AlN	593	9.75	0.52 μm	0.7 μm	0.3 μm	0.015	0.009
AlN	793	25	0.54 μm	0.7 μm	0.4 μm	0.006	0.007

T: Deposition Temperature, in Kelvin. t: Deposition Period. AvgThk: Average Thickness.
MaxThk: Maximum Thickness Measured. MinThk: Minimum Thickness Measured.

$\bar{\dot{s}}$: Average Measured Deposition Rate on Particulate Substrate.

$\dot{s}_e$: Estimated Deposition Rate on Particulate Substrate (= $0.052\,\bar{\dot{s}}_{pl}$).

were 0.5 μm, with an error bar of ±0.1 μm.

With similar deposition conditions, as stated in Chapter 3, the average deposition rates on planar substrate were 0.46 nm/sec for the oxide film, 0.18 nm/sec for the nitride film deposited at 593 K, and 0.14 nm/sec for the nitride film deposited at 793 K, respectively. For an estimated ratio of 0.052[1] between the effective deposition rate on particulate substrate ($\dot{S}_e$) and the rate for the planar substrate ($\dot{S}_{pl}$), the estimated effective deposition rate for the oxide film on SiC particles was calculated to be 0.024 nm/sec. The estimated effective rate was 0.009 nm/sec for the nitride film deposited on SiC particles at 593 K, and 0.007 nm/sec for the film deposited on SiC particles at 793 K, respectively. Table 4.1 summarizes the results of the film thickness on SiC particles.

For the nitride films deposited at 793 K and the Al_2O_3 films, the measured effective deposition rates on SiC particles were comparable to their estimated values. However, the measured rate of the nitride film deposited on SiC particles at 593 K was 0.015 nm/sec that was 167% of the estimated value of 0.009 nm/sec.

Because the effective deposition rates for the nitride film deposited at 593 K was much higher than the estimated rate, the film on SiC particles was probably not as dense as the film deposited on the planar substrate. A different film structure was likely to be present on the particulate substrates compared with that on the planar substrate. Studies on film structures, discussed next, support this conclusion.

---

[1] The estimated ratio (r) between $\dot{S}_e$ and $\dot{S}_{pl}$ is calculated as $r = (Ad\rho)/(6W)$, where W is the amount of the particle charge used in a deposition, d is the nominal size of the particles, ρ is the density of the particles, and A is the deposition exposure area [Cai, 1992]. In this study, W was 1.0 gram, d was 60 μm, A was in an average of 16 cm^2, and ρ was 3.22 g/cm^3. Hence, this ratio was estimated to be 0.052.

Film Structure and Morphology

Aluminum Nitride Film Deposited at 593 K Aluminum nitride films deposited on planar substrates at 593 K had dense structures with smooth, reflective surfaces. At 0.4 μm thick, the films were transparent and non-conductive. Figure 4.2 (a) shows the surface of the film deposited on a glass slide. Figure 4.2 (b) shows the film's cross-section. The film consisted of small crystallites with a size of 0.1 – 0.2 μm. The structure was classified as the Zone T structure.

On the SiC particulate substrates, however, the nitride film had a different structure. After a 9.75-hour deposition, the nitride film was formed with a globular structure of grain clusters on the SiC substrate surface. Figure 4.3 shows SEM images of film morphology at both low and high magnifications.

The globular clusters in the films on SiC particles were of 0.3 μm in average size, with visible voids in between the clusters. The globular feature of the films resembled the Zone I structure [Movchan, 1969]. Within each globular cluster, grains were densely packed. The grains were of different sizes (0.2 μm or smaller). A Zone T structure was a good description for the structure within each globular cluster [Movchan, 1969]. Therefore, the overall film structure was determined as a mixture of Zone I and Zone T structures.

The large number of voids associated with the globular structure may explain the difference between the measured effective deposition rate on particulate substrates and the estimated one. It may be estimated, by using the difference in the estimated and the effective deposition rates, that the void space in the as-deposited film was about 40% of the total film volume.

Aluminum Nitride Film Deposited at 793 K Unlike the nitride films on SiC particles deposited at 593 K with a globular structure, the nitride films deposited at 793 K had a dense and smooth morphology on both planar and particulate substrates. Figure 4.4 shows SEM images of the film morphology on SiC particles after a 25-hour coating. A cross-section of the film was shown earlier in Figure 4.1. Grains in the film were varied in sizes (0.2 μm or smaller). A small amount of voids was also found in the film.

Because of the densely packed grains and the various grain sizes in the film, the film was of a classic Zone T film structure. Although the deposition temperature of 793 K (0.31 T_m of aluminum nitride) could result in a Zone II structure of columnar grains [Movchan, 1969; Ohring, 1991], the discontinuous deposition process postponed the Zone II structure from forming. Hence, the nitride films deposited at 793 K on SiC particles had a Zone T type in film structure.

Aluminum Oxide Film Deposited at Room Temperature The Al_2O_3 film deposited on both planar substrate and the SiC particles at room temperature using an IBAD process were opaque and black in color. The film, shown in Figure 4.5 (a), had a relatively smooth and dense morphology on its SiC particulate substrate. A more detailed SEM photo with a higher magnification, shown in Figure 4.5 (b), indicates that the film also had globular features.

As compared with the nitride films deposited at 593 K, the globular clusters in the oxide films were smaller and averaging 0.15 μm in size. The grains in the clusters were also smaller (less than 0.1 μm). Fewer voids in between the clusters were shown as compared with the nitride film deposited at 593 K as well. The globular feature was more evident in the oxide films covering areas with steps on SiC particles. The film

structure of the oxide film was classified as the Zone T structure [Movchan, 1969], with some globular features.

Discussion on the Globular Structure in Nitride Films The globular structure in the nitride film deposited on SiC particles at 593 K was quite unusual. Such a feature could be resulted from a combined influence of the deposition temperature and the constant levitation of the particulate substrates.

At a deposition temperature of 593 K (0.24 T_m of aluminum nitride), the enhanced atomic mobility promoted both continued nucleation of grains during deposition and subsequent grain growth [Thornton, 1977 and 1989]. With a continuous deposition such as in the situation of deposition on planar substrates, the resultant films consisted of both small and large grains, as well as of a dense structure (the Zone T Structure). On particulate substrates, however, the films were formed discontinuously because the constant levitation of the substrates interrupted the film growth.

It was observed in this study that, at an early stage of the film formation on SiC particles at 593 K, individual crystallites and clusters of crystallites were formed on the substrate surface. Figure 4.6 (a) shows the morphology of a SiC particle after being coated with aluminum nitride at 593 K for 2 hours. A magnified SEM picture, Figure 4.2 (b) indicates that the aluminum nitride had not formed a continuous film on the SiC particle after the 2-hour deposition period yet. The individual crystallites and clusters of crystallites had a size of 0.3 μm or smaller.

The development of the globular structure in the nitride films deposited at 593 K is speculated as a result of following steps. The deposition temperature was in favor of large crystals developing on substrate surfaces when the film was initiated. The

levitation of the substrates, however, stopped the further deposition necessary to form a continuous film on the substrate, leaving islands of large crystallites on the substrate surface. These islands of crystallites increased the degree of roughness on the surface.

Because of the levitation effect, the incident angle of the depositing flux changed constantly when the particles were exposed to the deposition flux. Combining the constant changing in the incident angle and the increasing in surface roughness, the extruding crystallite islands eventually grew into globular grain clusters on the substrate surfaces. The globular clusters stopped to grow after being in contact with each other. Voids were left at the boundaries in between globular clusters. Therefore, the formation of thin films on levitated particulate substrates at 593 K was a repetition of the formation of individual islands of crystallites and the subsequent growth of the islands into spheres.

As compared with the film deposition at 593 K, substrate surface provided more suitable sites for film nucleation at higher deposition temperatures (such as 793 K). The higher temperature increased surface atomic mobility, enabling the film to horizontally grow along the substrate surface. Hence the degree of self-roughening on the substrate surface was less for films deposited at a higher temperature regime. Consequently, films deposited at higher temperature regime were denser and less "globular" in film structure.

Composition of Aluminum Oxide Films

XPS[1] was used to study the composition because of XPS' good depth resolution and fairly good compositional accuracy. The oxide film was found to be predominately aluminum oxide. Figure 4.7 (a) and (b) show an oxygen peak (530.3 eV) and an aluminum peak (74.2 eV), both originating from aluminum oxide. No other chemical

[1] The principles of the XPS technique are stated in Appendix I.

bonds were found by XPS. The composition of the film was calculated to be $Al_{38}O_{62}$. The composition of the oxide film was also measured using an EDX quantitative method. Using a commercially pure Al_2O_3 rod as a standard, the result from the EDX method yielded a composition of $Al_{37}O_{63}$ for the deposited oxide film.

The difference in the calculated film composition and the stoichiometry (Al_2O_3) might not be significant after considering the errors associated with the measurement techniques. For light elements such as oxygen, both techniques offered an uncertainty of 10% in quantitative calculation [Moulder, 1992; Russ, 1984]. Hence, a stoichiometric Al_2O_3 sample could yield a measured composition result in a range between $Al_{46}O_{54}$ and $Al_{34}O_{66}$. Therefore, the oxide film was considered to be nominal stoichiometry.

Composition and Constituents in Aluminum Nitride Films

The composition in the nitride films was complex due to the employment of the reactive IBAD process. XPS was used to study the atomic and molecular composition of the nitride films on planar substrates. Samples with *i/a* ratios of 0.42 and 0.60 were used to reflect the deposition conditions for the particulate substrates.

The molecular concentration of the nitride films was estimated by assuming that all components in the film were stoichiometric [Hentzell, 1985; Kingery, 1976]. In Appendix II of this dissertation, detailed calculations of determining film molecular concentration are presented.

Nitride Film Deposited with an i/a Ratio of 0.42 With an *i/a* ratio of 0.42, the nitride film was deposited with an atomic arrival ratio of *N-to-Al* between 0.75 to 0.82[1]. Elements of aluminum, nitrogen, and oxygen were found in the film.

Below the first 5 nm depth from the film surface, the film composition was nearly constant at 55 at% aluminum, 40 at% nitrogen, and 5 at% oxygen. A 15 at% of oxygen was found at the film surface. Figure 4.8 shows an XPS concentration profile in the near-surface region of the film. On the surface, the composition was measured to be 48 at% aluminum, 37 at% nitrogen, and 15 at% oxygen.

The interior region of the film consisted of aluminum nitride, aluminum nitrate, and metallic aluminum. Table 4.2 lists the XPS results from the interior region of the film. The nitrogen XPS peak with a binding energy of 397.2 eV demonstrated a strong

Table 4.2. Composition of the Nitride Film Deposited with an *i/a* = 0.42, at a Region 40 nm below the Film Surface.

Element	Peak (eV)	Bond Type	at% of Total Content
Al (Aluminum)	73.8	Mixed [1]	43
	72.9	Al	11
O (Oxygen)	532.7	Nitrate	5
N (Nitrogen)	397.2	Mixed [2]	41
Film Molecular Concentration: 72.8% AlN + 26.1% Al + 1.1% $Al(NO_3)_3$			

[1]: A possible mixture of aluminum nitride and nitrate.

[2]: Aluminum nitride with possible nitrate.

[1] As discussed previously, the percentage of N_2^+ existing in a nitrogen ion beam from a Kaufman ion source was ranged from 78.7% to 96% [Netterfield, 1988; Taylor, 1981]. The remaining species in the ion beam were mostly N^+. Hence an *i/a* ratio of 0.42 was equivalent to a *N/Al* ratio between 0.75 to 0.82.

aluminum nitride (*AlN*) characteristic. The oxygen XPS peak, as shown in Figure 4.9 (a), indicated that the oxygen in the film was in a form of aluminum nitrate ($Al(NO_3)_3$). The aluminum peak indicated the presence of both a metallic aluminum (*Al*) component and a possible mixture of nitride and nitrate, as shown in Figure 4.9 (b).

Compared with the interior region, the film surface region had an additional component of aluminum oxide. Table 4.3 lists the XPS results from the surface region of the film. As indicated in Figure 4.10 (a), the oxygen XPS peak from the film surface showed a component at 531.8 eV that originated from aluminum oxide (Al_2O_3) molecules. The aluminum XPS peak, as shown in Figure 4.10 (b), was a convoluted result of characteristic peaks from components of metallic aluminum (*Al*) and a mixture consisting probably aluminum nitride, nitrate, and oxide.

Table 4.3. Composition of the Nitride Film Deposited with and $i/a = 0.42$, at the Surface Region.

Element	Peak (eV)	Bond Type	at% of Total Content
Al (Aluminum)	74.1	Mixed [1]	39
	72.9	Al	9
N (Nitrogen)	397.4	Mixed [2]	37
O (Oxygen)	532.5	Nitrate	7
	531.8	Al_2O_3	8
Film Molecular Concentration:76.5% AlN + 15.9% Al + 1.7% $Al(NO_3)_3$ + 5.9% Al_2O_3			

[1]: A possible mixture of aluminum nitride, oxide and nitrate.

[2]: Aluminum nitride with possible nitrate

Based on the calculations in Appendix II of this dissertation, the film had a molecular concentration of 72.8% *AlN*, 26.1% *Al* (metallic aluminum), and 1.1% $Al(NO_3)_3$ in the film interior. At the surface region, the calculated film composition was 76.5% *AlN*, 15.9% *Al*, 1.7% $Al(NO_3)_3$, and 5.9% Al_2O_3. The results are listed in Table 4.2 and Table 4.3

Nitride Film Deposited with an i/a ratio of 0.60 With an *i/a* ratio of 0.60, the nitride film had a N:Al arrival ratio between 1.07 to 1.18 during deposition. The XPS study found a film composition of 44 at% aluminum, 43 at% nitrogen, and 13 at% oxygen in the top surface layer of 10 nm thick. The oxygen concentration was reduced to a level of 7 at% inside the film, with 47 at% aluminum and 46 at% nitrogen in balance.

Table 4.4 lists the measured atomic composition and the calculated molecular composition of the film surface region. On the film surface, the XPS study showed the

Table 4.4. Composition of the Nitride Film Deposited with an *i/a* = 0.60, at the Surface Region.

Element	Peak (eV)	Bond Type	at% of Total Content
O (Oxygen)	531.7	Al_2O_3	6
	533.3	$Al(NO_3)_3$	7
N (Nitrogen)	397.2	Mixed [1]	43
Al (Aluminum)	73.9	Mixed [2]	44
Film Molecular Concentration: 94.3% AlN + 3.4% Al_2O_3 + 2.3% $Al(NO_3)_3$			

[1]: Aluminum nitride with possible nitrate.

[2]: A possible mixture of aluminum nitride, oxide, and nitrate.

dominant component of aluminum nitride (*AlN*). The oxygen XPS peak indicated the existence of both aluminum oxide (Al_2O_3) and aluminum nitrate ($Al(NO_3)_3$), as shown in Figure 4.11. The calculated film molecular composition, as described in Appendix II, was 2.3% $Al(NO_3)_3$, 3.4% Al_2O_3, and 94.3% *AlN*.

In the interior region 20 nm below the film surface, aluminum nitride (*AlN*) and aluminum nitrate ($Al(NO_3)_3$) were found. The XPS peak of oxygen in this area, as shown in Figure 4.12, indicated the existence of an aluminum nitrate ($Al(NO_3)_3$) component.

To calculate the molecular composition in the film, a small amount of metallic aluminum (*Al*) was also assumed to exist in the film, even though the XPS deconvolution method did not separate the *Al* component from the dominant aluminum peak at 74.1 eV. Calculations, detailed in Appendix II, yielded the film's molecular composition of 92.9% *AlN*, 1.7% $Al(NO_3)_3$, and 5.4% *Al*. In atomic composition terms, the calculation indicated that the *Al* component constituted 2.5 at% in the film. Table 4.5 lists both the measured atomic composition and the calculated molecular composition of the film.

Table 4.5. Composition of the Nitride Film Deposited with an $i/a = 0.60$, at a Region 20 nm below the Film Surface.

Element	Peak (eV)	Bond Type	at% of Total Content
Al (Aluminum)	74.1	Mixed [1]	47
N (Nitrogen)	397.4	Mixed [2]	46
O (Oxygen)	532.5	Nitrate	7
Film Molecular Concentration: 92.9% AlN + 5.4% Al + 1.7% $Al(NO_3)_3$			

[1]: A mixture of aluminum nitride and nitrate. Small amount of metallic aluminum may also exist.

[2]: Aluminum nitride with possible of nitrate.

Origin of Oxygen inside Nitride Films The existence of oxygen in the so-call "nitride" films was attributed to the incorporation of oxygen atoms in the films by the impingement of residual oxygen and water molecules during the deposition process.

In the deposition environment, oxygen atoms resided in two types of residual gas molecules: O_2 and H_2O. Both molecules produced a finite impingement rate on the growing film surface. As discussed in Chapter 2, the molecular concentration of an impurity due to residual gas molecule impingement was calculated by comparing the impinging rate of the residual gas molecules with the arrival rates of coating materials [Chambers, 1989; Ohring, 1991]. In the deposition chamber, the impinging rate of residual gas molecules (J_g) was expressed as:

$$J_g = 2.635 \times 10^{20} \frac{P}{\sqrt{M_g T}} \qquad (\text{molecules} \cdot \text{cm}^{-2} \cdot s^{-1}).$$

Here, P is the partial pressure (in Pa) for the residual gas, and T is the environment temperature (in K). M_g is the molar weight of gas molecules, which are 32 g/mole for oxygen and 18 g/mole for water. Hence, at an environment temperature of 300 K and a partial pressure of 1.3×10^{-5} Pa, the impinging rate of residual oxygen molecules was calculated to be 3.5×10^{13} molecules/cm^2/sec. For residual H_2O molecules, an impinging rate of 4.7×10^{13} molecules/cm^2/sec was estimated with the same conditions.

The water molecular impinging rate was equivalent to the oxygen atomic impinging rate contributed by water molecules. The oxygen atomic impinging rate from oxygen molecules was equivalent to twice the molecular impinging rate given by the above equation.

Assuming the oxygen atomic concentration in the film was low and all the impinging materials (including aluminum, nitrogen, and oxygen) were incorporated into the growing film, the oxygen atomic concentration (C_O) in the film was then calculated as

$$C_O = \frac{A_O}{A_{Al} + A_N + A_O} \approx \frac{A_O}{A_{Al} + A_N} = \frac{A_O}{A_N\left(1 + \frac{A_{Al}}{A_N}\right)} = \frac{J_O}{J_N\left(1 + \frac{J_{Al}}{J_N}\right)}.$$

Here, J_O, J_{Al}, and J_N are the arrival rate of oxygen, aluminum, and nitrogen atoms, respectively. A_{Al}, A_N, and A_O are the number of aluminum, nitrogen, and oxygen atoms in the film, respectively.

In the reactive IBAD used for nitride film depositions, the arrival rate of nitrogen atoms (J_N) was proportional to the ion beam density (J_i) received on the film surface from the assist-nitrogen ion beam. According to Netterfield [1988], $J_N = 1.787J_i$. Because J_i/J_{Al} is the same as the *i/a* ratio, hence, the oxygen atomic concentration in the film due to the impingement of the water vapor molecules was rewritten as:

$$C_O^{H_2O} = 3.47\times10^{19}\frac{P_{H_2O}}{J_i\left(1 + \frac{J_{Al}}{1.787J_i}\right)\sqrt{T}} = 3.47\times10^{19}\frac{P_{H_2O}}{J_i\left(1 + \frac{1}{1.787\cdot i/a}\right)\sqrt{T}}.$$

The oxygen atomic concentration due to the residual oxygen molecules was then

$$C_O^{O_2} = 5.21\times10^{19}\frac{P_{O_2}}{J_i\left(1 + \frac{J_{Al}}{1.787J_i}\right)\sqrt{T}} = 5.21\times10^{19}\frac{P_{O_2}}{J_i\left(1 + \frac{1}{1.787\cdot i/a}\right)\sqrt{T}}.$$

Therefore, the total oxygen atomic concentration in the film was then

$$C_O = C_O^{H_2O} + C_O^{O_2} = \left(3.47P_{H_2O} + 5.21P_{O_2}\right)\times10^{19}\frac{1}{J_i\left(1 + \frac{1}{1.787\cdot i/a}\right)\sqrt{T}}.$$

During the nitride film deposition with an *i/a* ratio of 0.42, the residual partial pressures for both oxygen (P_{O_2}) and water (P_{H_2O}) were about 1.3×10^{-5} Pa. The ion beam density (J_i) was about 3.4×10^{14} ($\text{ions}\cdot\text{cm}^{-2}\cdot s^{-1}$). The environment temperature (T) was 350 K. Therefore, the total oxygen concentration in the film was estimated to be 7.6 at%. The measured oxygen concentration was 5 at% in the interior of the film.

For the film deposited at 593 K with an *i/a* ratio of 0.6, the ion beam density (J_i) during the deposition was 5.2×10^{14} ($ions \cdot cm^{-2} \cdot s^{-1}$), and the environment temperature (T) was at 300 K. The residual partial pressures for both oxygen and water molecules were 1.3×10^{-5} Pa. Based on the above conditions, the oxygen concentration in the film was estimated to be 6.0 at%. The measured value was 7 at%.

Hence, the oxygen content in the nitride films probably originated from the impingement of the residual oxygen and water molecules during the film depositions. The results reaffirmed the notion that even high vacuum conditions may lead to a significant contamination when deposition rates are low [Ohring, 1991].

Discussion of Nitride Film Deposition Process on Planar Substrates Based on the composition study, nitride films were actually formed in two stages of Active Deposition and Oxidization. In the first stage of Active Deposition, the atomic concentrations of aluminum, nitrogen, and oxygen in the film were determined by the relative atomic arrival rates during the deposition process. Originating from the impingement of residual oxygen and water molecules during deposition, oxygen atoms were bound with nitrogen and aluminum atoms as aluminum nitrate ($Al(NO_3)_3$). Under the deposition conditions used in this study, small amount of metallic aluminum was left in the film after the first deposition stage. The dominant component in the film was aluminum nitride (AlN).

During the second stage of Oxidization, all or part of the metallic aluminum component was further oxidized upon exposure to air after deposition. Because of the dense structure of the film, the second stage of the film formation only affected the top surface region of the film. The oxidized depth of the film was about 5 to 10 nm.

With different *i/a* ratios, deposited nitride films differed in the amount of metallic aluminum content inside the films. At higher *i/a* ratios, more aluminum atoms were bonded with nitrogen forming aluminum nitride (*AlN*). For instance, in terms of molecular concentration, the nitride film with an *i/a* ratio of 0.60 consisted of 5.4% metallic aluminum, whereas 26.1% of metallic aluminum was left in the film deposited with an *i/a* ratio of 0.42. On the surface, the film with a lower *i/a* ratio formed more aluminum oxide (Al_2O_3) component by oxidation. Some of the metallic aluminum component on the surface might even remained.

Discussion of Composition of Nitride Films on SiC Particles Because SiC particles were levitated during deposition, the growth of the nitride films on SiC particles was of an intermittent nature. The resultant film on SiC particles experienced a multiple alternation of the two deposition stages of Active Deposition and Oxidization. Each second stage of oxidization was occurred in the deposition environment by the impingement of residual oxygen and water molecules.

Each first stage (the Active Deposition stage) of the film deposition on SiC particles actually resembles to the film deposition process on planar substrates in terms of deposition rate and conditions. The duration of each active deposition stage on SiC particles, which was the same as the time of a particle exposing itself to the depositing fluxes each time, was observed in this study to be no more than 10 seconds. Hence, the thickness of the film laid down at each first stage was no more than 2 nm (based on the measured deposition rate on planar substrates).

After each active deposition stage, the particle was levitated away from the incoming depositing fluxes. Because of the continuation of the impingement of residual oxygen and water molecules at the absence of the incoming aluminum flux, the freshly

deposited film layer underwent the second stage (the Oxidization stage) of film formation inside the deposition environment.

As observed in this study, the second stage of the film formation took place at the top surface region of 5 to 10 nm thick of the films. Because the thickness of the freshly deposited film layer after each first stage was no more than 2 nm on SiC particles, the subsequent oxidization stage was able to take place in the entire thickness of the freshly deposited film layer. Under current deposition conditions, the impingement of residual oxygen and water molecules during each oxidization stage supplied enough oxygen atoms to oxidize the entire metallic aluminum component in the freshly deposited film layer. Hence, the resultant nitride film on particles should consist of aluminum nitride, aluminum nitrate, and aluminum oxide.

To estimate the nitride film atomic composition and molecular constituents, it was assumed that the *N-to-Al* atomic ratio in the films was the same as the ratio of the arriving coating fluxes. The oxygen content in the film after each first stage of the film formation was presumably determined by the impingement of residual oxygen and water molecules. After the each first stage of the film formation, metallic aluminum component in the film was presumably oxidized into aluminum oxide in the subsequent oxidation stage.

For the conditions of the 593 K deposition of nitride film on SiC particles, an averaged *i/a* ratio of 0.56 gave an *N-to-Al* ratio of unity [Netterfield, 1988]. Using above assumptions, the film atomic composition was calculated to be 45.4 at% aluminum, 45.4 at% nitrogen, and 9.2 at% oxygen. In terms of molecular composition, the film consisted of 1.8% aluminum nitrate ($Al(NO_3)_3$), 1.8% aluminum oxide (Al_2O_3) and 96.4% aluminum nitride (AlN). (Appendix II of this paper presents detailed calculations of the estimation of the nitride film composition on the SiC particles.)

Similar estimations were also made for the nitride films deposited on the SiC particles at 793 K with an *i/a* ratio of 0.53. It was estimated that the film had an atomic composition of 45.7 at% aluminum, 43.3 at% nitrogen, and 11.0 at% oxygen. The molecular composition of the film was 94.4% *AlN*, 1.5% $Al(NO_3)_3$, and 4.1% Al_2O_3.

The above estimations were based on a *N-to-Al* ratio converted from the *i/a* ratio by using a factor of 1.787 [Netterfield, 1988]. Taylor [1981] suggested a higher converting factor of 1.96[1]. Based on Taylor's factor, a higher nitrogen atomic concentration was estimated in the film, which resulted in a higher concentration of *AlN* in the film with less $Al(NO_3)_3$ and Al_2O_3. Using Taylor's data, films under our experiment conditions yielded more than 98% of *AlN* with a balance of $Al(NO_3)_3$ only. However, the measured results from this study indicated that the films consisted of oxide content. Therefore, the estimations based on Netterfiled's data were more reliable.

In conclusion, nitride films deposited on SiC particles had a dominant aluminum nitride molecular content. The molecular concentration of aluminum nitride was estimated between 94% to 96%, with aluminum nitrate and aluminum oxide in balance.

Summary

With IBAD techniques, averaged 0.5 μm thick aluminum oxide and nitride films were deposited on SiC particulate substrates. On SiC particles, the oxide film had a Zone T structure with some globular feature. The grains were 0.1 μm or smaller. The nitride film deposited on SiC particles at 593 K had a voided globular film structure with

---

[1] The difference in conversion factor between Netterfield's and Taylor's study is due to the difference in their N_2^+ *-to-* N^+ ratio measurement in the ion beam from a Kaufman ion source. Netterfield's study [1988] reported a 78.7-to-21.3 ratio, whereas Taylor [1981] reported a 96-to-4 ratio. Hence, the ratio between nitrogen atom and ion density in the ion beam (the conversion factor) is 1.787 based on the Netterfield's result. Based on Taylor's measurement, the ratio is 1.96.

clusters of small grains. The structure for the nitride film was a mixture of Zone I and Zone T types. The grains in the film were less than 0.2 μm in size, and grouped into clusters sizing of 0.3 μm in average. The nitride films deposited at 793 K had a dense Zone T structure with a grain size of 0.2 μm or smaller. The composition of the oxide film was nominally stoichiometric. The nitride films on SiC particles were estimated of a *N/Al* ratio similar to the *N/Al* arrival ratio in the coating fluxes, and an oxygen concentration near 10 at%. Within the "nitride" films, aluminum nitride constituted about 95% of film molecules, balanced with aluminum nitrate and aluminum oxide.

2. Thin Film Thermomechanical Behavior: Annealing Tests

It was crucial for thin diffusion barrier films to maintain a full coverage on their substrates during applications. An understanding of film structural evolution helped to study the viability and the effectiveness of the thin diffusion barrier films. Annealing tests were designed to reveal the thermomechanical behaviors of the films.

Annealing at 1273 K in Air: Nitride Films on SiC Particles

SiC particles with aluminum nitride coatings were heated in air to 1273 K, and subsequently air-cooled to room temperature. Both nitride films (deposited at 593 K and 793 K) showed adequate adhesion to their SiC particle substrates during the test. Neither film showed any significant change in morphology in the process, as compared with the films' original states. Figure 4.13 shows the morphology of the film deposited at 793 K after the test. No cracks were found in the films under magnifications up to 7000×.

The nitride films deposited on 593 K SiC particles also survived after being quenched in liquid nitrogen (77 K) from 1273 K. No film delamination from the SiC particulate substrates was found. Even though some of the SiC particles themselves were cracked during the process, the films on these cracked SiC particles remained attaching to their substrates, as shown in Figure 4.14.

Annealing at 1273 K in Air: Oxide Films on SiC Particles

As a comparison, the Al_2O_3 films deposited on SiC particles were studied at the conditions of annealing at 1273 K in air and subsequent air-cooling to room temperature. Numerous cracks were found in the film after the process, as shown in Figure 4.15.

At 1273 K (0.55 T_m for Al_2O_3), the annealing temperature facilitated the grain growth in the film. As shown in Figure 4.15, the average grain size in the oxide film increased from their as-deposited size (as shown in Figure 4.5) after annealing. The grains in the oxide film after annealing had a size comparable to the film thickness averaged at 0.5 μm. Consequently, a large amount of grain boundaries extended from the film surface to the SiC substrate. Furthermore, an agglomeration of pores at the grain boundary region [Kingery, 1976] widened the boundaries, resulting in micro-cracks.

As a diffusion barrier to nickel aluminide matrices, Al_2O_3 films on SiC particles were usually subjected to a consolidation process with a temperature of 1373 K or higher. As indicated in this experiment, the oxide films could not retain a full coverage on SiC substrates in such a consolidation condition. For this reason, the Al_2O_3 film deposited on SiC particles was not a suitable diffusion barrier material in SiC particle reinforced nickel aluminide matrix composites.

Summary of Annealing Tests in Air

The annealing tests demonstrated that the oxide film had little tolerance for a moderate annealing temperature (1237 K). The aluminum nitride films were capable of retaining adhesion and a full coverage on SiC particulate substrates. The results indicated that the oxide film deposited on SiC particles was not a practical candidate as a diffusion barrier in SiC particle reinforced nickel-bearing matrix. The nitride films, on the other hand, showed their potential as effective barriers in the composites. The nitride films were studied further, as presented next, with respect to film structural stability under the annealing conditions of composite consolidations employed in this research.

Annealing in Vacuum: Nitride Films Deposited at 793 K

Films Annealed at 1373 K for One Hour This experiment simulated the composite consolidation conditions for SiC particle reinforced γ-Ni_3Al composites. In vacuum, the coated SiC particles were annealed for one hour at 1373 K.

Figure 4.16 shows SEM images of film morphology on an annealed particle. The aluminum nitride film retained adhesion to the SiC substrate. Neither cracks nor visible voids were found on the surface of the film under a magnification of 20,000×. There were no obvious changes in film morphology in the annealed films as comparing with the as-deposited films as shown in Figure 4.4.

Films Annealed at 1573 K for Four Hours The nitride films deposited on SiC particles at 793 K were annealed in vacuum at 1573 K for four hours. Although 1573 K was not used to consolidate the composites in this study, the annealing condition

was studied because it was the highest temperature at which all the nitride films retained a full coverage on the SiC substrates. At temperatures above 1573 K, cracks were found in some of the films.

Figure 4.17 shows the morphology of the film after the annealing. The grain boundaries in the film and voids in between grains became visible, as compared with the film morphology after being annealed at 1373 K. Besides a few large globular-structured grain clusters on the film surface, the grains in the film were also different in size. Some of the grains were about 0.2 μm in size, and were surrounded by smaller grains. Such a mixing of different grain sizes was a classical phenomenon in grain growth process in which the larger grains enlarged at the expense of the smaller ones [Kingery, 1976].

The appearance of visible voids on the film surface after the annealing indicated the progress of pore agglomeration at grain boundaries accompanied the grain growth [Kingery, 1976].

Films Annealed at 1673 K for Four Hours This annealing condition was used for the consolidation of β-NiAl matrix composites in this research. After annealing, the nitride films deposited at 793 K lost full coverage over the SiC particulate substrates. Small patches of SiC substrate surface were observed in SEM images. Figure 4.18(a) is a SEM image showing an annealed SiC particle with the nitride film. Figure 4.18(b) and (c) show more details of the morphology of the film at higher magnifications.

Most of grains in the annealed film ranged from 0.3 to 0.6 μm in size, which was comparable to the film thickness of 0.5 μm in average. Smaller spherical particles of less than 0.1 μm in size were found surrounding the bigger ones, as shown in Figure 4.18(c). As discussed in the section of film composition, the nitride film consisted of about 5%

secondary phases (aluminum oxide and aluminum nitrate). The smaller spherical particles around the bigger grains were presumably those secondary phases.

Because the grain size in the nitride film was comparable to the film thickness after the annealing at 1673 K, the grain boundaries in the film extended from the film surface to the SiC substrates. During grain growth process, pores in the film traveled along with the grain boundaries, and agglomerated there [Kingery, 1976]. The agglomerated pores widened the grain boundaries, resulting in micro-cracks in the film.

This experiment suggested that the aluminum nitride films deposited on SiC particles at 793 K would not be able to maintain an effective coverage on the SiC substrates during a 1673 K annealing process for 4 hours. Because this annealing condition was necessary to consolidate the β-NiAl matrix composite, therefore, the aluminum nitride film deposited at 793 K would not be able to protect the SiC particles from chemical reactions with the β-NiAl matrix during the consolidation process.

Annealing in Vacuum: Nitride Films Deposited at 593 K

As compared with nitride film deposited at 793 K, aluminum nitride films deposited on SiC particles at 593 K had a different film structure after deposition. The as-deposited films of 593 K consisted of globular clusters of grains, as comparing with the films of 793 K with a smooth and dense structure. For the annealing tests in vacuum, two temperatures (1573 K and 1673 K) were applied to the film deposited at 593 K.

Films Annealed at 1573 K for Four Hours The annealed nitride films on SiC particles showed a globular structure of grain clusters, similar to the structure of a non-

annealed film. Figure 4.19 shows an annealed SiC particle with the nitride coating and the film morphology on the coated particle. The nitride film retained the coverage over the SiC particle.

Compared with the as-deposited film shown in Figure 4.3, boundaries between individual grain clusters in the annealed film were better defined, and voids in between the clusters were more visible. The agglomeration of pores at the cluster boundaries indicated grain growth in the films during the annealing process [Kingery, 1976]. Because there was no obvious difference between the cluster sizes before and after the annealing, as indicated in Figure 4.3 and 4.19, the grain growth process likely occurred within each individual grain clusters.

Films Annealed at 1673 K for Four Hours The SiC particles were entirely covered with the nitride film after the annealing at 1673 K for 4 hours. Figure 4.20 shows a coated SiC particle and the film after the annealing.

The structure of the annealed film was classified as globular, with an averaged grain cluster size of 0.4 - 0.5 μm. Comparing images in Figure 4.19 and 4.20, the 1673 K annealing produced a denser film than the 1573 K annealing. The annealed film appeared slightly denser than the as-deposited films (shown in Figure 4.3) as well.

Grains in individual grain clusters coalesced into larger ones as compared with the original grain sizes. Some of the grains in the clusters were 0.3 - 0.4 μm in size. Much smaller grains (less than 0.1 μm) were found surrounding the large ones.

The grain coalescence (growth) was a process in which some grains increased their size at the expense of their neighboring grains. Because of the voided globular structure of the film, the grain growth process was primarily developed within each grain

cluster. As a result, the size of the large grains in the film approximately equaled to the original grain cluster size of 0.3 μm. The smaller grains of a size of 0.1 μm or less were presumably the secondary phases (aluminum oxide and aluminum nitrate).

The denser structure in the annealed film was attributed to a solid-state sintering process occurring in the film during the 1673 K annealing. Sintering process densified the film by eliminating the original voids in the film [Kingery, 1976]. However, the primary globular structure of the annealed film indicated that the densification via solid-state sintering was not completed.

Therefore, the original globular structure of the nitride film did not change after the annealing process at 1673 K. The grain growth process was primarily limited within the original grain clusters, resulting in a grain size comparable to the original cluster size. Limited solid-state sintering process during the annealing helped to densify the originally voided film. The resultant films after the annealing retained their coverage on the SiC particulate substrates.

Discussion of Nitride Film Annealing in Vacuum

The vacuum annealing tests of the nitride films strongly indicated the influence of the original film structure on the thermomechanical behavior of the films. At elevated temperatures, the extent of grain growth in a thin film determined the survivability of the integrity of the film. Grain growth hinderer such as voids in the film played a profound role in film's thermomechanical behavior.

As an inevitable high-temperature process, grain growth increased average grain size in materials by combining several smaller grains into a larger one [Kingery, 1976]. Without a grain growth hinderer such as voids, films with small grains experienced an

uninhibited, homogeneous grain growth in the film at elevated temperatures. Such a grain growth in the film eventually led to a grain size comparable to the film thickness, extending the grain boundaries in the film from the film surface to the substrate. Agglomerating of pores at the grain boundaries during grain growth further compromised the integrity of the annealed film. The nitride film deposited on SiC particles at 793 K was such an example.

By being a voided structure, films with an originally globular structure not only provided the grain growth hinderer such as voids, but also set a stage for solid-state sintering taking place at high temperatures [Kingery, 1976]. The original voided globular structure confined the grain growth process primarily within individual grain clusters. The sintering process densified the film to a certain extent. Because voids in film stalled the grain growth process [Kingery, 1976], the progress of grain coalescence in the originally voided film was less advanced than that in a film with an original dense structure. The grain size in the film deposited at 593 K was found to be less than that in the film deposited 793 K after the same annealing.

Therefore, the original voided globular structure was actually preferred in this study for thin films under high-temperature ($>0.5T_m$ of the film material) applications, as comparing to the originally dense film structure with small grains. In this study, the nitride film deposited on SiC particulate substrate at 593 K consisted of a globular film structure with clusters of fine grains. This nitride film was preferred as diffusion barrier at high temperatures to nitride films deposited at 793 K with a dense structure.

3. Ni Diffusion in Aluminum Nitride, a Cursory Study

There was limited information available regarding nickel diffusion in aluminum nitride. A cursory study was conducted to determine if Ni has low lattice diffusivity in the nitride at temperatures applied in this research. The extent of Ni diffusion in both monolithic aluminum nitride plate and deposited aluminum nitride film were studied. In this investigation, only the extent of Ni diffusion in the nitride was studied.

Ni Diffusion at the Interface of Aluminum Nitride and Nickel Aluminide Plates

An aluminum nitride plate was diffusion bonded in vacuum with a γ-Ni_3Al plate at 1473 K for 32 hours. After revealing the interface of the diffusion couple, an EDX Ni line-profile showed that there was no significant lattice diffusion of Ni across the interface. The interfacial bond strength between these two plates was very weak.

Assuming a constant diffusant source situation[1], the extent of Ni diffusion in aluminum nitride was estimated by measuring the width of Ni concentrational transition at the interface on SEM/EDX photos. Measured from an EDX Ni line-profile shown in Figure 4.21(a), the Ni diffusion extent was less than 1 μm (which is the spatial resolution for the EDX technique [Russ, 1984]). An upper-bound lattice diffusivity for Ni diffusing in the aluminum nitride lattice was therefore estimated to be less than 2.2×10^{-14} cm^2/sec under the conditions of the diffusion bonding. Accordingly, for an one-hour diffusion at

[1] A constant diffusant source situation represents an ideal diffusion model where the diffusant concentration remains constant at the interface of a diffusion couple, and the same as in the source material. This model is best fit in a diffusion couple situation that diffusant has a high diffusivity in the diffusant source comparing with the diffusivity in the diffusion matrix material.

1473 K, an upper-bound distance of Ni diffusing in the nitride via lattice diffusion was estimated to be 0.18 μm[1].

A diffusion couple of planar aluminum nitride and β-NiAl was subjected to a bonding treatment at 1673 K for 12 hours. As shown in Figure 4.21(b), the transition distance of Ni concentration at the interface was also less than 1 μm. Hence, an upper-bound diffusivity of Ni diffusing in the β-NiAl lattice at this temperature was estimated to be less than 5.8×10^{-14} cm^2/sec. An upper-bound lattice diffusion distance was estimated to be 0.58 μm under a hot-pressing condition of 1673 K for 4 hours.

Ni Diffusional Penetration in a Deposited Aluminum Nitride Film

This experiment was designed to measure the extent of Ni diffusion in a deposited aluminum nitride film. A γ-Ni_3Al plate was chosen as the source for Ni. After the nitride film coated plate was annealed in vacuum at 1373 K (the consolidation temperature for γ-Ni_3Al matrix composites) for 30 minutes, the extent of Ni diffusion in the nitride film from the γ-Ni_3Al substrate was studied by XPS.

Figure 4.22 shows a Ni concentration profile in the aluminum nitride film. In the profile, a concentration ratio of *Ni-to-Al* was used for the *y*-axis. A 6/5 power of the distance from the film surface was used for the *x*-axis, for which was proportional to the diffusant concentration due to grain-boundary diffusion [LeClaire, 1961].

---

[1] The maximum distance (x)of a diffusant can be expressed as:

$$x = 2\sqrt{D_l t}$$

Here, the D_l is the lattice diffusivity, and t is the diffusion duration. For diffusion at 1473 K between aluminum nitride and γ-Ni_3Al, x = 1 μm, t = 32 hours. Hence, D_l was calculated to be 2.2×10^{-14} cm^2/sec. For an one-hour diffusion duration, the upper-bound distance of Ni lattice diffusion in the nitride is then 0.18 μm.

As indicated in the profile, the concentration of Ni content reduced sharply within a region about 10 nm wide in the nitride film at the film-substrate interface. Following that region, the concentration decreased gradually and penetrated into the film further. No Ni content was found on the film surface. The total distance of Ni diffusing in the nitride film after the 0.5 hour annealing duration was extrapolated to be about 200 nm (0.2 μm) from the interface.

The transition region with high Ni concentrations at the film-substrate interface was interpreted as a result of the lattice diffusion of Ni in the film. The region with a gradually changed concentration profile was most likely caused by grain-boundary diffusion [Gilmer, 1976a]. The small grain size of the film facilitated the extent of the Ni diffusion in the film.

For a condition of an one-hour annealing in vacuum at 1373 K, the extent of Ni diffusion in the nitride film was estimated to be roughly 0.3 μm from a γ-Ni_3Al source. This estimation was based on the relationship of the diffusion distance being proportional to the square root of diffusion duration.

Summary and Discussion

This cursory study showed, with both β-NiAl and γ-Ni_3Al as nickel sources, nickel has very low lattice diffusivities in aluminum nitride. From a γ-Ni_3Al source, the upper-bound lattice diffusivity of Ni in the nitride was 2.2×10^{-14} cm^2/sec at 1473 K. At 1673 K, the upper-bound diffusivity was 5.8×10^{-14} cm^2/sec from a β-NiAl source.

The study of Ni diffusion in a deposited aluminum nitride film showed a greater diffusional distance than the estimated distance based on the lattice diffusion. Because of

the grain-boundary diffusion effect, the diffusional penetration was about one order of magnitude greater than the prediction from the lattice diffusion data.

From a γ-Ni_3Al source, the extent of Ni diffusing in the nitride film at the consolidation condition of γ-Ni_3Al composites (1373 K/1 hour) was estimated to be about 0.3 μm. This distance was less than, but comparable to the thickness of the films deposited on SiC particulate substrates used in this study (As discussed in Section 1 of this chapter, the film thickness in this study was about 0.5±0.1 μm.).

As to the Ni diffusion in the nitride film from a β-NiAl source, the upper-bound lattice diffusion distance at the consolidation condition of β-NiAl composites (1673 K/4 hours) was estimated to be less than 0.58 μm.

Hence, with a nominal thickness of 0.5 μm, the deposited aluminum nitride film on SiC substrates was a good candidate to evaluate the chemical potential effect on the effectiveness of diffusion barriers in different composite systems.

4. Effectiveness of Diffusion Barriers in Two Composites: SiC Particle Reinforced β-NiAl and γ-Ni_3Al Composites

The chemical potentials were different in composite systems of SiC/β-NiAl and SiC/γ-Ni_3Al. The interaction between SiC and β-NiAl was moderate as compared with the interactions in a SiC/γ-Ni_3Al composite [Chou, 1991a&b]. The reaction zone between SiC and γ-Ni_3Al was about an order of magnitude wider from a 1273 K annealing than the reaction zone in a SiC/β-NiAl diffusion couple annealed at 1573 K. With a higher Ni content in the matrix, the SiC/γ-Ni_3Al composite system offered a higher chemical potential, and a much more challenging task for the diffusion barriers than the β-NiAl matrix composite did.

In Section 2 of this chapter, three barrier films (aluminum oxide deposited at room temperature, aluminum nitride film deposited at 593 K, and aluminum nitride film deposited at 793 K) demonstrated different thermomechanical behaviors during annealing at temperatures for composite consolidation. This section addresses the effectiveness of the films as diffusion barriers in both SiC particle reinforced β-NiAl and γ-Ni_3Al composites under the composites' respective "hot-press" consolidation conditions.

The Control Composite Samples

The control composite samples, which used non-coated SiC particles, were consolidated with both β-NiAl and γ-Ni_3Al matrices under the composites' respective consolidation conditions. The β-NiAl matrix composites were hot-pressed for 4 hours at 1673 K. The γ-Ni_3Al matrix composites were consolidated at 1373 K for one hour.

As shown in Figure 4.23(a), the non-coated SiC particles reacted with the β-NiAl matrix. A 20 μm thick reaction zone was formed at the interface region between the SiC particles and the β-NiAl matrix. As shown in Figure 4.23(b) of an EDX spectrum from the reaction zone, the reaction product was a Ni-Al-Si ternary compound with a low Si content that was qualitatively in agreement with the previous report by Chou [1991a].

Figure 4.24 shows the reaction zone in a γ-Ni_3Al matrix composite sample where the non-coated SiC particles were used. The γ-Ni_3Al reacted severely with the SiC reinforcements at the consolidation conditions. Layers of reaction products were formed in the area previously occupied by the SiC particles. No remnant of the SiC particle was found after the consolidation.

Aluminum Nitride Films Deposited at 593 K as Diffusion Barrier

In β-NiAl Matrix Composite After consolidated with the β-NiAl matrix at 1673 K for 4 hours, the coated SiC particles were protected from the chemical reactions with the matrix by an average 0.5 μm thick nitride film deposited at 593 K.

More than 90% of the coated SiC particles were preserved with the nitride film intact. Figure 4.25(a) and (b) are SEM images of a coated SiC particle in the composite after the consolidation. On this particle, part of the nitride film was damaged, showing a relatively smooth area. Only one strong Si signature was shown in an EDX spectrum collected from the smooth area, as shown in Figure 4.25(c), which indicated that the film was damaged during the SEM sample preparation. The revealed SiC substrate in this area showed no sign of the reaction products.

On fewer than 10% of the coated particles in the composite, the nitride films were broken during the hot-pressing process. In these regions with film damages, the SiC substrate was exposed to and chemically reacted with the NiAl matrix during the consolidation process. Figure 4.26(a) shows one of the few such particles. The particle was released by electropolishing to remove the matrix material. In Figure 4.26(b), a magnified picture of the film damaged region shows reaction products similar to those in the control samples in Figure 4.23. Figure 4.26(c) is an EDX spectrum from the substrate at the film-damaged region, indicating the presence of a ternary Ni-Al-Si compound.

In γ-Ni_3Al Matrix Composite The aluminum nitride film deposited on SiC particles at 593 K did not prevented the reactions in the γ-Ni_3Al matrix composite system. A reaction zone was formed in the composites after the consolidation.

Figure 4.27 presents an optical micrograph of the reaction zone in the composite containing the coated SiC particles. The structure of the reaction zone in the composite was almost identical to the zone in the control samples shown in Figure 4.24. A broken line at the outer perimeter of the reaction zones showed some evidence of the location, or might even the remnants of the nitride film.

Discussions The results of this experiment indicated that an average 0.5 μm thick nitride film deposited at 593 K was an effective diffusion barrier for SiC particles in a β-NiAl matrix composite during the composite consolidation process at 1673 K. However, the same nitride film was not adequate to protect the SiC particles in a γ-Ni_3Al matrix composite at 1373 K.

This experiment demonstrated the importance of the chemical potential in the composite system in determining the effectiveness of the diffusion barrier. Although the nitride film was an effective diffusion barrier in the β-NiAl matrix composite with a modest chemical potential, the film did not offer any sign of stalling the reactions in the γ-Ni_3Al matrix composite with a higher chemical potential.

The consolidation process for β-NiAl at 1673 K probably had an additional advantage for the nitride film deposited on SiC particles at 593 K. As discussed in the section of Thermomechanical Behavior, the film underwent a limited solid-state sintering process on the SiC particles at 1673 K. The film structure after the sintering process was denser than the non-annealed state. As for the film after a 1373 K consolidation process for γ-Ni_3Al, the annealed film was as voided as the film in the original state. A voided film offered more fast-diffusion baths than a densely packed thin film.

Aluminum Nitride Films Deposited at 793 K as Diffusion Barrier

In β-NiAl Matrix Composite SiC particles used in the composite were coated with nitride film at 793 K. The average film thickness was 0.5 μm. After consolidation with the β-NiAl matrix at 1673 K for 4 hours, the coated SiC particles were found to react with the matrix. Figure 4.28 shows a reacted SiC particle in the β-NiAl matrix composite. The reaction zone was similar to that in the control sample. There was no evidence that the nitride film had any effect in stalling the matrix-reinforcement reaction.

In γ-Ni_3Al Matrix Composite The aluminum nitride film deposited at 793 K did not prevented the reactions in the SiC/γ-Ni_3Al matrix composite system. Reaction zones were formed in the composites after the consolidation. Figure 4.29 shows the reaction zone at a location formerly occupied by a coated SiC particle. The composite was fractured in tension at room temperature after the consolidation. The reactions between the γ-Ni_3Al matrix and SiC particle consumed the entire SiC particle. No remnant of the SiC particle was found after the consolidation.

Discussions The results of this test indicated that an average 0.5 μm thick nitride film deposited at 793 K was not adequate to protect the SiC particles in both β-NiAl matrix and γ-Ni_3Al matrix composites during the composites' respective consolidation processes. In the γ-Ni_3Al matrix composite, the high chemical potential in the system was blamed as the cause of the ineffectiveness of the diffusion barrier.

In the β-NiAl composite, the thermomechanical behavior of the nitride film probably cost the film's effectiveness as the diffusion barrier. As discussed in the section of Thermomechanical Behavior, the nitride film deposited at 793 K lost integrity over the

SiC particulate substrates under the conditions for β-NiAl consolidation at 1673 K. Uninhibited grain growth resulted in grain boundaries extending from the film surface to the substrate. The breakage of the film's continuity presumably led to the film's failure to protect the substrates.

Aluminum Oxide Films as Diffusion Barrier

An average 0.5 μm thick oxide film on SiC particles was not sufficient to protect the SiC particles from chemical reactions in both β-NiAl matrix and γ-Ni_3Al matrix composites during the composites' respective consolidation processes. As shown in Figure 4.30, there was no evidence of stalling the reactions in both matrices as compared with the control composite samples. Figure 4.30(a) shows the reaction products around the remnant of a SiC particle in a β-NiAl matrix composite. Figure 4.30(b) presents the reaction zones in a γ-Ni_3Al matrix composite.

As discussed in the section of Thermomechanical Behavior, the oxide film exhibited a higher tendency of grain growth at lower temperatures than the nitride films did. Because of a film structure of densely packed small grains in the as-deposited oxide film on SiC particles, uninhibited grain growth in the film during annealing eventually cost the film's continuity. Numerous cracks were observed in the oxide film after the coated SiC particles had been annealed at 1273 K (Figure 4.15). It was not a surprise that the oxide film failed to protect the SiC substrates during the composite consolidation processes at temperature of 1373 K or above.

Summary

Although SiC was chemically ready to react with β-NiAl at temperatures above 1573 K [Chou, 1991a], the imposition of an aluminum nitride diffusion barrier could stall the reaction long enough for the success of consolidating the composite at 1673 K. With an original globular film structure and an average thickness of 0.5 μm, the nitride film deposited on SiC particles at 593 K was an effective diffusion barrier in SiC particle reinforced β-NiAl matrix composites processed at a temperature of 1673 K.

This study indicated that the chemical potential in the composite system played an important role in determining the effectiveness of the diffusion barrier. Although the nitride film deposited at 593 K functioned effectively as a diffusion barrier in the SiC/β-NiAl composite system, the same film failed to protect the SiC particles in a higher chemical potential composite system (the SiC/γ-Ni_3Al composite system) during the composite's consolidation process at 1373 K.

The thermomechanical behavior of the barrier films was also important. Both densely packed fine-grain films, the oxide film deposited at room temperature and the nitride film formed at 793 K, lost the film integrity on the SiC particulate substrates because of the uninhibited grain growth in the films at elevated temperatures. None of the densely packed fine-grain films functioned as the effective diffusion barrier in SiC reinforced aluminide matrix composites in this study .

CHAPTER 5. CONCLUSIONS

In this study, aluminum nitride and aluminum oxide films were used as diffusion barriers in SiC particle reinforced nickel aluminide matrix composites (both SiC/β-NiAl and SiC/γ-Ni_3Al systems). Several factors were found to affect the effectiveness of the diffusion barrier films. These factors included barrier film materials, barrier film deposition conditions and resultant film structures, barrier film thermomechanical behavior during compositing process, and chemical potential in the composite system. In this study, a nitride film with an average thickness of 0.5 μm demonstrated its capability as an effective barrier to the catastrophic reinforcement-matrix reactions in SiC particle reinforced β-NiAl matrix composites at a temperature of 1673 K.

A cursory investigation done in this study indicated that Ni has low lattice diffusivity in aluminum nitride (*AlN*) at high temperatures. Only the upper-bound value of the diffusivity of Ni in *AlN* lattice was estimated in this study. The estimated upper-bound diffusivity of Ni from a γ-Ni_3Al source was 2.2×10^{-14} cm^2/sec at 1473 K, and 5.8×10^{-14} cm^2/sec at 1673 K from a β-NiAl source. In an aluminum nitride film deposited on a γ-Ni_3Al plate, Ni penetration was measured to be about 0.2 μm deep into the nitride film after annealing at 1373 K for 0.5 hour. The diffusion depth was contributed predominantly by the grain-boundary diffusion in the fine-grained film.

In this study, the nitride and oxide films were fabricated by ion-beam assisted deposition (IBAD) processes. Both films were deposited on SiC particulate substrates in a specially designed particle levitation system. The oxide film was formed at room temperature with an assisted argon ion beam. The nitride films were formed at elevated temperatures reactively using a nitrogen ion beam.

By using the reactive IBAD technique, the nitride film was formed in a two-stage process of Active Deposition and subsequent Oxidization. After the active deposition stage, the constituents in the nitride film were found to be aluminum nitride (*AlN*), aluminum nitrate ($Al(NO_3)_3$), and metallic aluminum (*Al*). Because of the low deposition rate on the particulate substrates, the entire *Al* component in the film was oxidized in situ by the impingement of residual oxygen and water molecules the second stage of film formation, the Oxidization stage.

While the oxide film had a nominally stoichiometric composition and a single Al_2O_3 component, the deposited nitride film on SiC particles consisted of about 10 at% oxygen content. The *N-to-Al* ratio in the nitride film was estimated to be between 0.95 and 1.0. An estimated 95% of molecules in the nitride films on SiC particles were *AlN*, with $Al(NO_3)_3$ and Al_2O_3 molecules in balance.

On SiC particulate substrates, the average thickness for both oxide and nitride films was about 0.5 μm. Grains in both films were smaller than 0.2 μm. However, films deposited at different temperatures were different in structures.

The nitride film deposited at 593 K had a globular structure with clusters of grains. Large amount of voids was visible in the film. The average size of the clusters in the film was 0.3 μm. The nitride film deposited at 793 K had a densely packed structure. The structure of the oxide film deposited at room temperature consisted of densely packed grains, with some globular features. The difference in film structure was attributed to the combined effect of the levitation of the particulate substrates during deposition and the difference in deposition temperatures.

At high temperatures, grain growth was observed in both oxide and nitride films. The film material affected the rate of the grain growth. The oxide film had a higher rate of grain growth than the nitride film did at elevated temperatures. At 1273 K, the grains

in the oxide film on SiC particles coalesced to an average size that was comparable to the film thickness. The grain boundaries in the oxide film extended from the film surface to the film-substrate interface. Agglomeration of pores at the grain boundaries in the oxide film widened the boundaries into micro-cracks. At higher temperature such as 1673 K, the nitride film with densely packed small grains (deposited on SiC particles at 793 K) experienced the similar process in which grain growth led towards larger grains and micro-cracks in the annealed film.

This study demonstrated the effect of film structure on film's thermomechanical behavior at high temperatures. The structure of the nitride film deposited at 593 K was globular with grain clusters. Because of large amount of voids in between the clusters, grain growth in the film was restricted within each cluster. At high temperatures, solid-state sintering also densified the film. As a result, the nitride film not only retained the coverage over the SiC particulate substrates after the annealing at 1673 K, but also evolved into a film with less voids.

This study showed the importance of the chemical potential in composite system in determining the effectiveness of a diffusion barrier film. In a composite system with a high chemical potential (such as in the SiC/γ-Ni_3Al system), a diffusion barrier film was less effective than the same film was in a composite system with a modest potential (such as in a SiC/β-NiAl system). With an average thickness of 0.5 μm, the nitride film deposited on SiC particles at 593 K was an effective barrier for Ni diffusing in the SiC/β-NiAl composite during the composite consolidation process at 1673 K. However, the same nitride film did not prevent reactions between the SiC reinforcement and the γ-Ni_3Al matrix during the SiC/γ-Ni_3Al composite consolidation process at 1373 K.

In conclusion, this study indicated that several key factors other than diffusivity were critical for the success of a diffusion barrier in a composite system. The chemical

potential in the composite system was the most crucial factor in determining the effectiveness of the diffusion barrier. By affecting film's thermomechanical behavior at elevated temperatures, the initial film structure significantly influenced the effectiveness of the diffusion barriers in high-temperature composites.

Though model composite systems were used in this study, it was clearly shown that, with a proper film structure, using aluminum nitride films on the SiC particles was a possible way to fabricate SiC particle reinforced β-NiAl matrix composite.

APPENDICES

APPENDIX I.

PRINCIPLES OF THE XPS TECHNIQUE

The technique of X-ray photoelectron spectroscopy (XPS, sometimes also called ESCA) was applied in this work for thin film composition study. In XPS, a sample is illuminated with X-rays that excite photoelectrons from the surface of the sample [Moulder, 1992; Walls, 1989]. The photoelectrons have binding energies that are characteristic of individual atoms to which the electrons were bound. Because of the shallow escape depth of the photoelectrons, XPS is a surface analysis tool with a depth resolution of 0.2 nm. With a complementary ion-gun, XPS can be used for composition profiling. The depth resolution for the profiling is poor compared with the static method.

The photoelectron energy is dependent on the precise chemical configuration of the atoms. For an element with several chemical bonds in a material, the element's XPS peak is a convolution of all the photoelectron energies from all the chemical bonds. These bonds and their relative amount on a sample surface can be analyzed from the XPS spectrum by deconvoluting the XPS peak. Hence, XPS is a tool to obtain chemical information from a material's surface. Table A lists some of the binding energies for three elements: *Al*, *N*, and *O* in some of their compounds [Moulder, 1992, Taylor, 1981].

For a sample that is homogeneous in the analysis volume, the molar concentration of any constituent in the sample, C_x, can be written as

$$C_x = \frac{I_x/S_x}{\sum I_i/S_i}$$

where I_x is the measured peak intensity for element x and S is the relative atomic sensitivity factor for that peak. The values of S are based on empirical data, and are matrix-dependent.

The XPS technique is a semi-quantitative one. It has a reasonable quantitative accuracy (better than ±10% with good calibration standards) among the surface analysis techniques. The accuracy is influenced by the homogeneity of the sample surface, the elements involved, and the degree of peak interference.

Table A. Standard XPS Binding Energy for *Al*, *N*, and *O* [Moulder, 1992; Taylor, 1981].

Material	Binding Energy (eV)		
	Al	N	O
Al	72.8	-	-
AlN	73.9 - 74.4	397.3	-
Al_2O_3	73.7 - 74.7	-	530.0 - 531.8
Nitrate	Not Available	407.0 - 408.1	532.5 - 533.6

APPENDIX II.

CALCULATION OF NITRIDE FILM MOLECULAR CONCENTRATION FROM XPS RESULTS

In this study, XPS results indicated that the as-deposited nitride films consisted of up to four components: aluminum nitride, aluminum nitrate, aluminum oxide, and metallic aluminum. Because of the limitation of XPS method, elemental information in some of the components could not be separated from each other. For instance, the aluminum characteristic peaks from nitride and oxide (located at 74.15 ± 0.25 eV and 74.2 ±0.5 eV, respectively) could not be separated by a deconvolution method. Additional assumptions were needed to calculate the molecular concentration of a sample using XPS measurement. In following estimations, all components in the film were assumed at their stoichiometric state.

Case 1. Nitride Film with an *i/a* Ratio of 0.42 on Planar Substrate

Interior Region

At the interior region of a nitride film deposited with an *i/a* ratio of 0.42, the XPS results showed three molecular components: aluminum nitride (*AlN*), aluminum nitrate ($Al(NO_3)_3$), and metallic aluminum (*Al*). The atomic composition of the film was found of 54 at% aluminum, 41 at% nitrogen, and 5 at% oxygen.

For every 100 atoms at the interior region of the film, let u be the number of aluminum atoms, v for nitrogen, and w for oxygen, respectively. Thus, $u+v+w = 100$. The 100 atoms formed a molecules of AlN and b molecules of $Al(NO_3)_3$, leaving c atoms (molecules) of Al. Hence, the film components were: $a\mathrm{AlN} + b\mathrm{Al(NO_3)_3} + c\mathrm{Al}$.

The amount of individual atoms in the film could be expressed as:

Aluminum Atom:	$a + b + c = u$
Nitrogen Atom:	$a + 3b = v$
Oxygen Atom:	$9b = w$

Therefore,

$$\begin{cases} a = v - w/3 \\ b = w/9 \\ c = u - v + 2w/9 \end{cases}$$

Because $u = 54$, $v = 41$, and $w = 5$, the number of molecules formed from the 100 atoms at the interior region of the film was therefore 39.33 for AlN (a), 0.56 for $Al(NO_3)_3$ (b), and 14.11 for Al (c). For a total of 54.0 molecules ($=a+b+c$), the molecular composition in the film was 72.8% AlN, 1.1% $Al(NO_3)_3$, and 26.1% Al.

The above estimation yielded a concentration of 14.1 at% metallic aluminum component at the film interior region. The measured concentration of metallic aluminum was 11 at% by the XPS deconvolution method.

Surface Region

At the surface region of the nitride film, four components were found: aluminum nitride (AlN), aluminum nitrate ($Al(NO_3)_3$), aluminum oxide (Al_2O_3), and metallic

aluminum (*Al*). The atomic composition was measured of 48 at% aluminum, 37 at% nitrogen, and 15 at% oxygen.

For every 100 atoms at the surface region, let u be the number of the aluminum atoms, v for nitrogen, and w for oxygen, respectively. Thus, $u+v+w = 100$. Furthermore, let w_1 and w_2 be the number of oxygen atoms bound in Al_2O_3 and $Al(NO_3)_3$, respectively. Hence, $w_1 + w_2 = w$. The 100 atoms formed a molecules of *AlN*, b molecules of $Al(NO_3)_3$, and c molecules of Al_2O_3, leaving d atoms (molecules) of *Al*. Hence, the film components were: aAlN + bAl$(NO_3)_3$ + c Al_2O_3 + dAl.

The amount of individual atoms in the film could be expressed as:

Aluminum Atom: $a + b + 2c + d = u$

Nitrogen Atom: $a + 3b = v$

Oxygen Atom:
$$\begin{cases} 3c = w_1 \\ 9b = w_2 \\ w_1 + w_2 = w \end{cases}$$

Therefore,

$$\begin{cases} a = v - {}^{w_2}\!/_{3} \\ b = {}^{w_2}\!/_{9} \\ c = {}^{w_1}\!/_{3} \\ d = u - v + {}^{2w_2}\!/_{9} - {}^{2w_1}\!/_{3} \end{cases}$$

For every 100 atoms at the surface region of the film, $u = 48$, $v = 37$, and $w = 15$. Furthermore, it was measured by XPS method that $w_1 = 8$ and $w_2 = 7$. The number of molecules formed from the 100 atoms at the surface region of the film was therefore 34.67 for *AlN* (a), 0.78 for $Al(NO_3)_3$ (b), 2.67 for Al_2O_3 (c), and 7.22 for *Al* (d). With a total of 45.34 molecules ($=a+b+c+d$), the above estimation yielded a molecular composition of 76.5% *AlN*, 1.7% $Al(NO_3)_3$, 5.9% Al_2O_3, and 15.9% *Al*.

The above estimation yielded a concentration of 7.2 at% metallic aluminum component at the film surface region. According to XPS deconvolution result, the atomic concentration of metallic aluminum was 9 at%.

Case 2. Nitride Film with an *i/a* Ratio of 0.60 on Planar Substrate

Interior Region

In the interior region, XPS results showed that the film consisted of components of aluminum nitride (*AlN*) and aluminum nitrate ($Al(NO_3)_3$). The atomic composition was 47 at% aluminum, 46 at% nitrogen, and 7 at% oxygen.

Although XPS study did not show any metallic aluminum in the film, the following estimation was assumed that a small amount of metallic aluminum (*Al*) existed in the film. For every 100 atoms at the surface region, let u be the number of the aluminum atoms, v for nitrogen, and w for oxygen, respectively. Thus, $u+v+w = 100$. The 100 atoms formed a molecules of *AlN* and b molecules of $Al(NO_3)_3$, leaving c atoms (molecules) of *Al*. Hence, the film components were: $a\mathrm{AlN} + b\mathrm{Al(NO_3)_3} + c\mathrm{Al}$.

The amount of individual atoms in the film could be expressed as:

Aluminum Atom: $a + b + c = u$
Nitrogen Atom: $a + 3b = v$
Oxygen Atom: $9b = w$

Therefore,

$$\begin{cases} a = v - w/3 \\ b = w/9 \\ c = u - v + 2w/9 \end{cases}$$

Because $u = 47$, $v = 46$, and $w = 7$, the number of molecules formed from these 100 atoms at the interior region of the film was therefore 43.67 for *AlN* (*a*), 0.78 for $Al(NO_3)_3$ (*b*), 2.56 for *Al* (c). With a total of 47.01 molecules (=*a*+*b*+*c*), the above estimation yielded a molecular composition of 92.9% *AlN*, 1.7% $Al(NO_3)_3$, 5.4% *Al*.

The above estimation suggested that a 2.56 at% of metallic aluminum component could probably exist in the film. The justification of this assumption was based on the existence of aluminum oxide on the film surface. The oxide was most likely formed by the oxidation of the metallic aluminum component at the surface. For a XPS peak from a component with such a low concentration, the neighboring dominant aluminum peaks from nitride/nitrate components would easily overshadow it.

Surface Region

At the surface region, the film consisted of three components: aluminum nitride (*AlN*), aluminum nitrate ($Al(NO_3)_3$), and aluminum oxide (Al_2O_3). The atomic composition was 44 at% aluminum, 43 at% nitrogen, and 13 at% oxygen.

For every 100 atoms at the surface region, let *u* be the number of the aluminum atoms, *v* for nitrogen, and *w* for oxygen, respectively. Thus, $u+v+w = 100$. The 100 atoms formed *a* molecules of *AlN*, *b* molecules of $Al(NO_3)_3$, and c molecules of Al_2O_3. Hence, the film components were: $a\mathrm{AlN} + b\mathrm{Al(NO_3)_3} + c\mathrm{Al_2O_3}$.

The amount of individual atoms in the film could be expressed as:

Aluminum Atom:	$a + b + 2c = u$
Nitrogen Atom:	$a + 3b = v$
Oxygen Atom:	$9b + 3c = w$

Therefore,

$$\begin{cases} a = 5v/8 + 3u/8 - w/4 \\ b = v/8 - u/8 + w/12 \\ c = 3u/8 - 3v/8 + w/12 \end{cases}$$

For every 100 atoms at the surface region of the film, $u = 44$, $v = 43$, and $w = 13$. The number of molecules formed from the 100 atoms in the surface region of the film was therefore 40.13 for *AlN* (*a*), 0.96 for $Al(NO_3)_3$ (*b*), and 1.46 for Al_2O_3 (*c*). With a total of 42.55 molecules (=*a*+*b*+*c*), the above estimation yielded a molecular composition of 94.3% *AlN*, 2.3% $Al(NO_3)_3$, and 3.4% Al_2O_3.

The above estimation yielded an atomic concentration of oxygen in nitrate of 8.6 at%, and of 4.4 at% bonded in oxide. According to the XPS, the atomic concentration of oxygen in nitrate was 7 at%, and 6 at% in oxide.

Also, because the aluminum oxide component was most likely formed by the oxidation of the metallic aluminum component in the film, the amount of the oxide component at the surface region required a molecular concentration of 6.6% metallic aluminum before the oxidation occurred. It was in a good agreement with the estimated result of 5.4% for the interior region.

Case 3. Nitride Film Deposited on SiC Particles

General Assumptions

For nitride films deposited on SiC particles, the films were presumably formed in two stages. The first stage was the Active Deposition where most of the film components were deposited from the coating fluxes. In the second stage, other components were

formed by oxidization. These two stages of deposition took place in turn during the film depositions because of the levitation of the SiC particles.

At the first stage where active depositions took place, all arrival aluminum and nitrogen atoms were incorporated into the film on the particle surface. Such an assumption gave the film a *N-to-Al* atomic ratio the same as the atomic arrival ratio of *N-to-Al* in the depositing fluxes. The arrival ratio of *N-to-Al* was converted from the *i/a* ratio using a factor of 1.787 [Netterfield, 1988].

Oxygen atoms from the impinging of the residual oxygen and water molecules in the deposition chamber were incorporated into the film, bonded in aluminum nitrate. After the first stage of deposition, the films consisted of aluminum nitride, aluminum nitrate, and metallic aluminum.

At the second stage of the film deposition, all the metallic aluminum component in the film was oxidized by the impingement of the residual oxygen and water molecules, in the absence of the aluminum and nitrogen fluxes. Hence, after the second stage of deposition, the film consisted of three molecular components: aluminum nitride, aluminum nitrate, and aluminum oxide.

The following two sections discussed in detail the composition of nitride films deposited at both 593 K and 793 K. Averaged data were used in estimations. All components in the films in both deposition stages were assumed stoichiometric.

Film Deposited at 593 K with an *i/a* Ratio of 0.56

The nitride film deposited at 593 K had an averaged *i/a* ratio of 0.56 that gave a *N-to-Al* atomic arrival ratio of unity [Netterfield, 1988]. The film composition was

expressed as $Al_1N_1O_x$ after the first stage of deposition. The oxygen content was originated from the impingement of oxygen and water molecules in the chamber.

During deposition, the partial pressures of oxygen molecules (P_{O_2}) and water molecules (P_{H_2O}) in the deposition chamber were both 1.3×10^{-5} Pa. The averaged arrival rate (J_i) of the nitrogen ions was 4.85×10^{14} (ions·cm^{-2}·sec^{-1}). The ambient temperature (T) was 300 K. The *i/a* ratio was 0.56. Using equations derived in Chapter 4, the oxygen atomic concentration in the film after the first stage was calculated as:

$$C_O = C_O^{O_2} + C_O^{H_2O} = (5.21\times10^{19}P_{O_2} + 3.27\times10^{19}P_{H_2O})\frac{1}{J_i(1+\frac{1}{1.787\cdot i/a})\sqrt{T}}$$

$$=(5.21\times10^{19} + 3.27\times10^{19})\frac{1.3\times10^{-5}}{4.85\times10^{14}(1+0.99)\sqrt{300}} = 0.07 = 7.0 \text{ at\%}.$$

Therefore, after the first stage of deposition, the atomic composition of the film was 46.5 at% aluminum, 46.5 at% nitrogen, and 7.0 at% oxygen.

After the first stage of deposition, the film was a mixture of aluminum nitride (*AlN*), aluminum nitrate ($Al(NO_3)_3$), and metallic aluminum (*Al*). For every 100 atoms in the film, 46.5 atoms were aluminum, 46.5 for nitrogen, and 7 for oxygen, respectively. The 100 atoms formed *a* molecules of *AlN*, *b* molecules of $Al(NO_3)_3$, and *c* atoms (molecules) of *Al*. Hence, the film components were: aAlN + bAl$(NO_3)_3$ + cAl. The amount of individual atoms in the film was expressed as:

Aluminum Atom:	$a+b+c=46.5$
Nitrogen Atom:	$a+3b=46.5$
Oxygen Atom:	$9b=7$

Therefore, the number of molecules formed from every 100 atoms in the film was 44.1 for *AlN* (*a*), 0.8 for $Al(NO_3)_3$ (*b*), and 1.6 for *Al* (*c*) after the first stage of deposition.

For every 100 atoms in the film after the first stage, 1.6 atoms were metallic aluminum. At the second stage of film deposition, the 1.6 atoms of metallic aluminum component was oxidized into aluminum oxide (Al_2O_3), incorporating an additional of 2.4 oxygen atoms into the film. Within the 102.4 (=100+2.4) atoms, 46.5 of them were aluminum, 46.5 for nitrogen and 9.4 for the oxygen. These 102.4 atoms in the film after the second stage would form 44.1 molecules of AlN, 0.8 molecules of $Al(NO_3)_3$, and 0.8 molecules of Al_2O_3.

Therefore, the nitride film deposited at 593 K with an averaged *i/a* ratio of 0.56 was estimated to consist of an atomic composition of 45.4 at% aluminum, 45.4 at% nitrogen, and 9.2 at% oxygen. The molecular composition of the film was estimated of 1.8% $Al(NO_3)_3$, 1.8% Al_2O_3, and 96.4% AlN.

Film Deposited at 793 K with an *i/a* Ratio of 0.53

The nitride film deposited at 793 K had an *i/a* arrival ratio of 0.53 that was equivalent to an atomic *N-to-Al* ratio of 0.95 [Netterfield, 1988]. After the first stage of deposition, the film composition was expressed as $Al_1N_{0.95}O_x$. The oxygen content was originated from the impingement of the oxygen and water molecules in the chamber.

During the deposition, the partial pressures of oxygen molecules (P_{O_2}) and water molecules (P_{H_2O}) in the deposition chamber were both 1.3×10^{-5} Pa. The averaged arrival rate (J_i) of nitrogen ions was 3.4×10^{14} (ions·cm^{-2}·sec^{-1}). The *i/a* ratio was 0.53. The ambient temperature (T) was 350 K. Using the equation derived in Chapter 4, the oxygen atomic concentration in the film after the first stage was estimated as the following:

$$C_O = C_O^{O_2} + C_O^{H_2O} = (5.21\times10^{19}P_{O_2} + 3.27\times10^{19}P_{H_2O})\frac{1}{J_i(1+\frac{1}{1.787\cdot i/a})\sqrt{T}}$$

$$=(5.21\times10^{19} + 3.27\times10^{19})\frac{1.3\times10^{-5}}{4.85\times10^{14}(1+1.06)\sqrt{350}} = 0.059 = 5.9 \text{ at\%}.$$

Thus, after the first stage of deposition, the atomic composition of the film was estimated of 48.3 at% aluminum, 45.8 at% nitrogen, and 5.9 at% oxygen.

After the first stage of film deposition, the film was a mixture of aluminum nitride (*AlN*), aluminum nitrate ($Al(NO_3)_3$), and metallic aluminum (*Al*). For every 100 atoms in the film, 48.3 atoms were aluminum, 45.8 for nitrogen, and 5.9 for oxygen, respectively. The 100 atoms formed *a* molecules of *AlN*, *b* molecules of $Al(NO_3)_3$, and *c* atoms (molecules) of *Al*. Hence, the film components were: $a\text{AlN} + b\text{Al(NO}_3)_3 + c\text{Al}$. The amount of individual atoms in the film can be expressed as:

Aluminum Atom:	$a + b + c = 48.3$
Nitrogen Atom:	$a + 3b = 45.8$
Oxygen Atom:	$9b = 5.9$

Therefore, the number of molecules formed from every 100 atoms in the film was 43.8 for *AlN* (*a*), 0.7 for $Al(NO_3)_3$ (*b*), and 3.8 for *Al* (*c*) after the first stage of deposition.

For every 100 atoms in the film after the first stage, 3.8 of them were metallic aluminum. At the second stage of film deposition, the 3.8 atoms of metallic aluminum component in the film was oxidized into aluminum oxide (Al_2O_3), incorporating an additional of 5.7 oxygen atoms into film. Within the 105.7 (=100+5.7) atoms after the second stage of deposition, 48.3 of them were aluminum, 45.8 were nitrogen, and 11.6 were the oxygen. These atoms formed 43.8 molecules of *AlN*, 0.7 molecules of $Al(NO_3)_3$, and 1.9 molecules of Al_2O_3.

After deposition, therefore, the nitride film deposited at 793 K with an averaged *i/a* ratio of 0.53 was estimated to have an atomic composition of 45.7 at% aluminum, 43.3 at% nitrogen, and 11.0 at% oxygen. In terms of molecular concentration, the film consisted of 94.4% *AlN*, 1.5% $Al(NO_3)_3$, and 4.1% Al_2O_3.

BIBLIOGRAPHY

BIBLIOGRAPHY

Balluffi, R.W., Blakely, J.M., *Thin Solid Films*, Vol. 25, pp. 363, 1975.

Behrisch, R., ed., *Sputtering by Particle Bombardment I.*, Springer-Verlag, 1981.

Behrisch, R., ed., *Sputtering by Particle Bombardment II.*, Springer-Verlag, 1983.

Behrisch, R., Wittmaack, K., ed., *Sputtering by Particle Bombardment III.*, Springer-Verlag, 1991.

Brindley, P. K., *High-Temperature Ordered Intermetallic Alloys. II*, pp. 419, 1987.

Broutman, L.J. and Krock, R.H., *Composite Materials Vol. 1: Interfaces in Metal Matrix Composites*, ed. by Metcalfe, A.G., Academic Press, 1974.

Bunshah, R.F., *Deposition Technologies for Films and Coatings. Developments and Applications*, ed. by Bunshah, R.F., et. al., pp. 83, 1984.

Bunshah, R.F., Deshpandey, C., in *Physics of Thin Films*, Vol. 13, ed. by Francombe, M.H., Vossen, J.L., Academic Press, New York, 1987.

Cai, Z., Thesis for the Degree of M.S., Michigan State University, 1992.

Cairns, J.A., Nelson, R.S., Baunfield, R.W., *British Patent 55466/72*, 1972.

Chambers, A., Fitch, R.K., Halliday, B.S., ed., *Basic Vacuum Technology*, 1989.

Chou, T.C., Joshi, A., Wadsworth, J., *J. Vac. Sci. Technol.*, Vol. 9(3), pp. 1525, 1991.

Chou, T.W., Kelly, A., and Okura, A., *Composites*, Vol. 16, pp. 187, 1985.

Chou, T.C., Nieh, T.G., (a), *Scripta, Metall.*, Vol. 25, pp. 2059, 1991.

Chou, T.C., Nieh, T.G., (b), *High-Temp. Ordered Intermetallic Alloys IV*, ed. by Johnson, L.A., et. al., pp. 1045, 1991.

Gardner, D.S., Flinn, P.A., *IEEE Transa.on Electron Devices*, Vol. 35(12), pp. 2160, 1988.

Gilmer, G.H., and Farrell, H.H., (a), *J. Applied Phy.*, Vol. 47(9), pp. 3792, 1976.

Gilmer, G.H., and Farrell, H.H., (b), *J. Applied Phy.*, Vol. 47(10), pp. 4373, 1976.

Glang, R., in *Handbook of Thin Film Technology*, ed. by Maissel, L.I., and Glang, R., McGraw-Hill, New York, 1970.

Goshtagore, R. N., *J. Appl. Phys.*, 40, pp. 4374, 1969.

Grayson, M., ed., *Encyclopedia of Composite Materials and Components*, 1983.

Gupta, D., Camplell, D.R., Ho, P.S., in *Thin Films - Interdiffusion and Reaction*, ed. by Poate, J.M., Tu, K.N., Mayer, J.W., 1978.

Gupta, D., Ho, P.S., ed., *Diffusion Phenomena in Thin Films and Microelectronic Materials*, Noyes Publications, 1988.

Hall, E.L., Kouh, Y.M., Jackson, M.R., Mehan, R.L., *Met. Trans. A.*, Vol. 14A, pp. 781, 1983.

Harper, J.M.E., Cuomo, J.J., Kaufman, H.R., *Ann. Rev. Mater. Sci.*, Vol. 13, pp. 413, 1983.

Harper, J.M.E., Cuomo, J.J., Kaufman, H.R., *J. Vac. Sci. Technol.*, Vol. 21(3), pp. 737, 1982.

Harper, J.M.E., Cuomo, J.J., Hentzell, H.T.G., *J. Appl. Phys.*, Vol. 58, pp. 550, 1985.

Hentzell, H.T.G., Harper, J.M.E., Cuomo, J.J., *J. Appl. Phys.*, Vol. 58, pp. 556, 1985.

Hillegas, W., Solohill Eng., Ann Arbor, Michigan, Private Communication, 1990.

Holland, L., *Science and Technology of Surface Coating*, ed. by Chapman, B.N., Academic Press, 1974.

Jackson, M.R., Mehan, R.L., Davis, A.M., Hall, E.L., *Metall. Trans. A.*, Vol. 14A, pp. 355, 1983.

Kattelus, H.P., Nicolet, M.-A., in *Diffusion Phenomena in Thin Films and Microelectronic Materisals*, ed. by Gupta, D., and Ho, P.S., pp. 432, 1988.

Kaufman, H.R., Cuomo, J.J., Harper, J.M.E., *J. Vac. Sci. Technol.*, Vol. 21(3), pp. 725, 1982.

Kaufman, H.R., Robinson, R.S., *Operation of Braod-Beam Sources*, Commonwealth Scientific Corporation, 1987.

Kingery, W.D., Bowen, H.K., Unlmann, D.R., ed., *Introduction to Ceramics*, second edition, John Wiley & Sons, 1976.

LeClaire, A.D., *Brit. J. Appl. Phys.*, Vol. 14, pp. 351, 1963.

Loretto, M.H., ed., *Electron Beam Analysis of Materials*, Chapman and Hall, 1984.

Lowell, C.E., Barrett, C.A., Whitternberger, J.D., *Intermetallic Matrix Composites*, ed. by Anton, D.L., et. al., pp. 355, 1990.

Mattox, D., *Materials Research Society Short Course on Films and Coating Deposition Techniques*, 1989.

Mehan, R.L., Bolon, R.B., *J. Mat. Sci.*, Vol. 14, pp. 2471 - 2481, 1979.

Metcalfe, A.G., *Composite Materials, Vol. 4: Metallic Matrix Composties*, ed. by Kreider, K.G.,.pp. 269,1974.

Moulder, J.F., Stickle, W.F., Sobol, P.E., Bomben, K.D., *Handbook of X-ray Photoelectron Spectroscopy*, ed. by Chastain, Perkin-Elmer Corporation, 1992.

Movchan, B.A., Demchishin, A.V., *Phys. Met. Metallogr.*, Vol. 28, pp. 83, 1969.

Netterfield, R.P., Muller, K.-H., McKenzie, D.R., Goonan, M.J., Martin, P.J., *J. Appl. Phys.*, Vol. 63(3), pp. 760, 1988.

Nicolet, M.-A., *Thin Solid Films*, Vol. 52, pp. 415, 1978.

Nieh, T.G., Stephens, J.J., Wadsworth, J., Liu, C.T., *Interfaces in Polymer, Ceramic, and Metal Matrix Composites*, ed. by Ishida, H., pp. 215, 1989.

Nourbakhsh, S., Margolin, H., and Liang, F. L., *Metall. Trans. A*, Vol. 20A , pp. 2159, 1989.

Ohring, M., ed., *The Materials Science of Thin Films*, 1991.

Poluboyarinov, D.N., Gordova, M.R., Kuznetsova, I.G., Bershadskaya, M.D., Avetikov, V.G., *Inorganic Materials*, Vol. 15(11), pp. 1617, 1980.

Pope, D. P., *High-Temperature Ordered Intermetallic Alloys II.*, pp. 3, 1987.

Pulker, H., *Coating on Glass*, Elsevier, Amsterdam, 1984.

Reddy, S.N.S., Betrabet, H.S., Purnshothaman, S.P., Narayan, C., *Ceram. Eng. Sci. Pro.*, Vol. 10(11/12), pp. 1696, 1989.

Russ, J.C., ed., *Fundamentals of Energy Dispersive X-ray Analysis*, Butterworths & Co. Ltd., 1984.

Schoutens, J. E., Tempo, K., *Introduction to Metal Matrix Copmposite Materials*, DOD MMCIAC #272, June 1982.

Shaffer, P.T.B., ed., *Plenum Press Handbooks of High-Temperature Materials. No. 1, Materials Index*, 1964.

Sheppard, L.M., *Ceramic Bulletin*, Vol. 69, pp. 1801, 1990.

Shewmon, P.G., ed., *Diffusion in Solids*, McGraw-Hill, 1963.

Smallman, R.E., *Modern Physical Metallurgy*, Butterworths, 1985.

Stelmack, L.A., Thurman, C.T., Thompson, G.R., *Nuclear Instruments and Methods in Physics Research, B*, Vol. 37/38, pp. 787, 1989.

Taylor, J.A., Rabalais, J.W., *J. Chem. Phys.*, Vol. 75, pp. 1735, 1981.

Thornton, J.A., *Ann. Rev. Mat. Sci.*, Vol. 7, pp. 239, 1977.

Thornton, J.A., Hoffman, D.W., *Thin Solid Films*, Vol. 171, pp. 5, 1989.

Walls, J.M., ed., *Methods of Surface Analysis*, Cambridege University Press, 1989.

Walters, R. P., Covino, B. S., Jr., *Metall. Trans. A.*, 19A, pp. 2163, 1988.

Westwood, W.D., *Materials Research Society Bulletin*, pp. 46, Dec. 1988.

Whipple, R.T.P., *Philo. Mag.*, Vol. 45, pp. 1225, 1954.

Yang, J.-M., Kao, W.H., Liu, C.T., (a), *Mat. Sci. Eng.*, Vol. A107, pp. 81, 1989.

Yang, J.-M., Kao, W.H., Liu, C.T., (b), *High Temp. Ordered Intermetallic Alloys III*, pp. 453, 1989.

Zangvil, A., Ruh, R., *Mat. Sci. Eng.*, Vol. 71, pp. 159, 1985.

FIGURES

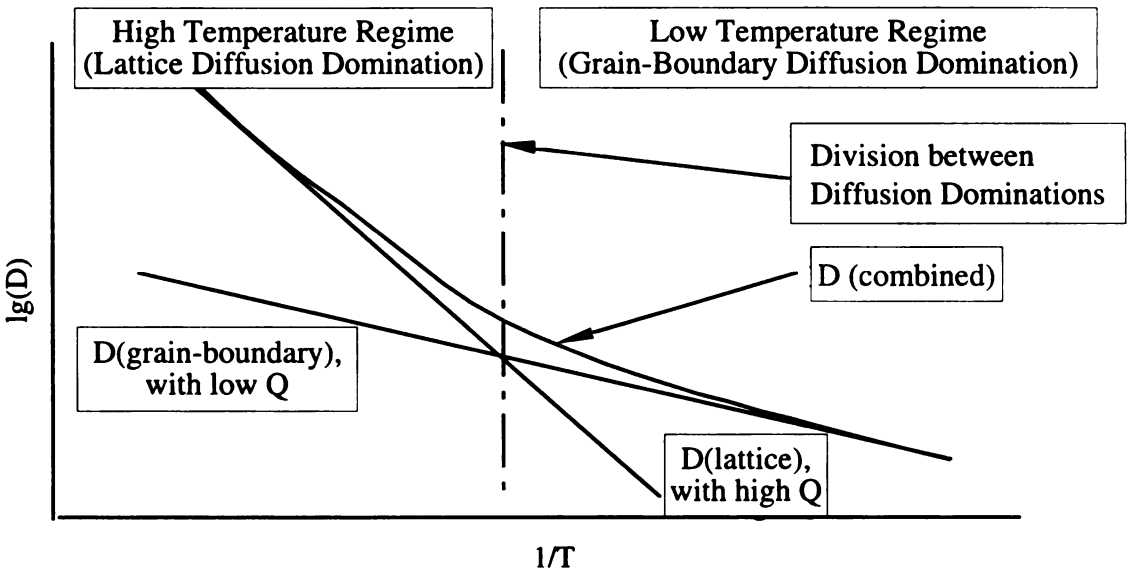

Figure 2.1. Illustration of Temperature Regimes of Dominant Diffusion Mechanisms.

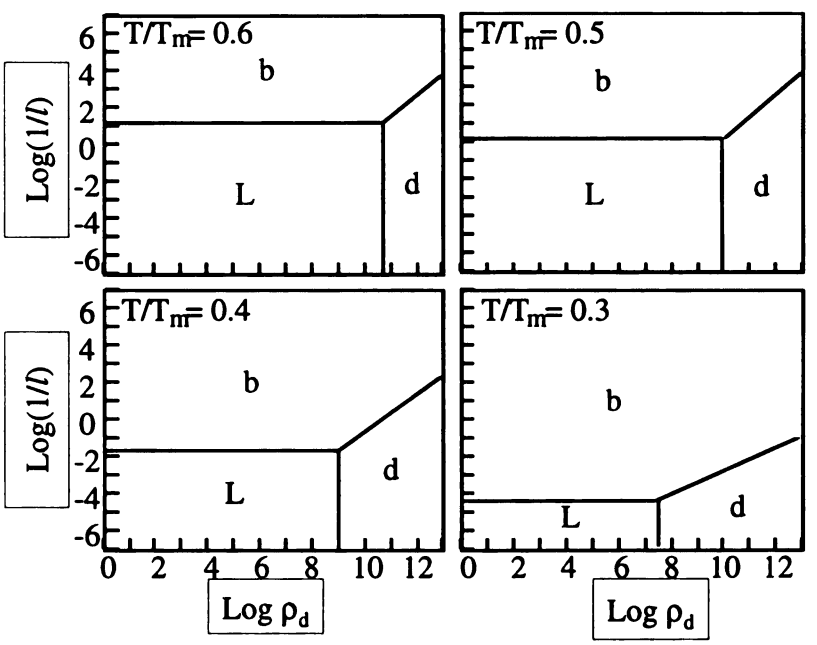

Figure 2.2. Regimes of Dominant Diffusion Mechanism in FCC Metal Films [after Balluffi, 1975].

l: Grain Size (in cm)
ρ_d: Dislocation Density (in cm^{-2})
L: Lattice Diffusion Dominant
b: Grain-Boundary Diffusion Dominant
d: Dislocation Diffusion Dominant

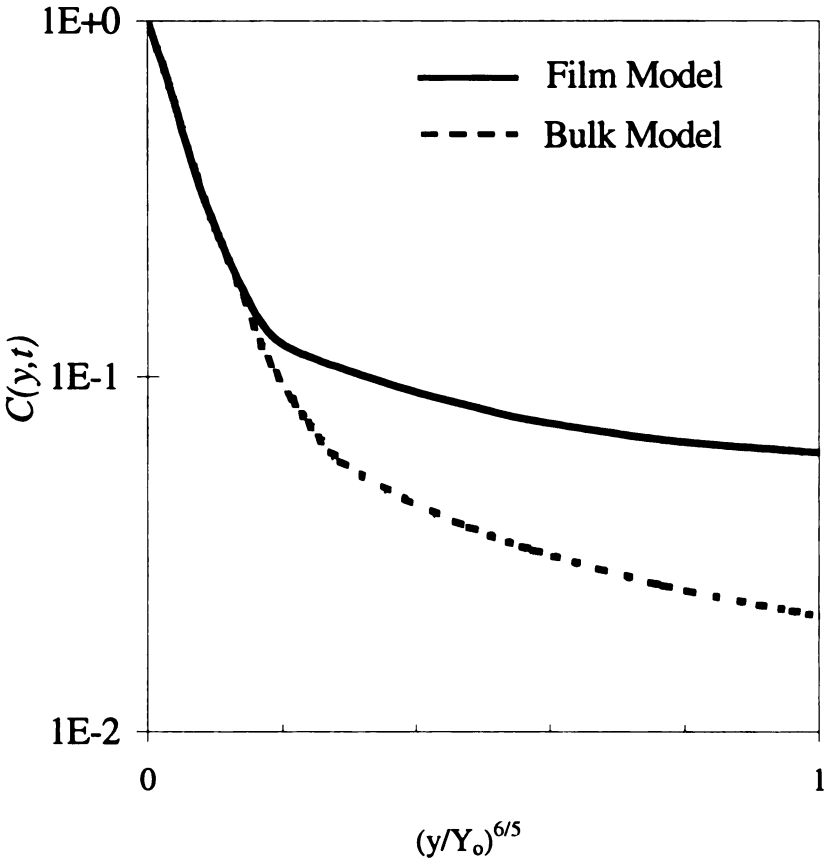

Figure 2.3. A Comparison of Concentrational Profiles between the Film and Bulk Models [after Gilmer, 1976a].
Y_o: Film thickness y: Distance from the source interface

The high diffusant concentration in thin film is attributed to the boundary condition of a free surface imposed to the thin film model.

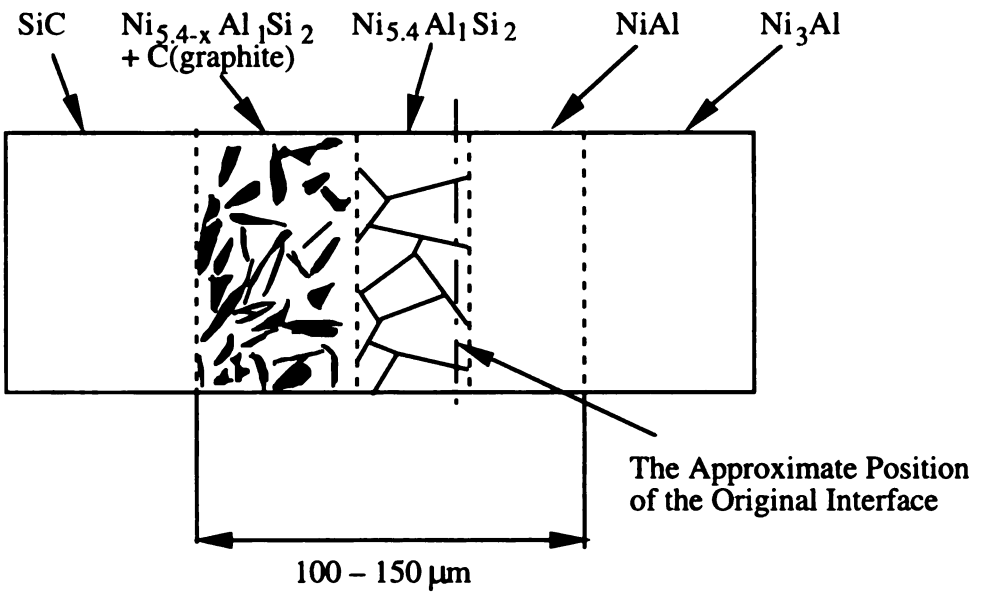

Figure 2.4. Schematic Presentation of Reaction Zone between SiC and γ-Ni_3Al at 1273 K for 23 Hours [Chou, 1991b].

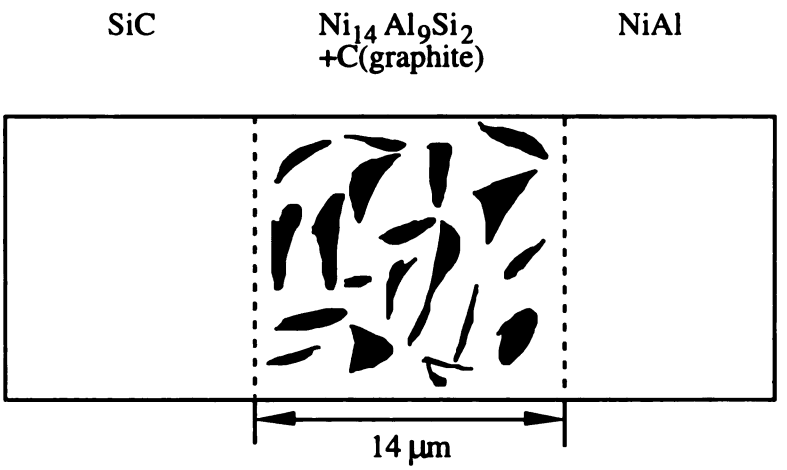

Figure 2.5. Schematic Presentation of Reaction Zone between SiC and β-NiAl at 1573 K for 20 Hours [Chou, 1991a].

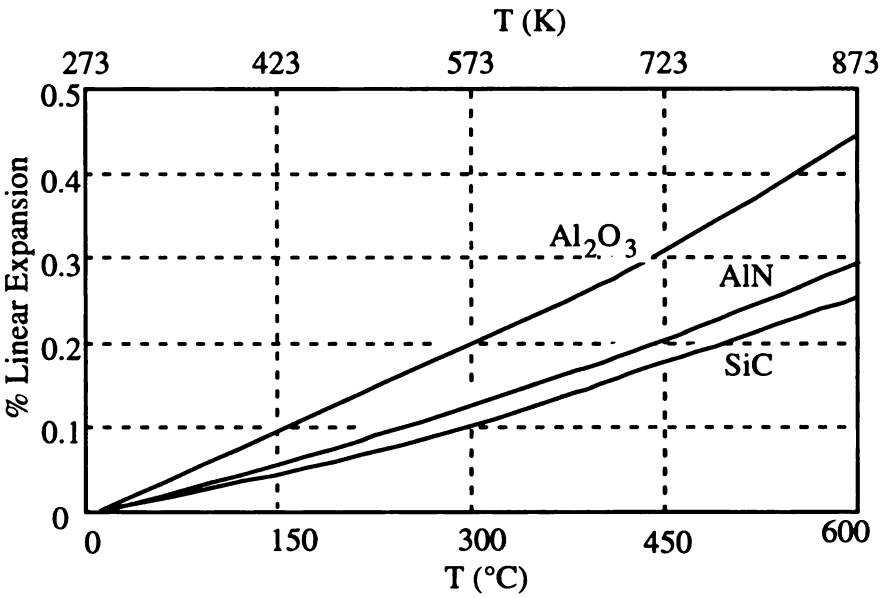

Figure 2.6. A Comparison of Linear Thermal Expansion of AlN, SiC, and Al_2O_3 [after Carborumdum Co., 1992].

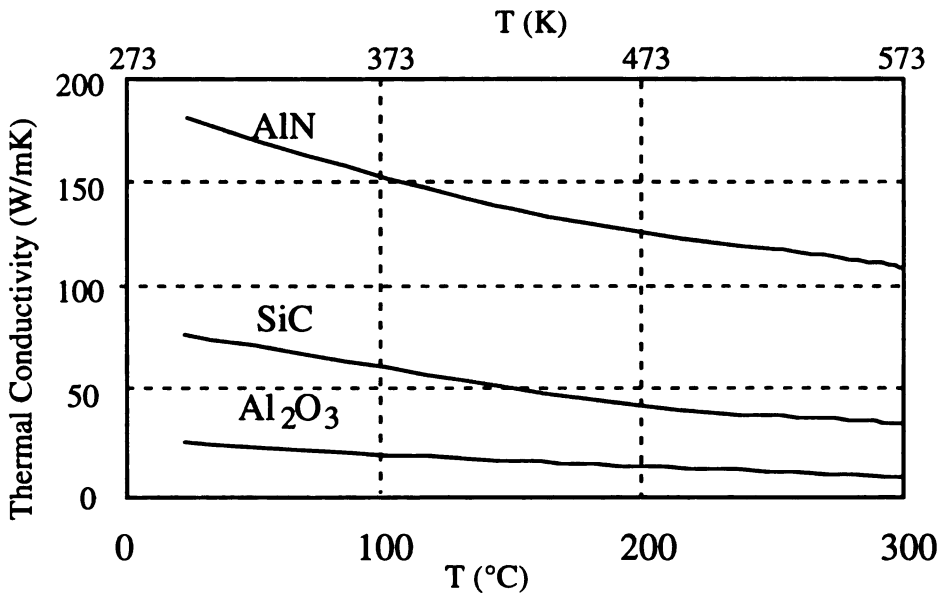

Figure 2.7. A Comparison of Thermal Conductivity of AlN, SiC, and Al_2O_3 [after Carborumdum Co., 1992].

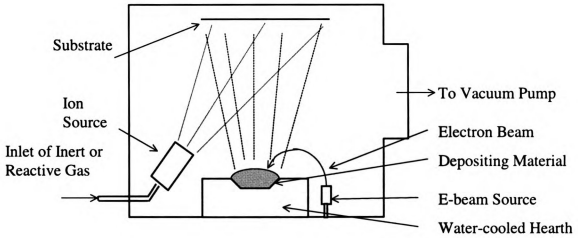

Figure 2.8. Schematic Configuration for Ion-Beam-Assisted Electron-Beam Evaporation.

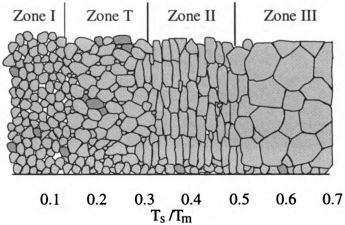

Figure 2.9. Schema of Zone Structures in Evaporated Thin Films [after Movchan, 1969].
Films with Zone I structure consist of small tapered crystals with voided boundaries. Zone T structure has a mixture of small and large grains, which produces a dense film. Zone II structure offers a columnar grains and dense grain boundaries. Zone III structure is only formed at high deposition temperature, consisting of large equiaxed grains.

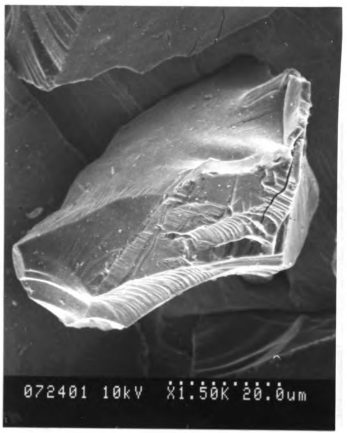

Figure 3.1. A SEM Photo of an As-Received SiC Particle.
The SiC particle was embedded in an Indium foil. The nominal SiC particle size was 60 μm.

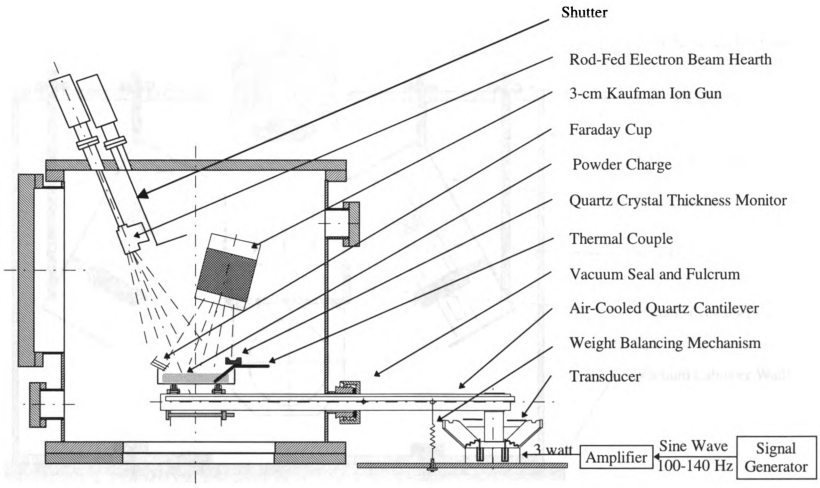

Figure 3.2. Configuration of an IBAD System for Deposition on Particulate Substrates.

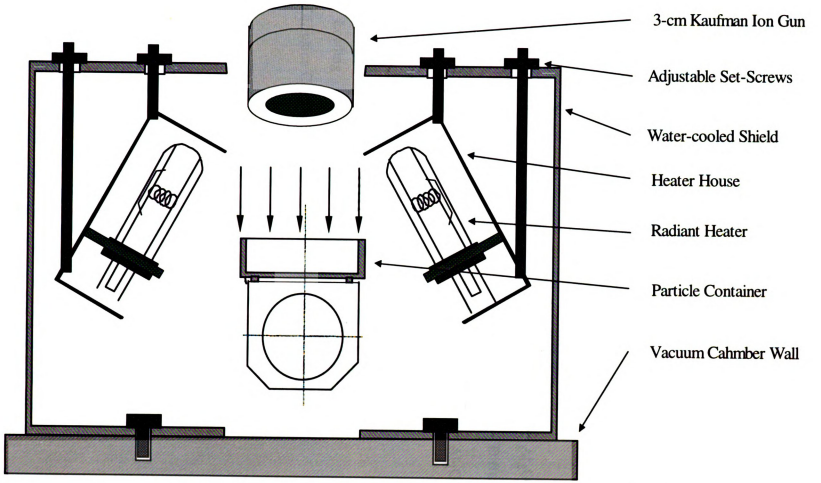

Figure 3.3. Illustration of the Arrangement of the Heater Compartment for the Particle Levitation System.

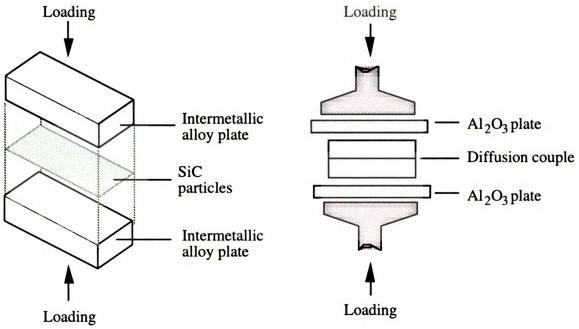

Figure 3.4. Configuration for Hot-Pressing.

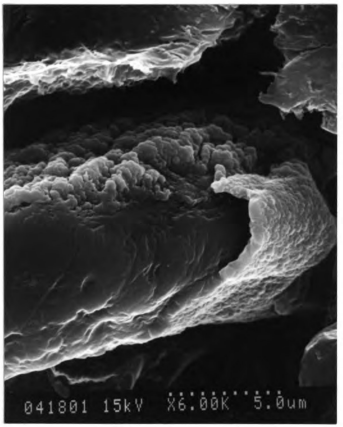

(a). A Polished As-deposited SiC Particle

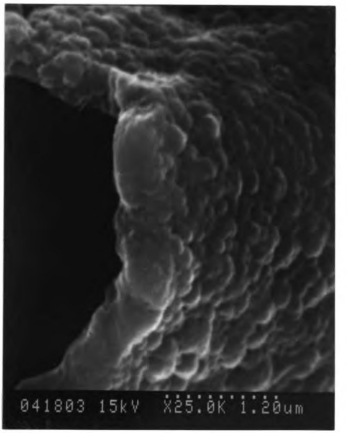

(b). Magnified Cross-section of the Aluminum Nitride Film

Figure 4.1. Cross-section of Aluminum Nitride Film on a SiC Particle, Deposited at 793 K.
The coated SiC particle was embedded in resin and polished to reveal film's cross-section. Part of the film was de-bonded during the polishing. The sample was gold-coated prior to the SEM study.

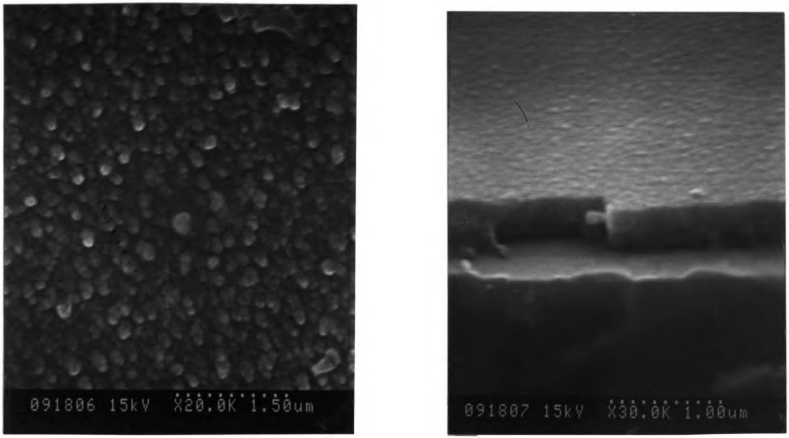

(a). Aluminum Nitride Film Surface

(b). Film Cross-section on a Glass Slide

Figure 4.2. Aluminum Nitride Film on a Planar Substrate, Deposited at 593K.

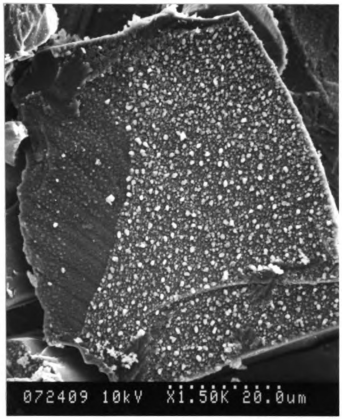

(a). An Aluminum Nitride Film Coated SiC Particle

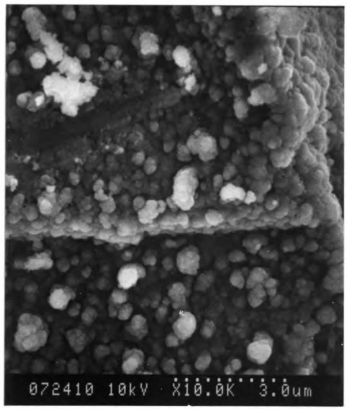

(b). Film Morphology on the SiC Particle

Figure 4.3. Aluminum Nitride Film on a SiC Particle, after a 9.75-hour Deposition at 593 K.
The nitride film on the SiC particle had a voided globular structure. The film consisted of clusters of small grains. The grains in the film were less than 0.2 μm in size. The size of the grain clusters were varied. The average cluster size was about 0.3 μm.

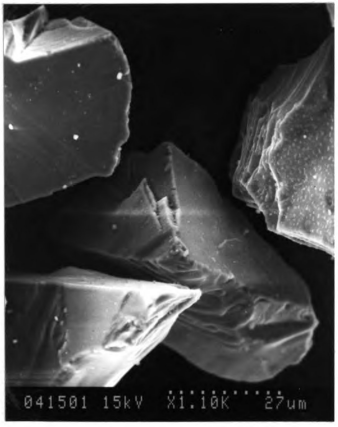

(a). Aluminum Nitride Film Coated SiC Particles

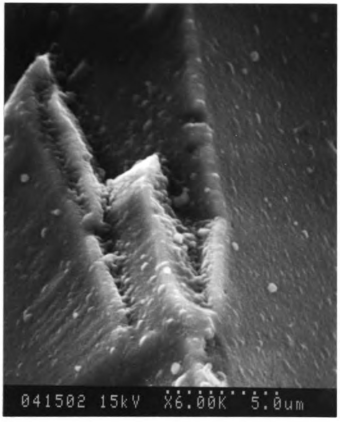

(b). Film Morphology on a SiC particle

Figure 4.4. Aluminum Nitride Film on a SiC Particle, after a 25-hour Deposition at 793 K.
The nitride film deposited on SiC particles at 793 K had a smooth film morphology. Edges of the SiC particles were well coated with the smooth nitride film.

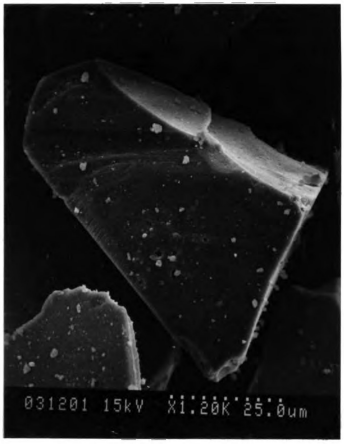

(a). Aluminum Oxide Film Coated SiC Particles

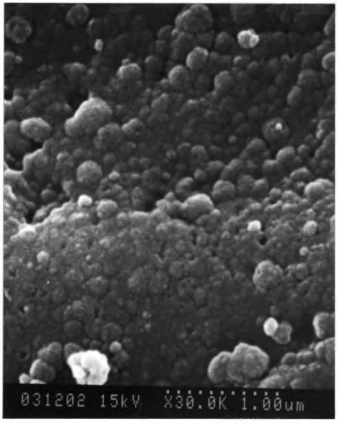

(b). Film Morphology near Edge Area on a SiC particle

Figure 4.5. Aluminum Oxide Film on SiC Particles, after a 6-hour Deposition at Room Temperature.
The oxide film deposited on SiC particles had an overall smooth film morphology. At the edges of the SiC particles, some globular feature was observed in film morphology.

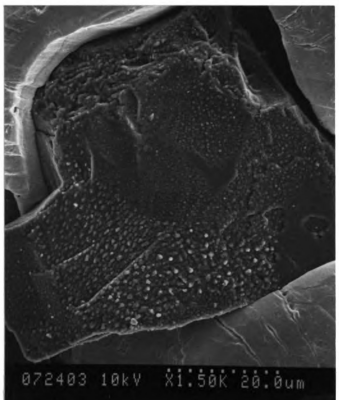

(a). An Aluminum Nitride Coated SiC Particle

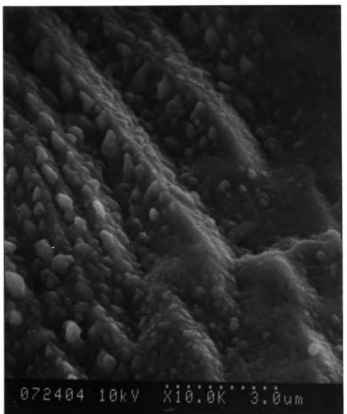

(b). Morphology of the Coated SiC Particle

Figure 4.6. Aluminum Nitride Film on a SiC Particle, after a 2-hour Deposition at 593 K.
The SiC particle was not fully covered by the nitride material. Some SiC surface was exposed after the 2-hour deposition. Individual crystallites and clusters of crystallites of the film material were observed on the SiC surface.

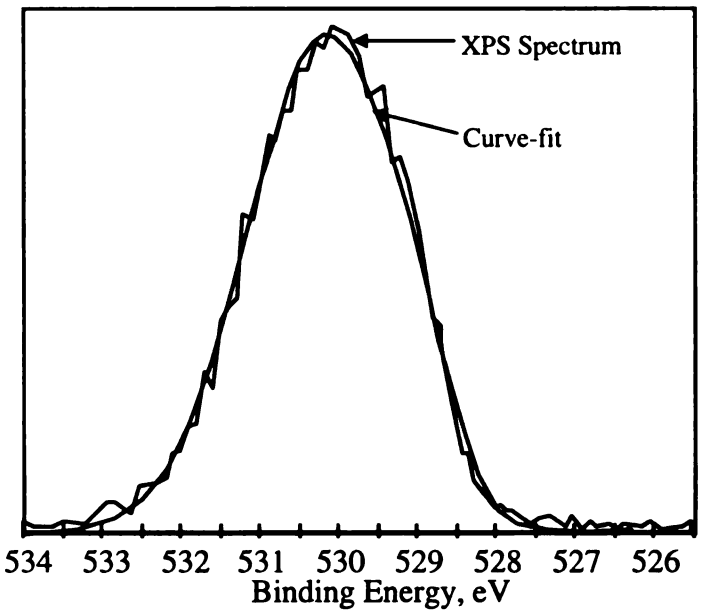

(a). Oxygen Peak

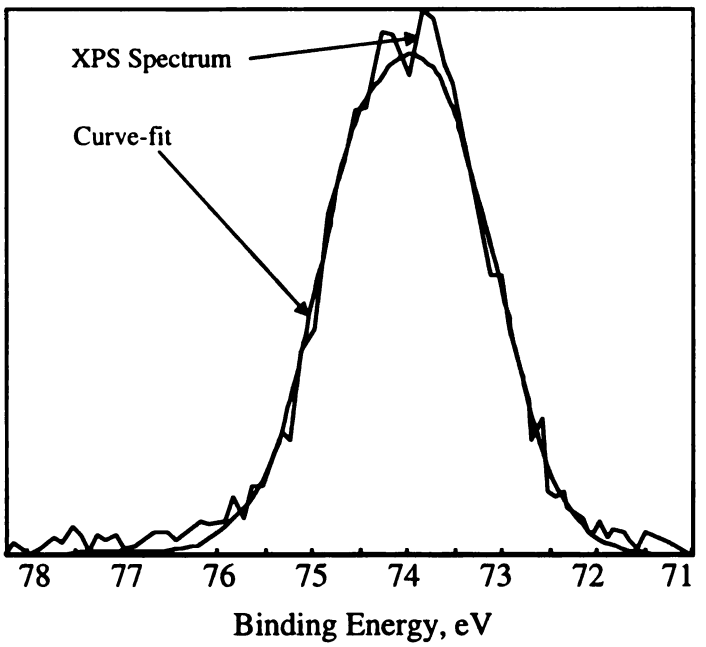

(b). Aluminum Peak

Figure 4.7. XPS Peaks from an Aluminum Oxide Film Deposited at Room Temperature, after Curve-fit.
Both peaks were generated from aluminum oxide. The composition was calculated to be $Al_{38}O_{62}$. The sample was determined to be nominally stoichiometric aluminum oxide.

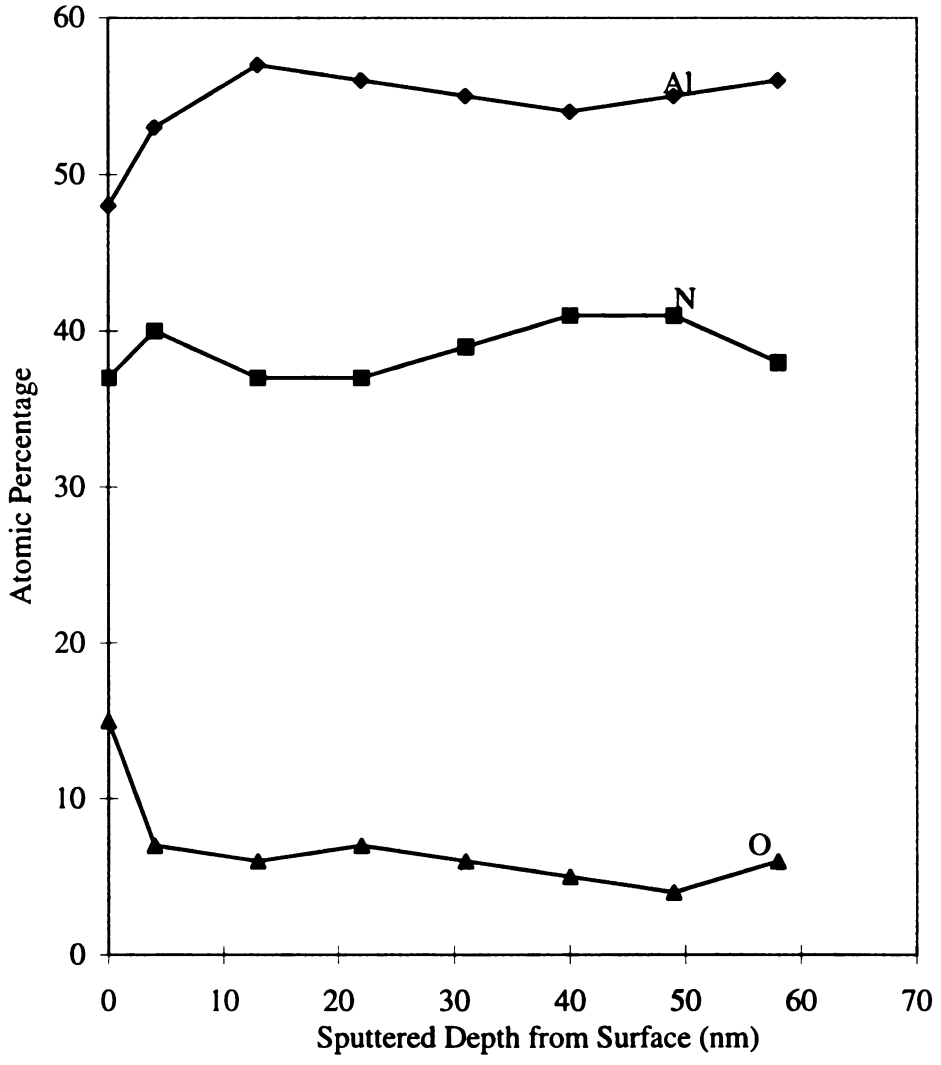

Figure 4.8. XPS Concentrational Profile of an Aluminum Nitride Film Deposited at 793 K with an *i/a* of 0.42.
The *N-to-Al* ratio in the film were corresponding to the *i/a* ratio of 0.42. A 5 – 7 at% oxygen content existed throughout the film. The higher oxygen content near film surface region was attributed to the oxidization after exposing the film to air.

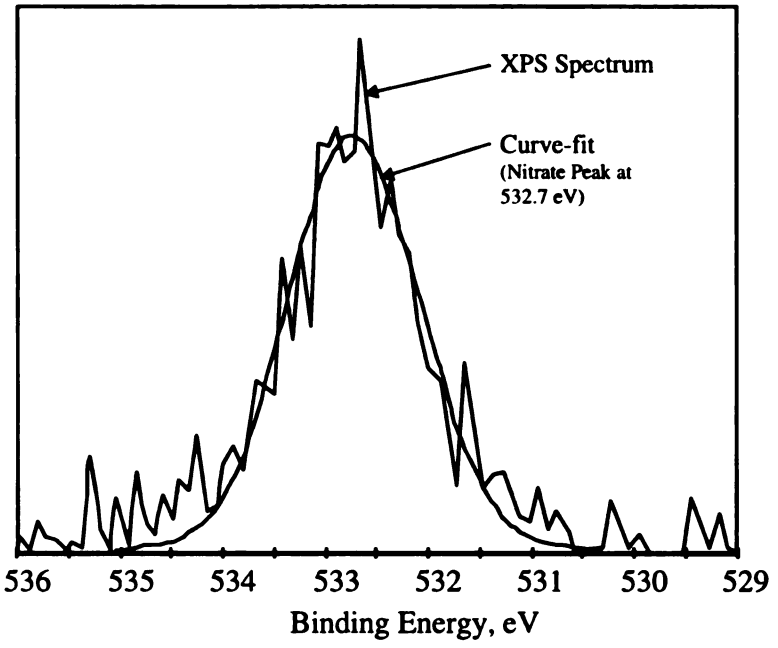

(a). Oxygen Peak, with Curve-fit

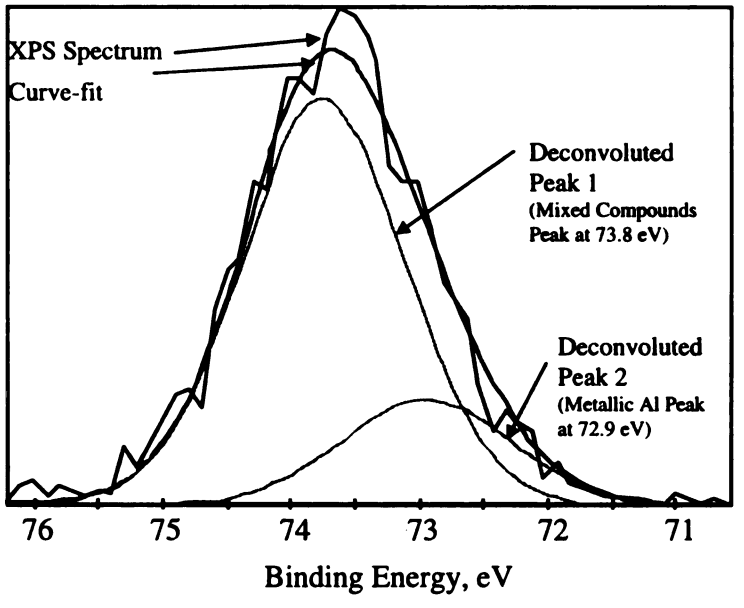

(b). Aluminum Peak, after Deconvolution

Figure 4.9. XPS Peaks from an Aluminum Nitride Film Deposited at 793 K with an *i/a* of 0.42, 40 nm below the Original Film Surface.
The XPS peaks of oxygen and aluminum indicated the existence of aluminum nitrate and metallic aluminum components inside the nitride film.

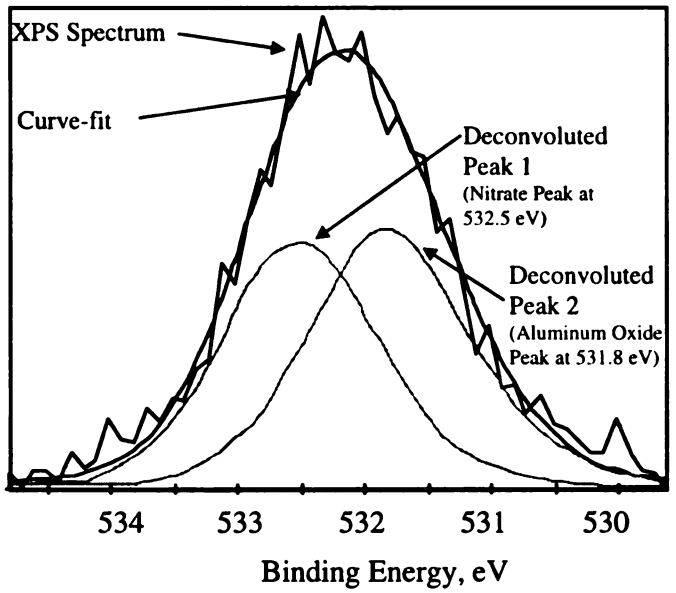

(a). Oxygen Peak, after Deconvolution

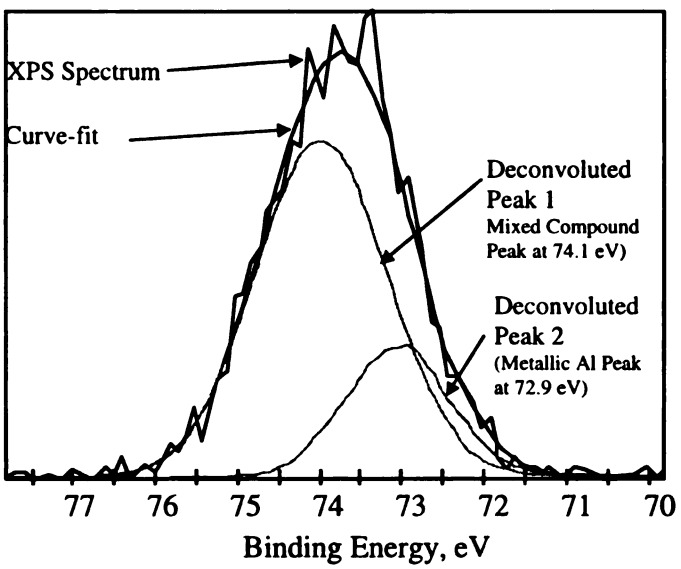

(b). Aluminum Peak, after Deconvolution

Figure 4.10. XPS Peaks from an Aluminum Nitride Film Deposited at 793 K with an *i/a* of 0.42, at Surface Region.
The XPS peaks of oxygen and aluminum indicated the existence of aluminum nitrate, aluminum oxide, and metallic aluminum components on the surface of the nitride film.

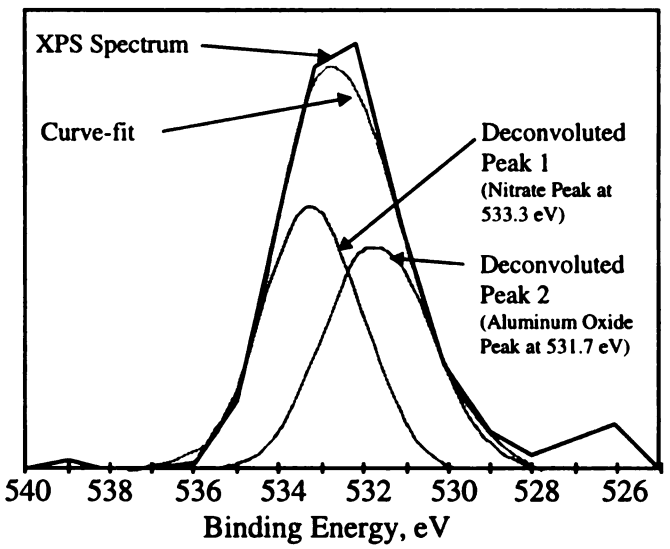

Figure 4.11. The XPS Oxygen Peak from an Aluminum Nitride Film Deposited at 593 K with an *i/a* of 0.60, Surface Region.
The oxygen XPS peak indicated the existence of aluminum nitrate and aluminum oxide components on the surface of the nitride film.

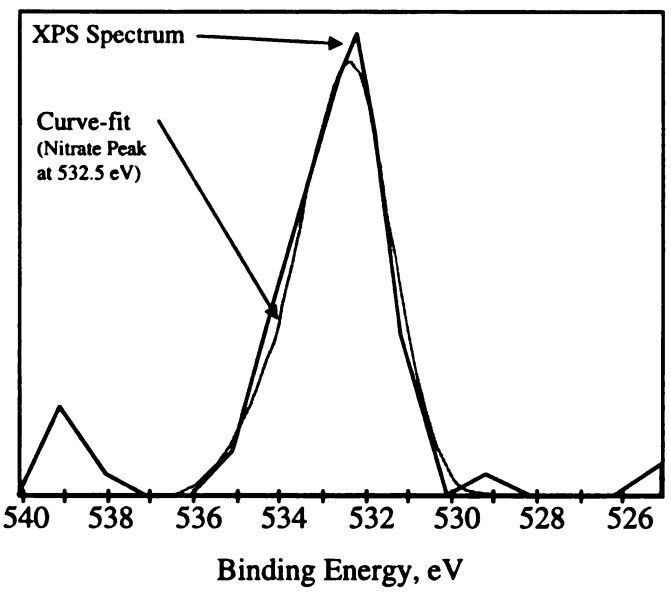

Figure 4.12. The XPS Oxygen Peak from an Aluminum Nitride Film Deposited at 593 K with an *i/a* of 0.60, 20 nm below the Original Film Surface.
The oxygen XPS peak indicated the existence of aluminum nitrate component inside the nitride film.

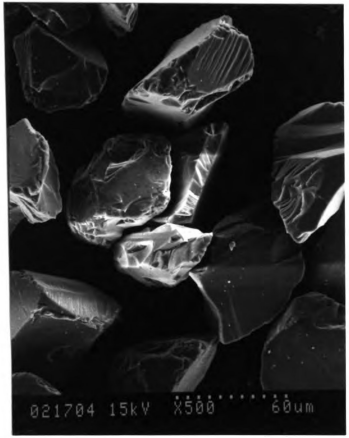

(a). Coated SiC Particles after Annealing

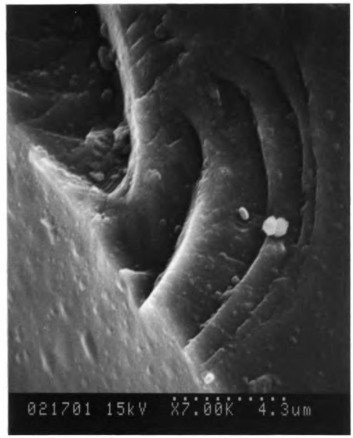

(b). Film Morphology on a SiC Particle

Figure 4.13. Aluminum Nitride Film Deposited on SiC Particles at 793 K, after Air-cooling from 1273 K to Room Temperature.
The film morphology after the annealing showed the same smoothness as compared with the film morphology before the annealing.

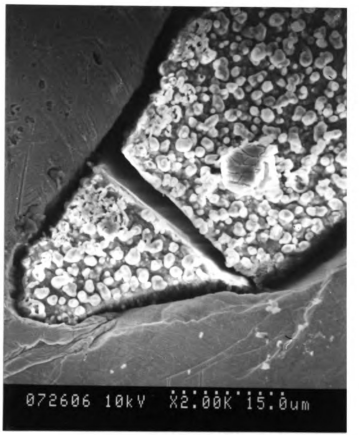

Figure 4.14. Aluminum Nitride Film Deposited on SiC Particle at 593 K, after Quenching in Liquid Nitrogen (77K) from 1273 K.
The nitride film retained the attachment on a fractured SiC particle after the annealing. The film structure was globular, similar to film's as-deposited structure.

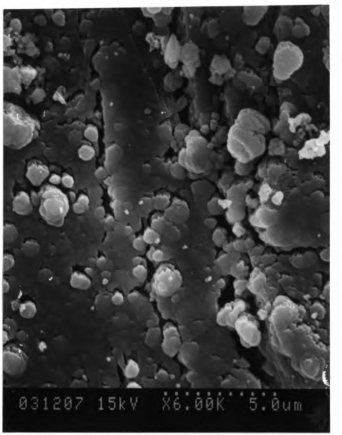

Figure 4.15. Aluminum Oxide Film on a SiC Particle, after Air-cooling from 1273 K to Room Temperature.
Grain growth occurred in the film during the annealing, resulting in micro-cracks in the film.

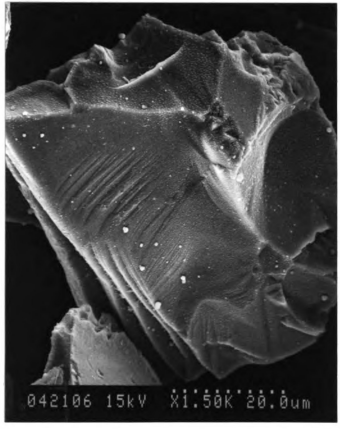

(a). A Coated SiC Particle after Annealing

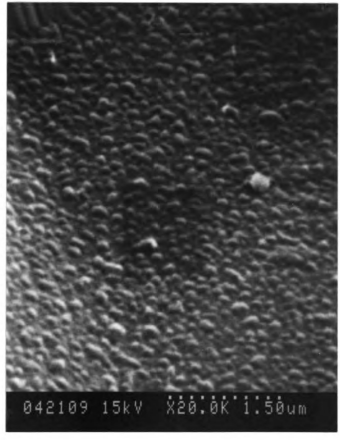

(b). Film Morphology on the SiC Particle

Figure 4.16. Aluminum Nitride Film Deposited on SiC Particles at 793 K, after Annealing at 1373 K in Vacuum for 1 Hour.

No change in film morphology was observed as compared with film's original morphology before the annealing.

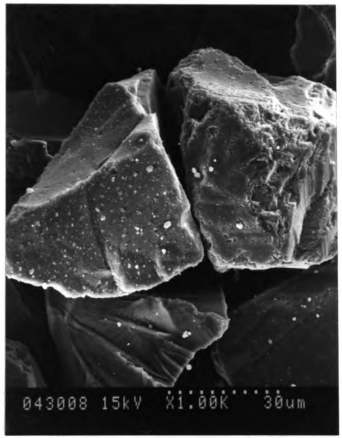

(a). Coated SiC Particles after Annealing

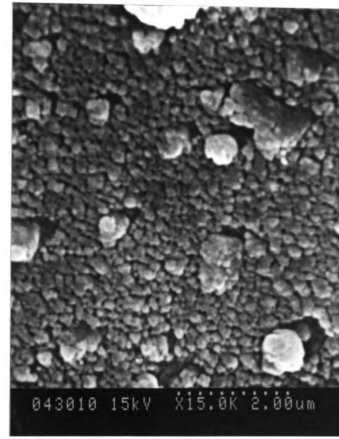

(b). Film Morphology on a SiC Particle

Figure 4.17. Aluminum Nitride Film Deposited on SiC Particles at 793 K, after Annealing at 1573 K in Vacuum for 4 Hours.

Better defined grain boundaries in the film was found as compared with the as-deposited film before the annealing. Voids became visible.

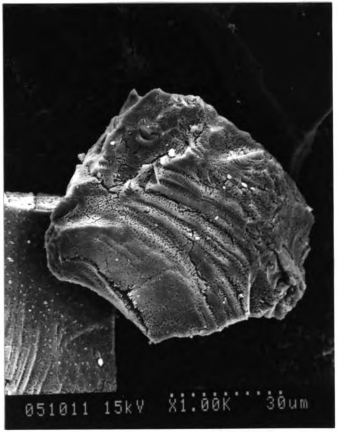

(a). A Coated SiC Particle after Annealing

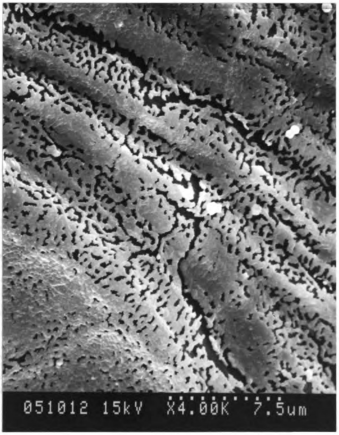

(b). Film Morphology on the SiC Particle

Figure 4.18. Aluminum Nitride Film Deposited on SiC Particles at 793 K, after Annealing at 1673 K in Vacuum for 4 Hours.

After annealing, micro-cracks were observed in the film. Surfaces of the SiC substrate were exposed. With a high magnification, Figure 4.18 (c) shows many small grains (<0.1 μm in size) of secondary phases.

Figure 4.18 (Cont.)

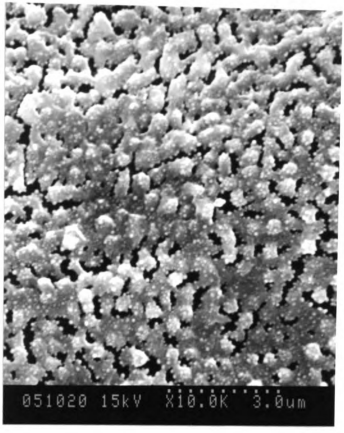

(c). A SEM Image of the Film Surface with High Magnification

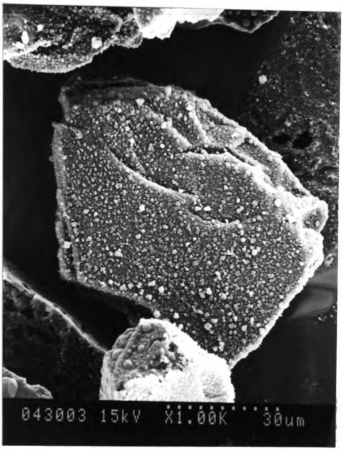

(a). A Coated SiC Particle after Annealing

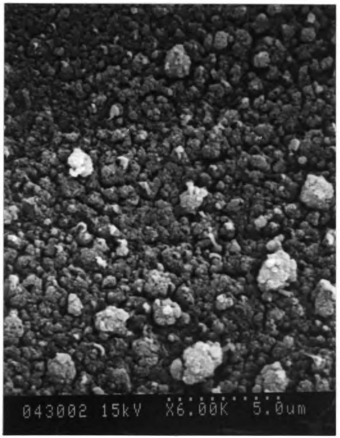

(b). Film Morphology on the SiC Particle

Figure 4. 19. Aluminum Nitride Film Deposited on SiC Particles at 593 K, after Annealing at 1573 K in Vacuum for 4 Hours.

Better defined grain boundaries inside each clusters was found as compared with the as-deposited film before the annealing. Voids were more visible in between the clusters.

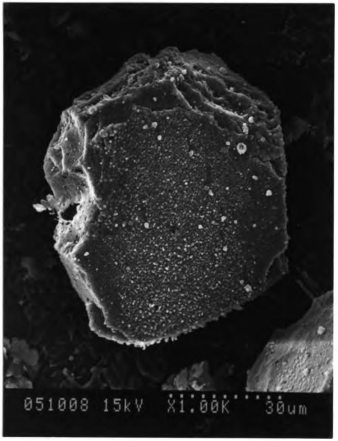

(a). A Coated SiC Particle after Annealing

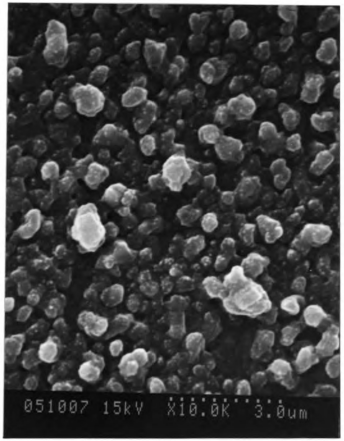

(b). Film Morphology on the SiC Particle

Figure 4.20. Aluminum Nitride Film Deposited on SiC Particles at 593 K, after Annealing at 1673 K in Vacuum for 4 Hours.

The annealed film retained the globular film structure, but with larger grains, as compared with film's original structure. Limited solid-state sintering took place, densifying the film.

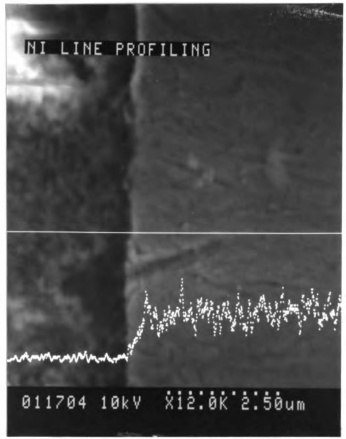

(a). AlN/Ni_3Al, after a 1473 K/32 Hours Annealing

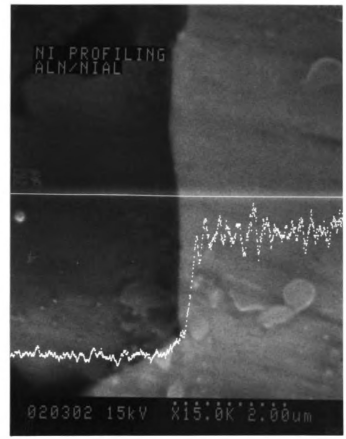

(b). AlN/NiAl, after a 1673 K/12 Hours Annealing

Figure 4.21. Ni Concentrational Profile at Interfaces in Diffusion Couples, by EDX.
The Ni concentrational transitions between aluminide and aluminum nitride plates were less than the spacial resolution of the EDX technique (of 1 μm).

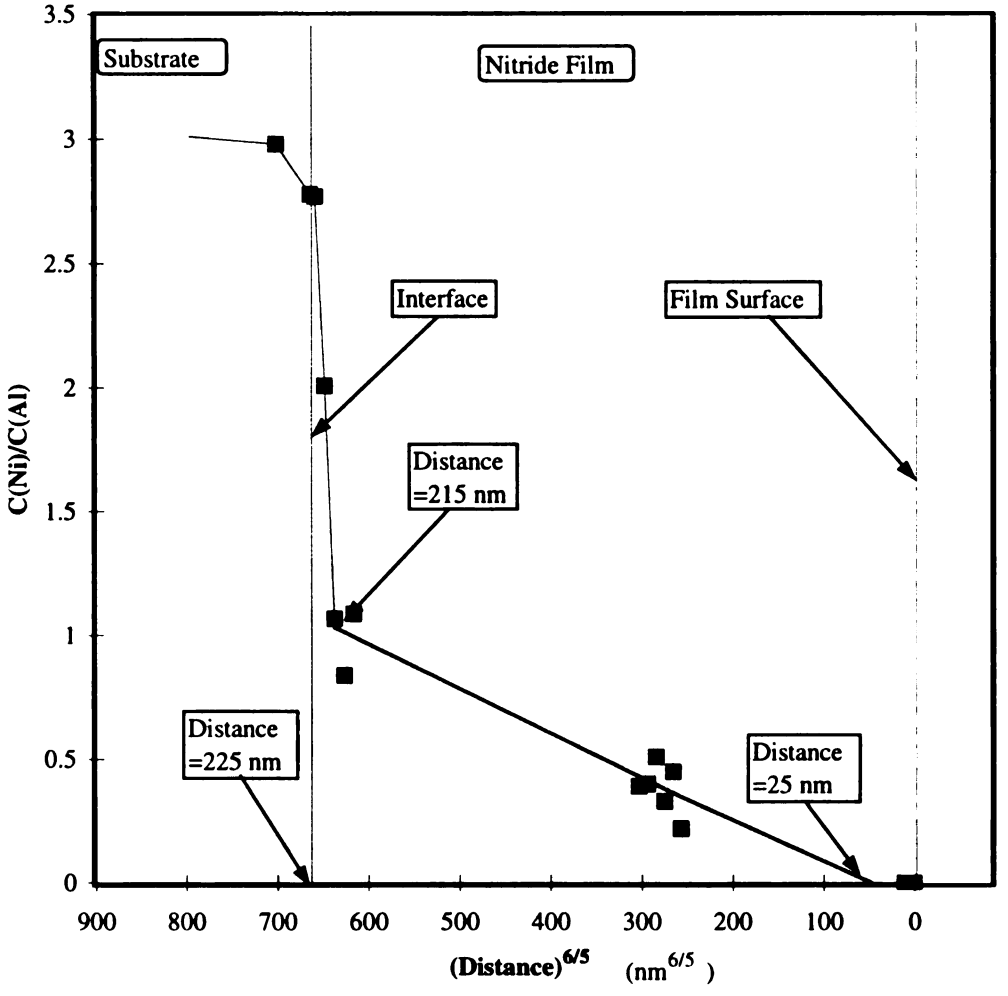

Figure 4.22. XPS Profile of Ni Diffusing in an Aluminum Nitride Film from a γ-Ni_3Al Source after a 1373 K/30 Minutes Annealing.
The film was deposited on a γ-Ni_3Al plate. The total distance of Ni diffusing in the film was about 200 nm (0.2 μm).

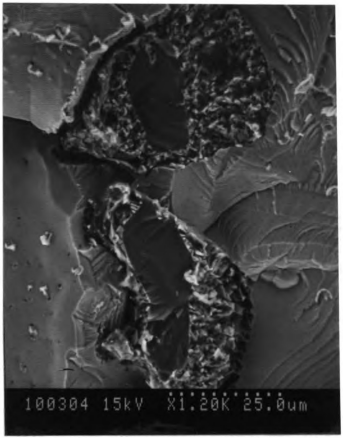

(a). The Reaction Zone between SiC and NiAl

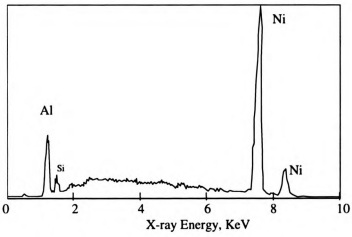

(b). EDX Spectrum from the Reaction Zone

Figure 4.23. Reaction Zone in a SiC Particle Reinforced β-NiAl Matrix Composite with Uncoated SiC Particles.
The reaction zone was found in between NiAl matrix and the remnant of the SiC particles.

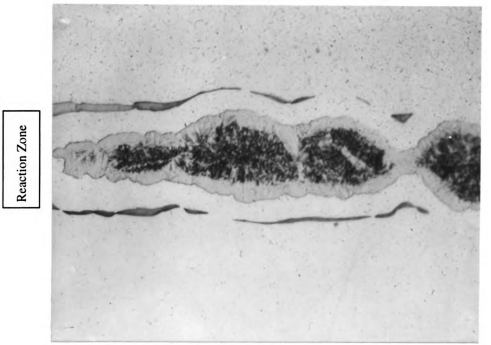

Figure 4.24. Reaction Zone in a SiC Particle Reinforced γ-Ni_3Al Matrix Composite with Non-coated SiC Particles.
(Magnification: 500x)
The reaction zone was found at the location previously occupied by the SiC particles. No remnant of the SiC particles was found in the composite.

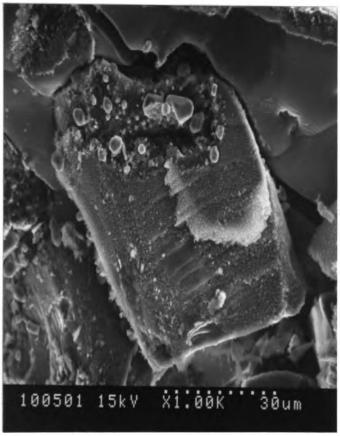

(a). A Coated SiC Particle in Composite

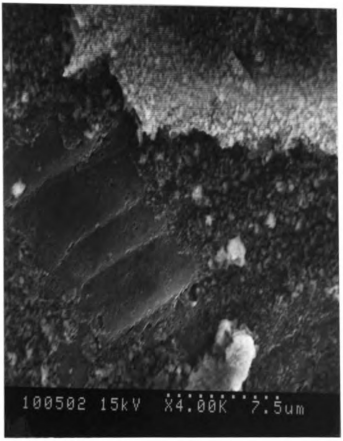

(b). Film Damaged Area on the SiC Particle

Figure 4.25. Aluminum Nitride Film Deposited at 593 K as a Diffusion Barrier in a SiC Particle Reinforced β-NiAl Matrix Composite.

The SiC particle was preserved by the nitride diffusion barrier film after the composite consolidation process. The nitride film on the SiC particle was damaged during SEM sample preparation process.

Figure 4.25 (Cont.)

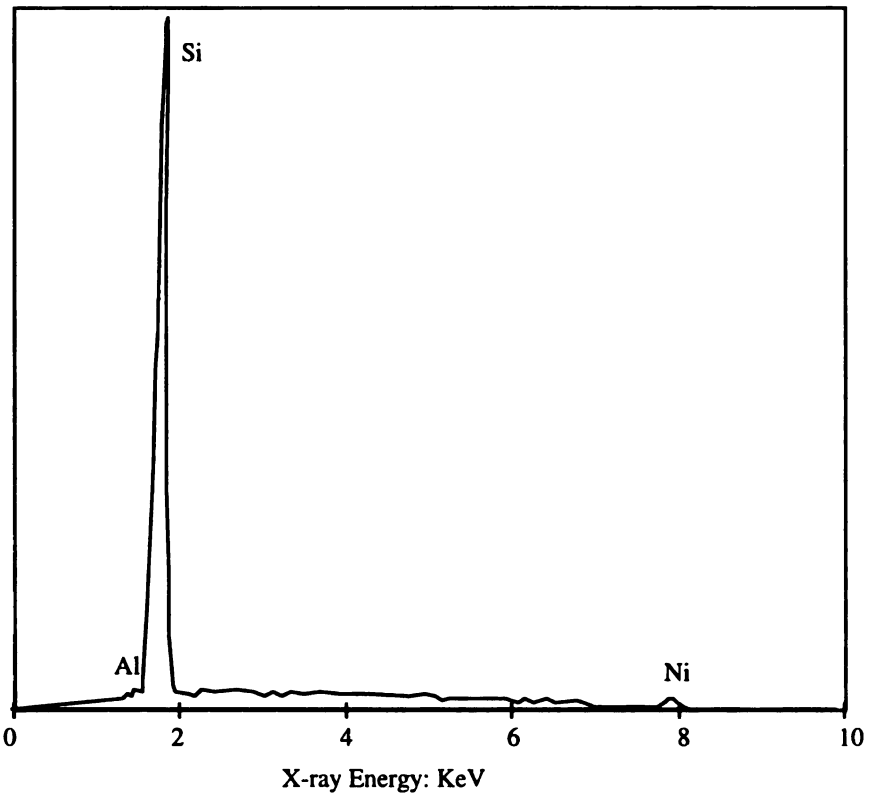

(c). EDX Spectrum from the Revealed SiC Surface Shown in Figure 4.25 (b)

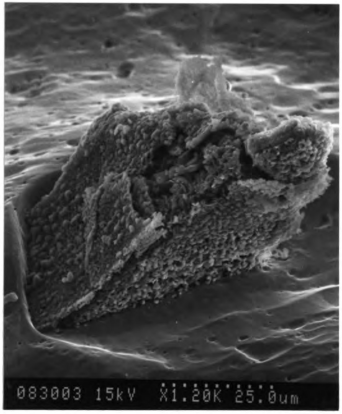

(a). A Coated SiC Particle, with Damaged Coating

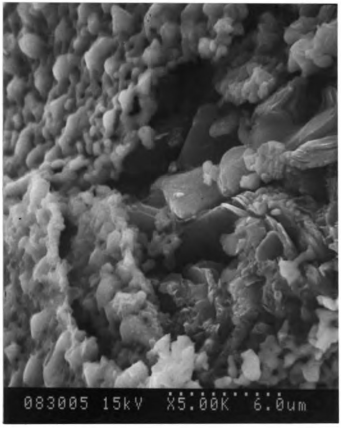

(b). Film Damaged Area on the SiC Particle

Figure 4.26. Aluminum Nitride Film Deposited at 593 K as a Diffusion Barrier in a SiC Particle Reinforced β-NiAl Matrix Composite, Film Damaged during Hot-Press Process.
The nitride film on the SiC particle was damaged during the composite consolidation process. The SiC substrate was chemically reacted with the NiAl matrix. Reaction products existed beneath the film.

Figure 4.26 (Cont.)

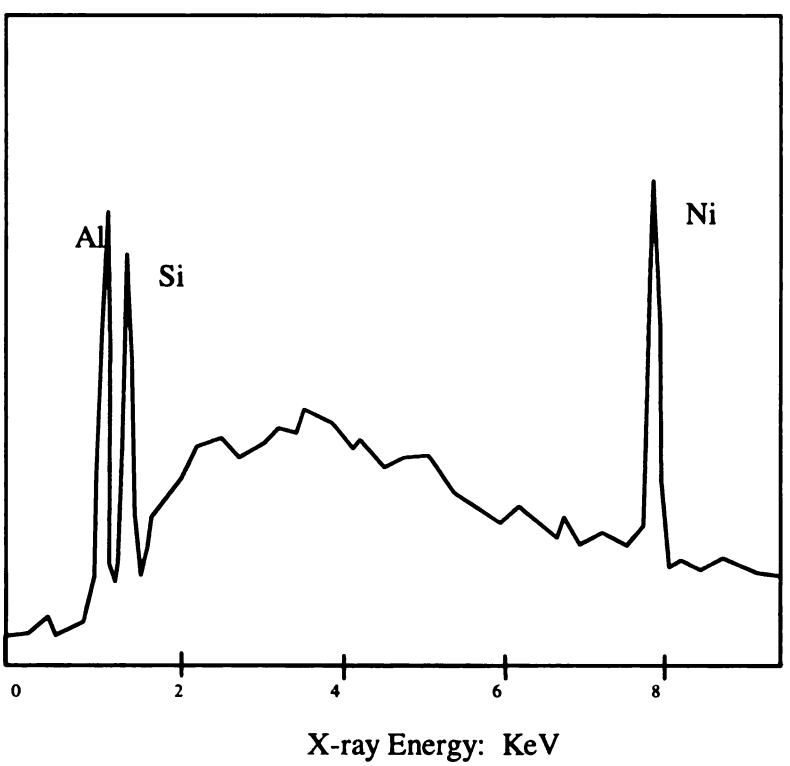

(c). EDX Spectrum from the Reaction Products Revealed at the Film Damaged Area

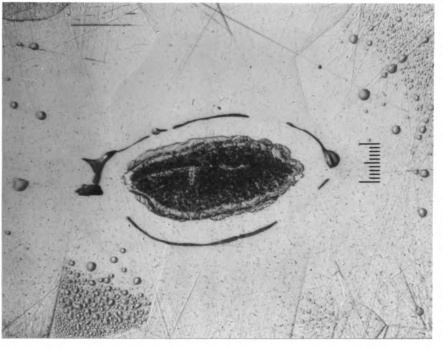

Figure 4.27. Reaction Zone in a SiC Particle Reinforced γ-Ni_3Al Matrix Composite with Aluminum Nitride Film Deposited at 593 K as a Diffusion Barrier. (Magnification: 500x)
The reaction zone was found at the location previously occupied by the SiC particles. No remnant of the SiC particles was found in the composite.

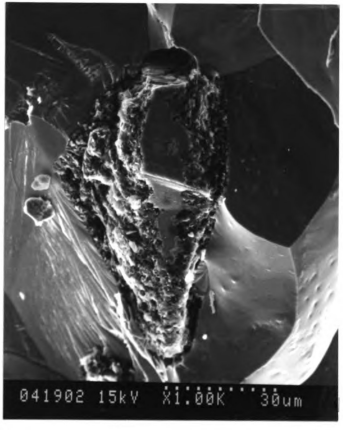

Figure 4.28. Reaction Zone in a SiC Particle Reinforced β-NiAl Matrix Composite with Aluminum Nitride Film Deposited at 793 K as a Diffusion Barrier.

The reaction zone was found in between NiAl matrix and the remnant of the SiC particles. No evidence of stalling the reaction by the imposition of the nitride barrier film was found.

Figure 4.29. Reaction Zone in a SiC Particle Reinforced γ-Ni_3Al Matrix Composite with Aluminum Nitride Film Deposited at 793 K as a Diffusion Barrier.

The SEM sample was prepared by fracturing the composite sample in tension. The reaction zone was found at the location previously occupied by the SiC particles. No remnant of the SiC particles was found. No evidence of stalling the reaction by the imposition of the nitride barrier film was found in the composite.

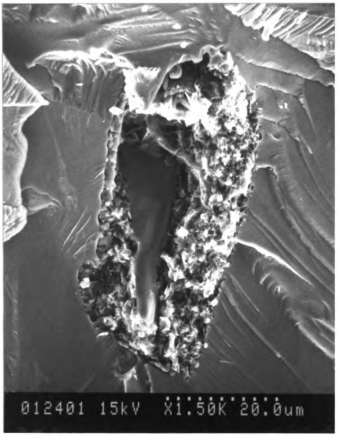

(a). Reaction Zone in SiC/β-NiAl Matrix Composite

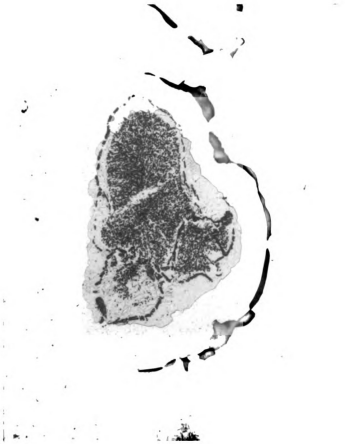

(b). Reaction Zone in SiC/γ-Ni_3Al Matrix Composite (Magnification: 500x)

Figure 4.30. Reaction Zone in SiC Particle Reinforced β-NiAl Matrix and γ-Ni_3Al Matrix Composites with Aluminum Oxide Film as a Diffusion Barrier.
No evidence of stalling the reactions by the imposition of the oxide barrier film was found in both composites.